

# FlowDike-D – Influence of wind and current on wave run-up and wave overtopping – Extracts of the final report –

*Stefanie Lorke, Antje Bornschein, Reinhard Pobl and Holger Schüttrumpf*

## Summary

In the past wave overtopping was a main reason of dike failures or dike breaches. These processes are induced by erosion and infiltration. To avoid overtopping induced dike failures the wave run-up height and wave overtopping rate has to be known. A lack of knowledge in this research field may result either in too high and expensive flood protection structures or in a higher risk of flooding because of weak designs. Within the project FlowDike-D physical model tests in the shallow water basin at DHI (Hørsholm, Denmark) on wave run-up and wave overtopping were performed measuring amongst others wave run-up height and wave overtopping rates. The new approach in this research project is to consider a current parallel and a wind perpendicular to the dike line combined with different angles of wave attack. During the analysis no influence of the wind on wave run-up or wave overtopping was detectable. The influence of the current can be considered by introducing a new defined influence factor for current  $\gamma_{\beta, cu}$ . Thereby it is important to distinguish between wave attack with and against the current.

## Keywords

dikes, wave run-up, wave overtopping, wind, current, freeboard design

## Zusammenfassung

*In der Vergangenheit war der Wellenüberlauf ein Hauptgrund für Deichversagen oder Deichbrüche. Diese Prozesse werden durch Erosion und Infiltration induziert. Um das von Überlauf induzierte Deichversagen zu vermeiden, müssen die Wellenauslaufhöhe und die Wellenüberlauftrate bekannt sein. Ein Mangel an Wissen in diesem Forschungsgebiet kann entweder in zu hohen und teuren Hochwasserschutzstrukturen oder in einem höheren Risiko für Überschwemmungen aufgrund schwacher Entwürfe resultieren. Im Projekt FlowDike-D wurden physikalische Modellversuche in einem flachen Wasserbecken bei DHI (Hørsholm, Dänemark) zu Wellenauslauf und Wellenüberlauf durchgeführt, um unter anderem die Wellenauslaufhöhe und die Wellenüberlauftrate zu messen. Der neue Ansatz in diesem Forschungsprojekt besteht darin, eine Strömung parallel und Wind senkrecht zur Deichlinie mit verschiedenen Winkeln zu betrachten. Während der Analyse war kein Einfluss des Windes auf den Wellenauslauf oder Wellenüberlauf nachweisbar. Der Einfluss der Strömung kann durch die Einführung eines neudefinierten Faktors für die Strömung  $\gamma_{\beta, cu}$  berücksichtigt werden. Dabei ist zwischen Wellenangriff mit und gegen die Strömung zu unterscheiden.*

## Schlagwörter

*Deiche, Wellenauflauf, Wellenüberlauf, Wind, Strömung, Freibordmessung*

## Contents

1	Introduction.....	3
2	Experimental procedure.....	4
2.1	Overview of test program.....	4
3	Model construction and instrumentation.....	5
3.1	Shallow water basin.....	5
3.2	Measurements.....	7
3.2.1	Overview.....	7
3.2.2	Wave field (wave gauges, ADV).....	10
3.2.3	Wind field (wind machine, Anemometer).....	12
3.2.4	Current (weir, ADV, micro propeller).....	13
3.2.5	Wave run-up (capacitive gauge, camera, step gauge).....	14
3.2.6	Overtopping velocity and layer thickness (micro propeller, wave gauge, pressure sensor).....	17
3.2.7	Overtopping water volume (load cell, pump).....	19
3.3	Model and scale effects.....	20
3.3.1	Model effects.....	20
3.3.2	Scale effects.....	21
4	Theory of the influence of current and wind.....	21
4.1	Wave and current interaction.....	21
4.1.1	General.....	21
4.1.2	Current induced shoaling.....	22
4.1.3	Current induced wave refraction.....	23
4.2	Wave run-up and wave overtopping influenced by current.....	25
4.3	Influence of wind on waves.....	25
4.4	Wave run-up and wave overtopping influenced by wind.....	26
5	Analysis of wave field and breaking processes.....	27
5.1	General.....	27
5.2	Verification of measurements.....	27
5.2.1	General.....	27
5.2.2	Measured wave heights.....	27
5.2.3	Reflection analysis – frequency domain.....	29
5.3	Wave breaking.....	33
6	Analysis of wave run-up and wave overtopping.....	35
6.1	Remarks.....	35

6.2	Analysis on wave run-up.....	36
6.2.1	Comparison between capacitive gauge and video.....	36
6.2.2	Reference tests .....	38
6.2.3	Influence of angle of wave attack .....	39
6.2.4	Influence of wind .....	43
6.2.5	Influence of current .....	45
6.2.6	Influence of current and oblique wave attack .....	47
6.2.7	Combination of all influence parameters .....	49
6.3	Analysis on wave overtopping.....	50
6.3.1	Reference test.....	50
6.3.2	Influence of wave spectra .....	52
6.3.3	Influence of oblique wave attack without current .....	52
6.3.4	Statistical spread of tests.....	55
6.3.5	Comparison with former investigations .....	56
6.3.6	Influence of current .....	57
6.3.7	Influence of wind .....	59
6.3.8	Influence of oblique wave attack and current .....	60
6.3.9	Angle of wave attack and absolute wave parameters .....	60
6.3.10	Angle of wave attack and relative wave parameters .....	61
6.3.11	Angle of wave energy and absolute wave parameters .....	62
6.3.12	Conclusion.....	64
6.4	Comparison of wave run-up and wave overtopping .....	64
6.5	Analysis of flow processes on dike crests .....	66
6.5.1	Plausibility of the measured data .....	66
6.5.2	Influence of oblique wave attack on flow processes on dike crests .....	71
7	Conclusion .....	72
8	List of abbreviations .....	74
9	Notation.....	74
10	References .....	76

## 1 Introduction

A variety of structures has been built in the past to protect the adjacent areas during high water levels and storm surges from coastal or river flooding. It is common practice to build smooth sloped dikes as well as steep or vertical walls as flood protection structures. The knowledge of the design water level with a certain return interval, wind surge, wave run-up and/or wave overtopping is used to determine the crest height of these structures.

The incoming wave parameters at the toe of the structure are relevant for the free-board design in wide rivers, estuaries and at the coast. At rivers waves are probably influenced by local wind fields and sometimes by strong currents – occurring at high water levels mostly parallel to the structure. In the past no investigations were made on the

effects of current and the combined effects of wind and current on wave run-up and wave overtopping. Only a few papers, dealing with wind effects, are publicized. To achieve an improved design of structures these effects should not be neglected, otherwise the lack of knowledge may result in too high and expensive structures or in too low flood protection structures which result in higher risks of flooding.

The aim of the research project presented is to achieve a better understanding about the influence of current and wind on wave run-up and wave overtopping by experimental investigations in an offshore wave basin. Data from previous KFKI projects “Oblique wave attack at sea dikes” and “Loading of the inner slope of sea dikes by wave overtopping” and from the CLASH-database are at hand for comparison purposes. They represent a set-up with perpendicular and oblique wave attack but without wind and without longshore current.

The research dealt with the wave run-up and wave overtopping due to long-crested waves on a dike slope with a smooth surface. The experimental set-up includes different longshore current velocities and onshore wind speeds, two different dike crest levels and various wave directions.

The experimental investigations were performed within two test phases in 2009 at DHI in Horsholm, Denmark. In the first test phase (EU-HYDRALAB-III project FlowDike) a 1:3 sloped dike (FlowDike 1) was investigated, while a 1:6 sloped dike (FlowDike 2) was tested in the second test phase (BMBF-KFKI project FlowDike-D, 03KIS075 (IWW), 03KIS076 (IWD)). The compilation of both test phases, using the results for the 1:3 dike as well as the results for the 1:6 dike, is done within the project FlowDike-D.

A first overall view of the experimental procedure and a more detailed description of the model set-up as well as the used measurements are given in sec. 2 and 3. After presenting the theory of the influence of current and wind on waves, wave run-up and wave overtopping in sec. 4, the analysis of the wave field is presented in sec. 5. The analyses on wave run-up and wave overtopping have been done in sec. 6, which includes the determination of run-up heights, mean overtopping discharges and evaluation of flow processes on dike crests. Finally a conclusion and outlook is given in sec. 7.

## 2 Experimental procedure

### 2.1 Overview of test program

The investigation was focused on long crested waves which were created using JON-SWAP spectrum. The test program covered model tests with and without current and with and without wind for normal and oblique wave attack. Tab. 1 presents a summary of the test program. The angle of wave attack covers a range of  $0^\circ$  to  $45^\circ$ . The maximum flow velocity was 0.4 m/s and the maximum wind speed was 10 m/s. Normal wave attack is here equal to an angle of  $\beta = 0^\circ$ . Waves with a positive angle of wave attack propagate in the direction of the current, while waves with a negative angle of wave attack are directed against the current.

The test program did consider dikes with different slopes too. In whole 119 tests were performed on a 1:3 sloped dike and 152 tests were done on a 1:6 sloped dike. Each tested combination of a certain angle of wave attack, a current velocity (including no current)

and a wind velocity (including no wind) provides the framework for six tests with six different sea states. Each sea state is characterized by a significant wave height  $H_s$  and a peak period  $T_p$ . The DHI wave synthesizer (DHI WASY WATER & ENVIRONMENT 2007) was applied to generate the time-dependent wave height according to the formulas of JONSWAP spectra so that one test includes at least 1000 approaching waves.

Table 1: Summary of the test program and test configurations.

freeboard height $R_C$ [m]	1:3 dike: 0.10 and 0.20 1:6 dike: 0.05 and 0.15
wave height $H_s$ [m] and wave period $T_p$ [s]	1:3 dike: $H_s$ 0.07 0.07 0.10 0.10 0.15 0.15 $T_p$ 1.474 1.045 1.76 1.243 2.156 1.529 1:6 dike: $H_s$ 0.09 0.09 0.12 0.12 0.15 0.15 $T_p$ 1.67 1.181 1.929 1.364 2.156 1.525
angle of wave attack $\beta$ [°]	-45 -30 -15 0 +15 +30
current $v_x$ [m/s]	0.00 0.15 0.30 0.40 (only 1:6 dike)
wind velocity measured at the dike crest $u$ [m/s]	1:3 dike 0 5 10 1:6 dike 0 4 8

### 3 Model construction and instrumentation

#### 3.1 Shallow water basin

The Danish Hydraulic Institute (DHI) in Hørsholm, Denmark provided a shallow water wave basin as test facility for the hydraulic model tests. It was 35 m long, 25 m wide and could be flooded to a maximum water depth of 0.9 m. At the eastern long side an 18 m long multidirectional wave generator composed of 36 segments (paddles) was installed (see Fig. 1). The 0.5 m wide and 1.2 m high segments can be used to generate multidirectional, long or short crested waves. The applied DHI software included procedures for active wave absorption. An automatic control system called AWACS (Active Wave Absorption Control System) used the measured data of the actual water depth at each paddle to identify and absorb reflected waves.

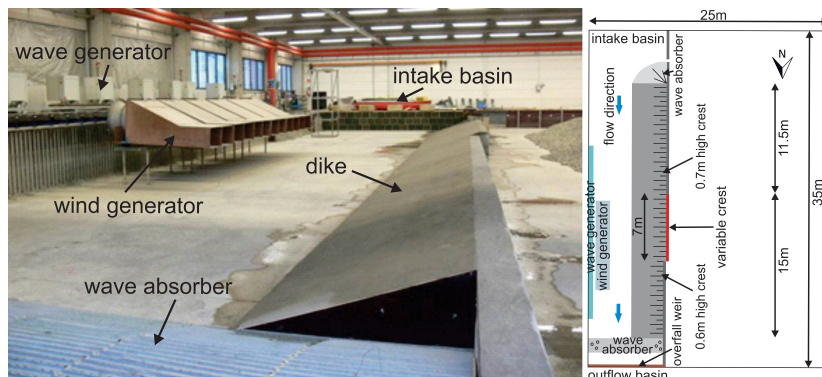


Figure 1: Completed dike slope (view from downstream), wave generator (paddles) and wind generator (fans) on the left side.

Wind machines were used to introduce wind as an influence parameter. They could generate a homogenous wind field over the free water surface. Six wind machines were placed in front of the wave generator 0.8 m above the basin floor.

An adjustable weir at the downstream end was used to ensure a constant water depth in the basin. To create a longshore current a closed water cycle was initiated. The pumped water discharge was adjusted for each current velocity so that the chosen water depth was assured. Three rows of beverage crates at the upstream end were used to straighten the inflow and to provide aligned and parallel streamlines within the channel (see Fig. 2). Wave absorbers at the upstream and downstream end ensured minimal reflection and diffraction. At the upstream end gravel heap was placed whereas at the downstream end a metallic wave absorber was used (see Fig. 2).



Figure 2: Left: upstream edge of the dike with wave absorption and beverage racks; right: metallic wave absorber in front of the weir.

The complete dike structure was 26.5 m long. Its length was determined by the domain where the fully developed sea state reaches the dike slope considering the different wave directions. The model dike looked like half a dike. A brick wall formed the landward side and the 0.28 m wide dike crest. On the seaward side a core of compacted gravel was covered with a 50 mm concreted layer.

The overtopping water was sampled by four overtopping units out of plywood which were mounted at the landward edge of the crest. A cross-section of one overtopping unit is given in Fig. 3. Two units have been installed at the lower and two at the higher dike part. The overtopping water was lead into an overtopping channel and then into the overtopping tank. The overtopping water in each tank was measured by a load cell and water level gauges in each tank. Standard pumps in the tanks were used to empty the tanks during and after each test. External boxes were constructed to contain the overtopping tanks, load cells and water level gauges and prevent these devices from uplift.

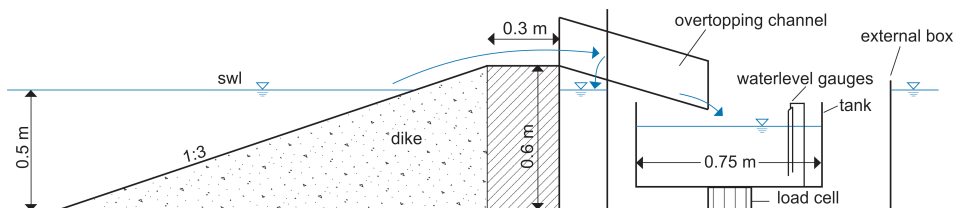


Figure 3: Cross section of overtopping unit exemplary for the 0.6 m high dike.

For the wave run-up a so called “run-up board” out of plywood (2 m x 2.5 m) was mounted on top of the concrete crest to facilitate the up rush measurement by a capacity gauge and video analysis. This plate could be moved easily in its position during the changes of set-ups. The gap between run-up board and crest edge was filled either with a wooden piece and silicone or with a cement cover. To get films with a better contrast the wave run-up board was enlightened by a 2000-W-spotlight which was positioned such as the light met the run-up board within an angle of  $120^\circ$  to the optical axis of the digital cameras. On the left side of the run-up plate a digital radio controlled clock with a 0.4 m x 0.4 m display was positioned due to the purpose of synchronizing the measurements (Fig. 4).

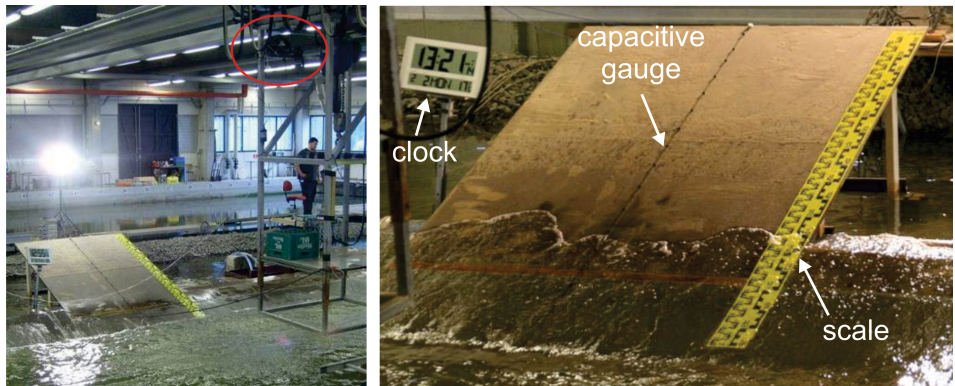


Figure 4: Wave run-up board and rack with both digital cameras marked with a red circle (left); capacitive gauge, clock and scale (right).

## 3.2 Measurements

### 3.2.1 Overview

An overview of the shallow water basin is given in Fig. 5 (1:3 sloped dike) and Fig. 6 (1:6 sloped dike). Flow direction of the current (blue arrows) was from left to right. The area marked in light yellow indicates the domain where the fully developed sea state occurred depending of the angle of wave attack. The position of all used measurement devices is marked and explained within the drawings. They are listed below in alphabetical order and are described in detail in the following sections. If there were changes in measurement devices between the tests on the 1:3 sloped dike and the 1:6 sloped dike they are explained too.

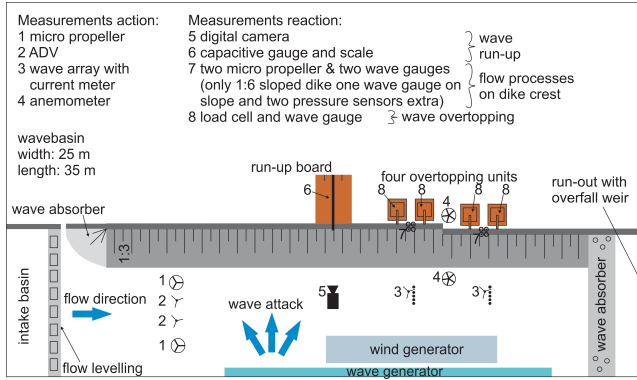


Figure 5: Model set-up FlowDike 1 with instruments and flow direction (1:3 sloped dike).

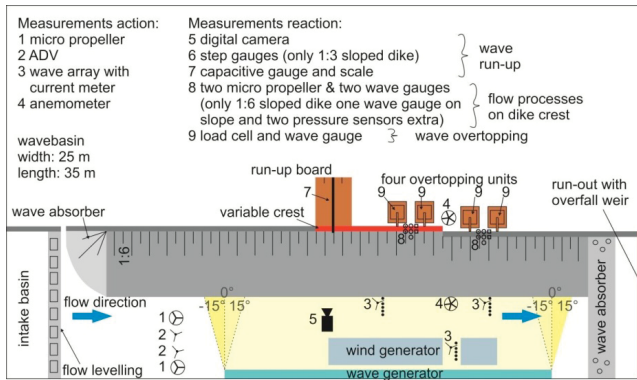


Figure 6: Model set-up FlowDike 2 with instruments and flow direction (1:6 sloped dike).

### Anemometer (TSI)

Wind velocity was measured by two anemometers. They were provided by DHI and installed in the model set-up. These thin transducers with a small window for the sensor were able to record a range of 0 V – 10 V (0 m/s – 20 m/s) with a sampling frequency of 5 Hz.

### Capacitive gauge

The capacitive gauge on a run-up plate was used to get quantitative data of time-dependent wave run-up and down. The main part, a 3.5 m long capacitor, was formed by one insulated and one non insulated wire. Air or water between the two wires forms the dielectric fluid. The scale of the voltage value ranged from 0 V to 5 V. A sampling frequency of 25 Hz was applied.

The capacitive gauge was insensitive to environmental conditions like changes in water temperature but it depends on the model set-up especially on the wire length and the mounting height. That is why the calibration was repeated for each model set-up.

### **Current meter (Acoustic Doppler Velocity meter (ADV), Minilab SD-12, Vectrino)**

Different devices were applied to measure current velocity at different locations in the shallow water basin. Both ADV's and Vectrino are single point Doppler current meters. The current velocity is measured using the Doppler Effect. The sampling frequency was set to 25 Hz and a nominal velocity range of  $\pm 1$  m/s. The Minilab SD-12 is an ultrasonic current meter. It contains a transducer, a reflector and four receivers that measure the velocity from time difference between the send and received signal. The resolution of this current meter is 1 mm/s.

### **Digital cameras**

The flow processes on the run up board were recorded by means of digital cameras too. The data analysis to obtain the run-up height could then be done later after the model tests. Two digital cameras were used for FlowDike 1 as well for FlowDike 2 but with different picture resolution and different frame rates.

### **Load cell**

The cubic shaped weighing equipment had a height of 0.1 m and was mounted beneath the overtopping tank. They were used to measure the amounts of overtopping water. Data analysis was focused on the z-component with a maximum capacity of 2150 N ( $\approx 220$  kg). Due to its accuracy ( $\leq 0.05$  %) it was used to detect single overtopping events.

### **Micro propeller (Schiltknecht)**

Vane anemometers of Schiltknecht, Switzerland were used to measure flow velocity on the dike crest. The vane rotation is closely linear to flow velocity and is unaffected by pressure, temperature, density and humidity. During FlowDike 1 model tests a MiniWater 20 Micro was used. Its measuring range lay between 0.04 m/s and 5 m/s and its accuracy was 2 % of the full scale. Several MiniWater 6 Micro anemometers have been provided by DHI for FlowDike 2 tests. Their measuring range is identical to that of the MiniWater 20 Micro.

### **Thermometer**

It was essential for some measurement devices e.g. wave gauges to assure a constant water temperature during the test. A significant change in water temperature could be caused by pumping in order to create a longshore current velocity. The water temperature was monitored during all tests.

## Wave gauges, water level gauges

Wave gauges and water level gauges were applied to measure water surface elevation and to gain data about the wave field and the flow depth on the crest. These sensors detect a change in water depth by means of change of conductivity between two thin, parallel stainless steel electrodes. An analog output signal is taken from the Wave Meter conditioning module, where the wave gauge is connected to, and compiled in the data acquisition system. Each wave gauge array included five wave gauges and one velocity meter. Calibration was only valid for a constant water temperature and had to be repeated if the water temperature deviated more than  $0.5^{\circ}\text{C}$ , generally at the beginning of each test day. Hereby a calibration factor of 0.1 m per 1 Volt was used. As an exception the calibration factor for the small wave gauges on the crest was 0.1 m per 0.5 Volt during FlowDike 1.

### 3.2.2 Wave field (wave gauges, ADV)

To analyze the wave field the water surface elevation as well as flow velocity has to be measured. These values were determined by two wave gauge arrays of 5 wave gauges (with a length of 0.6 m each) and a current meter. An overall view given in Fig. 7 and Fig. 8 demonstrates that each of them is orthogonal aligned between the wave machine and the dike. Each array was assigned to one crest height and placed at the toe of the structure positioned between the two overtopping channels.

Non-equal distances between the single gauges of the wave gauge arrays were necessary for the reflection analysis. That is why the wave gauges were placed at 0.00 m, 0.40 m, 0.75 m, 1.00 m and 1.10 m from the first wave gauge along a line. A current meter, ADV or Minilab SD-12, was positioned close to one wave gauge of the array. Reflection and crossing analysis were carried out for each array and its associated velocity meter.

In order to observe the development of the wave field while propagating through the longshore current a third wave gauge array, which was placed in front of the wave generator, was added to the model set-up of the 1:6 sloped dike. A vectrino was assigned as current meter to this array. The two other wave gauge arrays were situated in similar positions as in FlowDike 1 (1:3 sloped dike). The distance between the two wave gauge arrays at the dike toe and the one near the wave generator was 1.5 m.

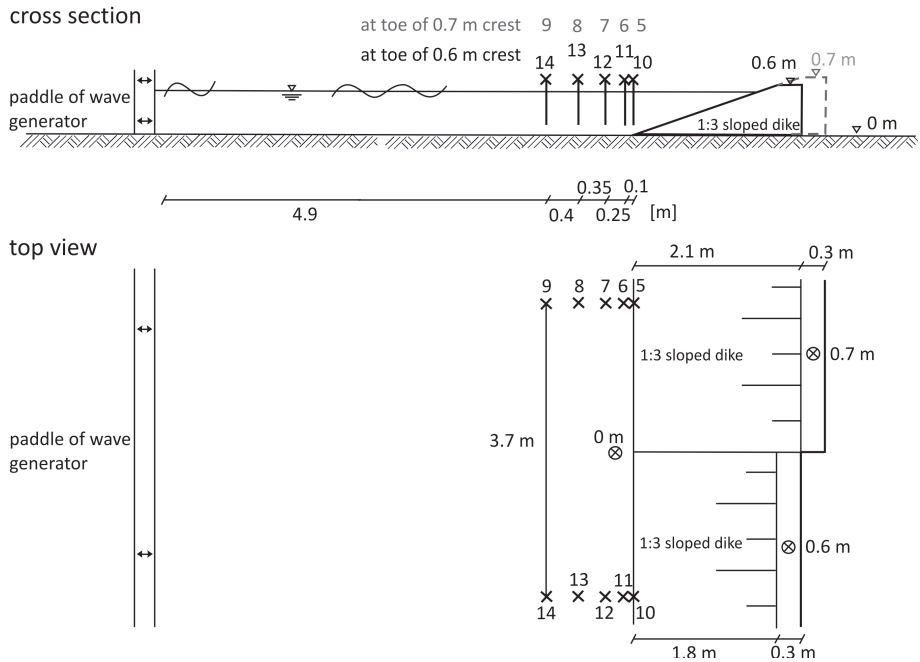


Figure 7: Configuration of the wave gauge arrays exemplary on the 1:3 sloped dike (cross sectional and top view).

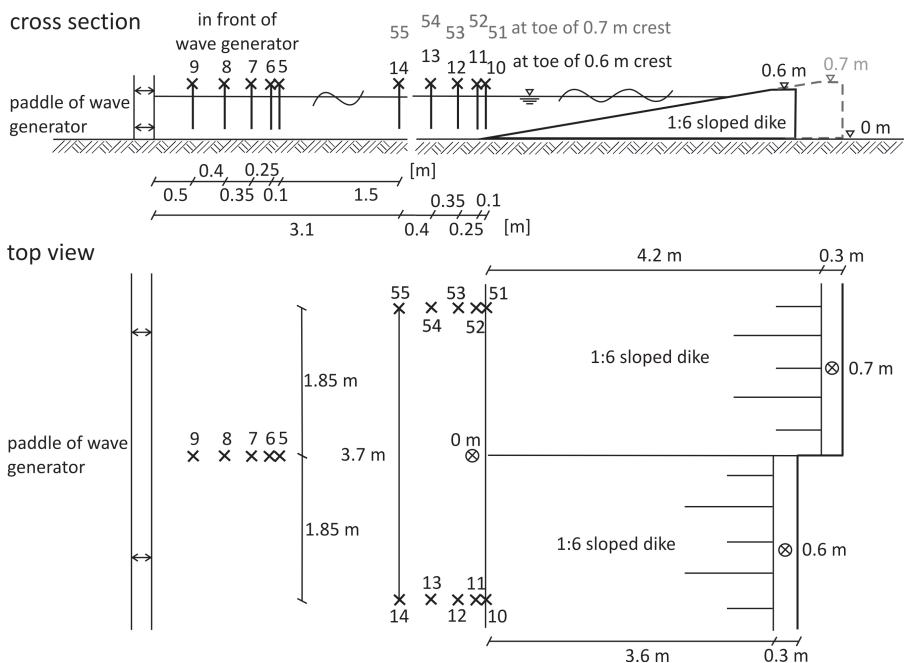


Figure 8: Configuration of the wave gauge arrays exemplary on the 1:6 sloped dike (cross sectional and top view).

### 3.2.3 Wind field (wind machine, Anemometer)

During the tests a wind field was generated by six wind machines using wind turbines. Wind direction was towards the dike and perpendicular to the dike crest. In order to create a homogeneous wind field on the dike slope and crest the distances between the six wind machines were not equally spaced (0.38 m – 0.45 m – 0.50 m – 0.45 m – 0.38 m).

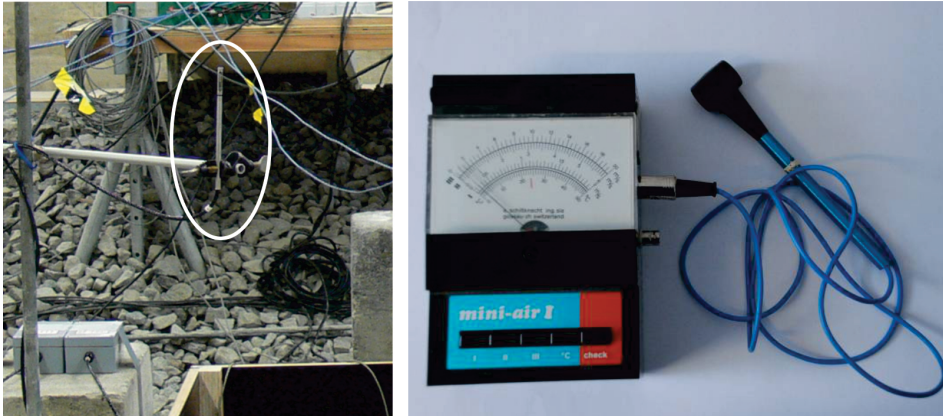


Figure 9: Anemometer (left) and fan wheel for air velocity measurement (right).

During the tests two different wind velocities have been created by setting two different propeller revolutions per second at the wind generators. To verify, if the wind field was spatially homogeneous, the wind velocity was measured along the dike crest with a fan wheel (see Fig. 9). The results are given in Fig. 10 and Fig. 11.

All measurement results prove a homogeneously distributed wind field. The average wind velocity in FlowDike 2 (1:6 sloped dike) was slightly lower than in FlowDike 1 (1:3 sloped dike). This was caused by the larger distance between the wind generator and the dike crest.

To control wind velocity during tests two anemometers for velocity measurements provided by DHI were installed in the model set-up. One was situated 2 m in front of the dike toe and the second was placed above the crest. Both measured within a height of 1 m above the basin ground, just in the middle between the overtopping unities for each crest as shown in Fig. 9.

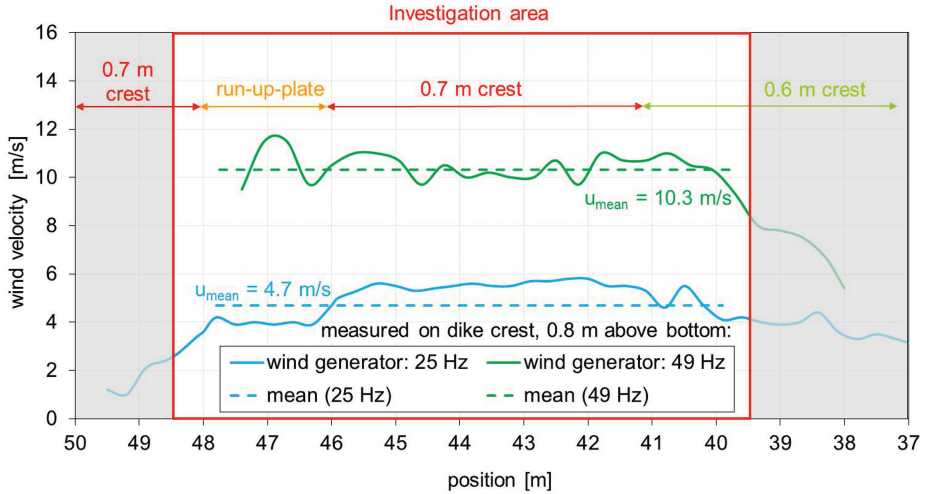


Figure 10: Wind velocity distribution for a frequency of 25 Hz and 49 Hz (1:3 sloped dike).

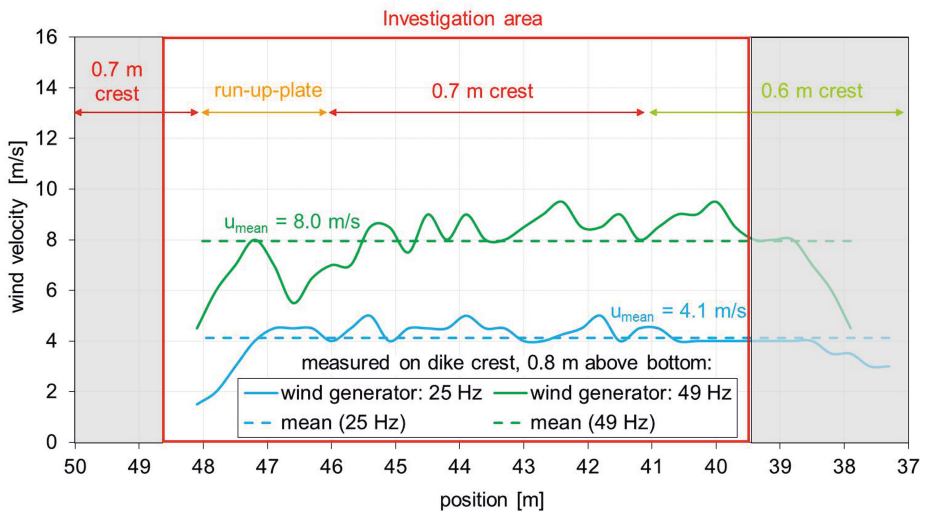


Figure 11: Wind velocity distribution for a frequency of 25 Hz and 49 Hz (1:6 sloped dike).

### 3.2.4 Current (weir, ADV, micro propeller)

Current velocities were controlled with two ADV's (a blue and a black one) and two big micro propellers. All these devices were fixed on a beam, which was situated 2 m upstream the wave machine (Fig. 12). The velocity was measured at a height of 2/3 water depth (circa 33 cm above the basin bottom) where an average velocity within the depth profile was assumed. Both ADV's were placed in a distance of 2 m and 3.5 m from the dike toe. For a better knowledge of the velocity distribution in the cross section two micro propellers were installed additionally, within a distance of 1.5 m, besides the ADV's.



Figure 12: Beam upstream the wave machine (on the left side), flow direction from right to left; ADV; Micro propeller (FlowDike 1).

An example of measured current velocity of the ADVs before starting the wave generator for a test with a current of 0.15 m/s is given in Fig. 13. These ADVs have been installed at the middle of the beam in the flow channel. The micro propeller did not give a clear signal.

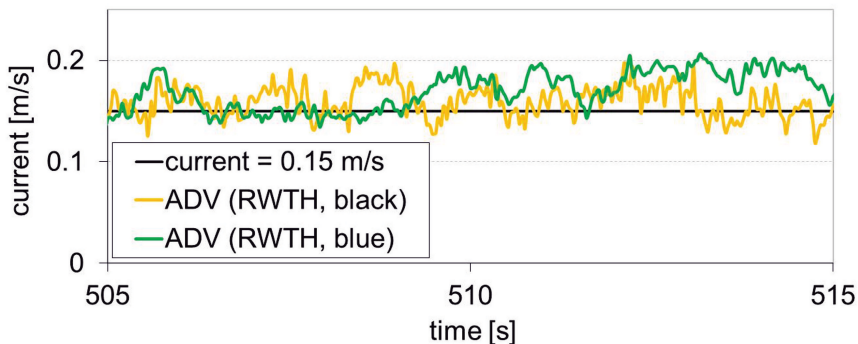


Figure 13: Signal of current meter (test s4\_35 with 15 m/s current).

### 3.2.5 Wave run-up (capacitive gauge, camera, step gauge)

In order to observe and measure wave run-up a 2 m wide and 2.5 m long ply-wood plate was installed as an extension of the dike slope (Fig. 15). Its surface was covered with sand which was fixed by means of shellac to provide a similar surface roughness as of concrete slope.

At the right side of the run-up board an adhesive tape with a black/yellow or black/white pattern was put on as the gauge board (see Fig. 14). This gauge had two different scales in the FlowDike 1 set-up. The original scale with its 0.01 m long sections showed the oblique wave run-up height. The distances at the second scale were multiplied with a factor depending on the dike slope and represented the vertical run-up height.

A capacitive gauge was mounted in the middle of the run-up board. Its capacitor (Fig. 14) was formed by two electrodes – one insulated and one non insulated wire each 3.5 m long. They were mounted on the run-up plate orthogonally to the dike base. One end was installed about 0.25 m above the bed which is equal to 0.25 m below still water level (SWL). The other end was fitted at the highest point of the run-up plate. Thus it is possible to measure both the wave run-up and the run-down. To avoid a water film between the two electrodes after a wave runs down several rubber bands assure a constant distance of about 5 mm between the two wires.

The air or the water between the two wires was the dielectric fluid. Because the permittivity of water is 80 times greater than that of air, the variation of the water level produced a measurable variation of the electrical value of the capacitor. A transducer allowed loading and unloading the capacitor 25 times per second which is equal to a sampling frequency of 25 Hz. Each value of the time constant of the capacitor  $\tau$  would be transmitted to an A/D-converter as a voltage value. The digital signal which came out of the A/D-converter would be transmitted to the data collection unit and put in storage together with the signals of the other measurement equipment.



Figure 14: Capacitive gauge and visual gauge on the run-up board (left: FlowDike 1, right: FlowDike 2).

In addition to the capacitive gauge the wave run-up height was measured by two digital gauges (*step gauges*) each 1.5 m long. They were mounted at the 0.7 m high dike slope within a distance of 2.2 m. It was only possible to measure the wave run-up till the dike crest with these gauges. These devices were not applied during FlowDike 2. There is no analysis available concerning the step gauges yet.

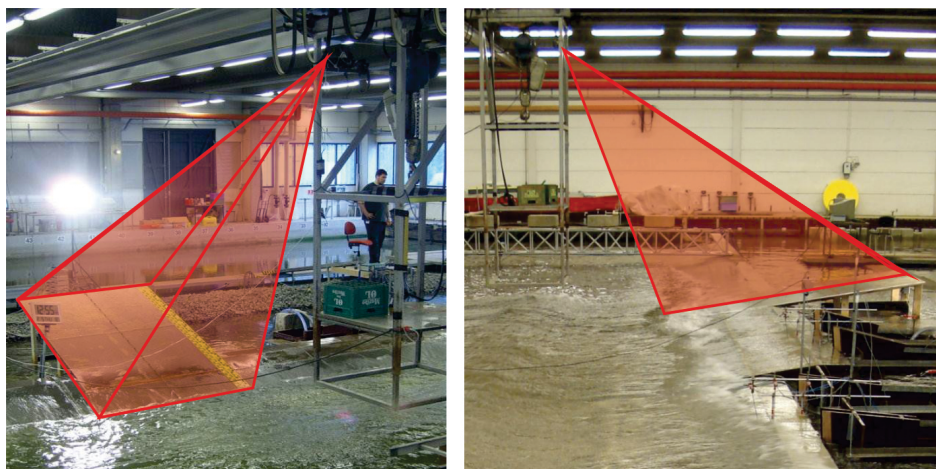


Figure 15: Wave run-up plate and rack with both digital cameras (left: FlowDike 1, right: FlowDike 2).

Two digital video cameras were used to record in parallel the wave run-up (Fig. 16). Both were mounted on a rack about 4 m above the ground (Fig. 15). The rack was fixed at a laboratory crane to make the positioning of the two cameras very easy.

In the FlowDike 1 model set-up a digital camera and SONY camcorder were applied. The digital camera was a compact, professional USB 2.0 camera from VRmagic GmbH which is suitable for industrial purposes. The used model VRmC-3 + PRO contained a 1/3 inch-CMOS-sensor which could record 69 frames per second. The picture resolution of 754 x 482 pixels was adequate for measurement purposes in the model tests presented herein. The camera was suitable for recording very fast motions like wave run-up on slopes. One benefit of this camera was the possibility to transmit the data to the computer directly by the high speed USB 2.0 interface and without any additional frame grabber hardware. The recorded films were AVI-files. These files were automatically analyzed after the end of the model tests.

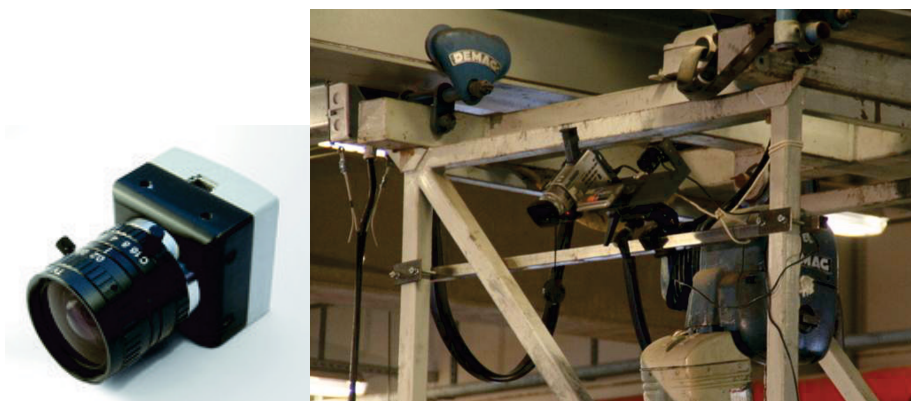


Figure 16: Left: USB-camera, Right: Both cameras mounted on a rack in the FlowDike 1 model set-up.

The SONY Camcorder (Model: *DCR-TRV900E PAL*) had a 3CCD (*Charge Coupled Device*, 1/4 inch). The objective had a focal distance between 4.3 mm and 51.6 mm and a 12 times optical zoom. The camcorder was employed as a redundant system in the event of a USB-camera malfunction. The camcorder used mini cassettes to store its films. Choosing the LP-modus the record time of the mini cassettes could be extended to 90 minutes. Because of test durations between 17 and 34 minutes the cassettes were able to store between 2 and 4 test films. For analysis purposes the films on mini cassettes had to be transformed into AVI-files. This is very time expensive and that is why USB camera was chosen as the main system though the SONY camcorder has a better resolution.

In FlowDike 2 both cameras were replaced by two others with better picture resolution. Since the image-processing algorithm works with grey-level images, one color camera was replaced by a more powerful monochrome camera (1/2" Progressive-scan-CCD sensor (*Charge Coupled Device*, 1/2 inch) JAI CM-140 GE of Stemmer Imaging). Its resolution of 1392 x 1040 pixels with 4.65  $\mu\text{m}$  pixel size allows producing pictures of the run-up plate with a precision of 0.5 mm. The second camera (a color area scan camera) was used for documentation purposes. It had the same features like the monochrome one but the output-files are three times greater (about 2.6 GB/min). The same objectives as in FlowDike 1 were reused.

A benefit of these cameras was their Gigabit Ethernet (C3 series) interface, which allowed placing the laptop in the office room outside the very humid air of the laboratory hall. Laptop and camera were connected with a 30 m cable. In addition the interface allowed a three times higher transfer rate. The MATLAB algorithm was upgraded considering the new output-file format.

To get films with a better contrast the wave run-up board was enlightened by a 2000 W-spotlight which was positioned such as the light met the run-up plate within an angle of 120° to the optical axis of the digital cameras. For the purpose of synchronizing all measurements a digital radio controlled clock with a 0.4 m x 0.4 m display was positioned on the left side of the run-up plate (Fig. 15).

Stored video data had a compacted AVI-format (*Codec VRMM*) with 10 frames per second.

### **3.2.6 Overtopping velocity and layer thickness (micro propeller, wave gauge, pressure sensor)**

To measure the flow processes on the dike crest, the width of the crest was enlarged to 0.3 m in the region where the measurement devices have been installed. Hence the flow processes are comparable with former investigations.

Micro propellers (SCHILTKNECHT) and small wave gauges (0.2 m long) were applied in FlowDike 1 to record flow velocities and flow depths on the crest. A testing section included two small micro propellers combined with two wave gauges between the two overtopping boxes at the seaward and the landward edge of the dike crest (see Fig. 17). An example of measured data is given in Fig. 18. They provide a good basis to distinguish between single overtopping events.

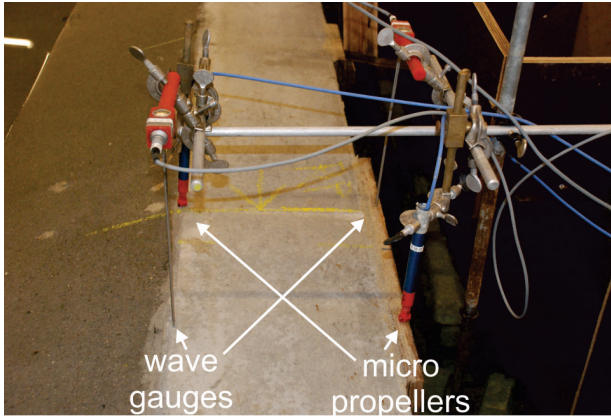


Figure 17: Measurement of velocity and depth of flow on the crest.

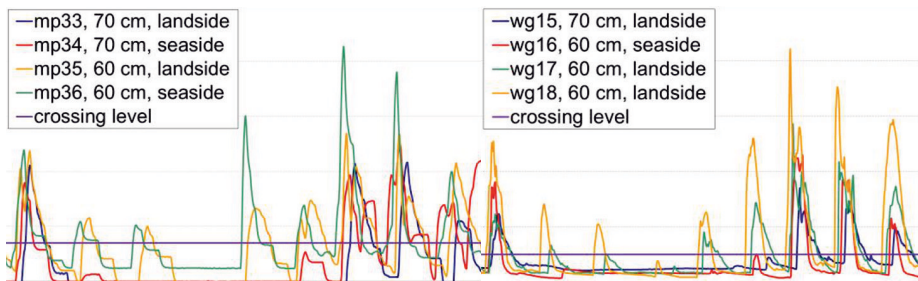


Figure 18: Micro propeller (left) and wave gauge (right) measurement for a sequence (s1\_03\_30\_w5\_00\_00).

Pressure sensors were used to measure flow depth additionally in FlowDike 2. Furthermore all devices were situated 0.03 m from each crest edge, so a distance of 0.24 m was kept between the aligned seaward and landward devices. To investigate the influence of the seaward edge another wave gauge was placed perpendicular onto the slope. The flow depth of the up rushing wave was measured in a horizontal distance of about 0.12 m downstream the crest edge (Fig. 19 and Fig. 20).

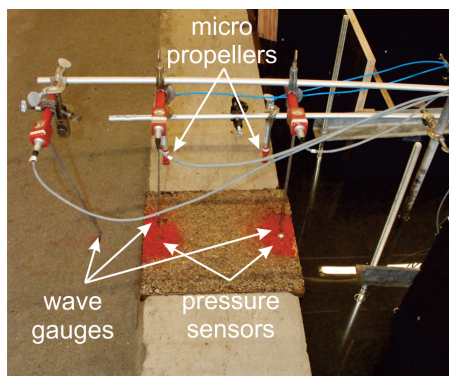


Figure 19: Measurement of pressure, velocity and depth of flow on the crest.



Figure 20: Plywood boxes and drilled holes for pressure sensors.

### 3.2.7 Overtopping water volume (load cell, pump)

Wave overtopping volume was measured by four similar overtopping units – two per crest section. Each overtopping unit consisted of an overtopping channel, an external box, a tank, a load cell and a water level gauge. The tank (0.35 m x 0.75 m x 0.75 m) was mounted on a load cell of 0.10 m height. This load cell was placed on the bottom of the separate watertight external box (0.55 m x 1.02 m x 1.18 m), which was built to avoid uplift of the tanks and load cells, when the shallow water basin was flooded. To avoid entering splash water into the overtopping tank next to the overtopping channel, the wall of the external box next to the dike was extended. A rectangular overtopping channel with a 0.10 m wide cross section led the incoming water into the tank, where its weight was recorded by the load cell over the time. The cross-section of an overtopping unit is sketched in Fig. 21.

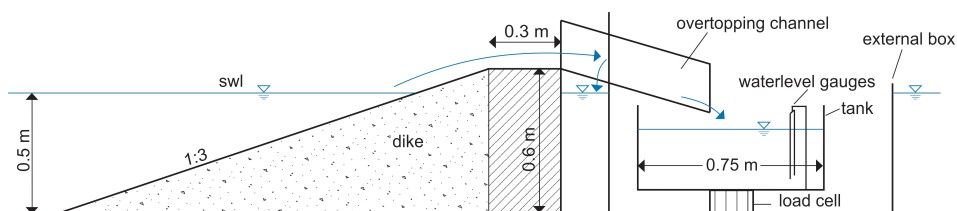


Figure 21: Cross-section of the overtopping unit on the 1:3 sloped dike.

A wave gauge (0.60 m length) was placed in every tank to gain redundant data regarding the water elevation. But wave gauge data could not be used to detect single overtopping events due to the disturbed water level.

The overtopping boxes were not capable to capture the whole overtopped water volume for each test of approximately 30 min. Therefore a pump (standard pump) with a predetermined sufficient flow was placed within each tank. All four pumps were connected with the data acquisition via a switch, so start and end time of pumping could easily be detected. This allowed recalculating the lost amount of water during the pumping time.



Figure 22: Overtopping units with channel and measurement devices for flow depth and flow velocity measurements.

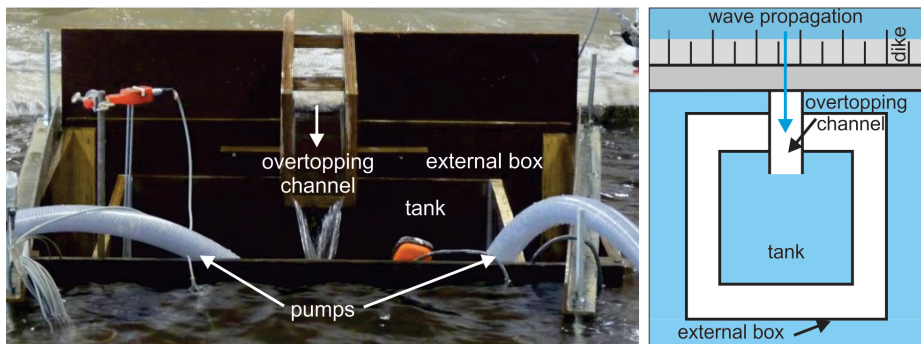


Figure 23: Overtopping unit seen from behind the dike.

### 3.3 Model and scale effects

#### 3.3.1 Model effects

Model effects could be caused by boundaries of the test facility which do not represent natural boundary conditions or by inadequate wave spectra creation. The FlowDike-D tests did not reproduce a specific natural dike. Nevertheless the results can be devolved to natural relations.

Model effects regarding FlowDike-D tests might be caused by

- wave reflection at the model boundaries
- distance between wave generator and dike (basin width)
- width of the run-up board
- inlet of the overtopping channel (shape, geometry)

In order to mitigate wave reflection different devices were installed within the shallow water basin as described in sec. 3.1.1. Due to the relatively short distance between the wave generator and the dike wave reflection influenced the incoming sea state. Therefore wave generation includes an algorithm to absorb reflected waves. It should be mentioned that this algorithm was not operational during FlowDike 2 (1:6 sloped dike) due to

technical problems. In case of very oblique wave attack the up rushing waves might not develop their full run-up height in a few tests because of the limited run-up board width. To ensure low turbulence during the wave overtopping process the edges of the overtopping channel were sharpened after the first test series.

### 3.3.2 Scale effects

The current research project was applied to consider the influence of wind and current on wave run-up and wave overtopping. In a first step the tests can be considered as prototype tests. In a second step the model set-up can be seen as a reduced model of a natural dike. That's why a relatively smooth surface on the dike slope was applied.

To ensure the similarity between the model and the prototype, the geometric similarity, the kinematic similarity and the dynamic similarity have to be considered. The geometric similarity assures the scaling of the design and the wave heights end lengths. The kinematic similarity describes the relation of the time scale for example of the wave period. More difficult is to ensure the dynamic similarity which includes the model laws by Froude, Reynolds, Weber, Thoma and Cauchy. The model law by Cauchy includes the equality of the elasticity and the inertia force. Thoma considers the inertia forces and pressure. Both Thoma and Cauchy are negligible for free surface applications.

The main complexity in scaling the wind tests is the different theory which has to be used for wind and water waves. Wind has to be scaled according to Reynolds, whereas waves are scaled according to the Froude-law. The law of Weber considers the interface between water and air. These three theories cannot be combined. That is why only few investigations considering the influence of wind on wave overtopping by means of physical model tests have been done (GONZÁLEZ-ESCRIVA 2006). Therefore the influence of wind on wave run-up and wave overtopping is analyzed only qualitative in the project FlowDike-D.

Regarding DE ROUCK et al. (2002) the roughness of the dike surface does only influence scaling for porous dikes. Therefore this factor is negligible in this study with a smooth dike.

According to LE MÉHAUTÉ (1976) the influence of the surface tension on scale effects of the incoming wave field is negligible for water depths higher 0.02 m and wave periods higher 0.35 s. Both conditions are achieved in the current project.

## 4 Theory of the influence of current and wind

### 4.1 Wave and current interaction

#### 4.1.1 General

The model tests were performed with and without a longshore current. Since the wave propagation is different in flowing water and in still water, it is required to interpret the following results with respect to the interaction of waves and current (TRELOAR 1986). Two main aspects have to be considered while interpreting the results:

- current induced shoaling: absolute and relative wave parameters
- current induced wave refraction: energy propagation

The wave propagation path can be divided into two parts. The first part reaches from the wave generator to the dike toe. The second part extends from the dike toe to the dike crest.

#### 4.1.2 Current induced shoaling

If a wave propagates on a current, a distinction has to be made between relative and absolute wave parameters and can be described by using the wave celerity. The relative wave celerity is the celerity relative to an observer who moves with the current, while the absolute celerity is defined as the velocity compared to a stationary observer and the ground, respectively.

The wave gauge arrays at the toe of the dike measured the wave field with its absolute parameters. According to HEDGES (1987), TRELOAR (1986) and HOLTHUIJSEN (2007) waves act only with its relative parameters. To determine the relative wave period  $T_{rel,m-1,0}$  from the measured absolute wave period  $T_{abs,m-1,0}$ , the absolute angular frequency  $\omega_{abs}$  has to be equalized to the sum of the relative angular frequency  $\omega_{rel}$  and the corresponding constituent of the current ( $k \cdot v_n$ ) (cf. HOLTHUIJSEN 2007):

$$\omega_{abs} = \omega_{rel} + k_{rel} \cdot v_{\beta} \quad (1)$$

with:  $\omega_{abs}$  absolute angular frequency [rad/s]  
 $\omega_{rel}$  relative angular frequency [rad/s]  
 $k_{rel}$  relative wave number [rad/m]  
 $v_{\beta}$  component of current velocity in the direction of wave propagation [m/s]  
 $d$  flow depth [m]

The absolute angular frequency can be determined using the measured absolute spectral wave period  $T_{abs,m-1,0}$

$$T_{abs,m-1,0} = \frac{m_{-1}}{m_0} \quad (2)$$

with  $m_{-1}$  minus first moment of spectral density [m<sup>2</sup>]  
 $m_0$  zero order moment of spectral density [m<sup>2</sup>/s]

and the following formula:

$$\omega_{abs} = \frac{2\pi}{T_{abs,m-1,0}} \quad (3)$$

The relative angular frequency  $\omega_{rel}$  is also defined as

$$\omega_{rel} = \sqrt{g \cdot k_{rel} \cdot \tanh(k_{rel} \cdot d)} \quad (4)$$

By using eq. (1) and (4), the relative wave number  $k_{rel}$  can be determined iteratively by using the measured absolute wave period  $T_{abs,m-1,0}$  (2), the known flow depth  $d$  and the current velocity in the direction of wave propagation  $v_{\beta}$ , which is defined as:

$$v_{\beta} = v_x \cdot \sin \beta \quad (5)$$

with the current velocity parallel to the dike  $v_x$  and the angle of wave attack  $\beta$  relative to a line perpendicular to the shore.

The relative angular frequency  $\omega_{rel}$  can be calculated using equation (4). Assuming deep water conditions the relative wave period  $T_{rel,m-1,0}$  and the relative wave length  $L_{rel,m-1,0}$  are determinable using the following formulae:

$$T_{rel,m-1,0} = \frac{2\pi}{\omega_{rel}} \tag{6}$$

$$L_{abs,m-1,0} = g \cdot \left( \frac{T_{abs,m-1,0}}{2\pi} \right)^2 \tag{7}$$

As shown in Fig. 24, the relative wave period  $T_{rel,m-1,0}$  decreases compared to the absolute wave period if a wave propagates against a current and increases if a wave propagates with a current (cf. formula (1) and (6)).

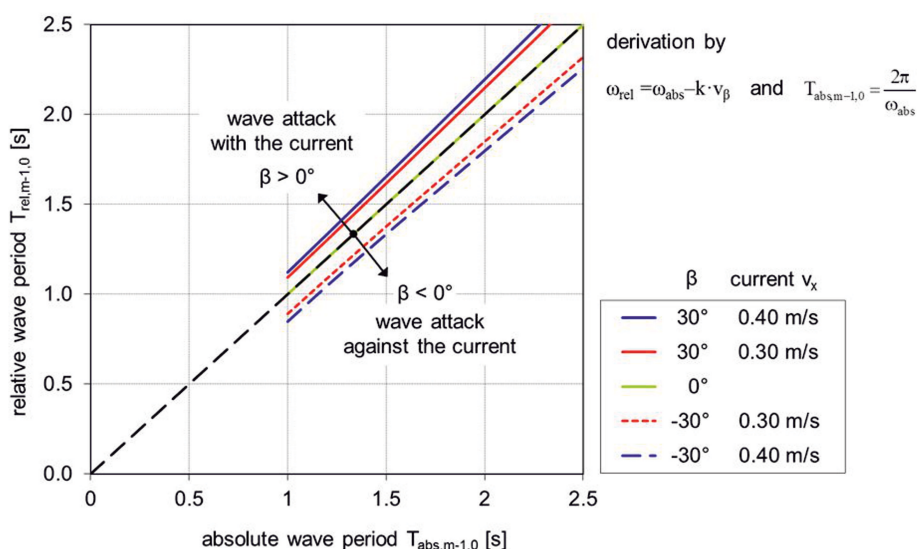


Figure 24: Absolute wave period  $T_{abs,m-1,0}$  against relative wave period  $T_{rel,m-1,0}$ , water depth  $d = 0.5$  m.

### 4.1.3 Current induced wave refraction

Fig. 25 shows schematically the combination of the two vectors for the current and the wave direction for negative (left) and positive (right) angles of wave attack. The dashed arrow describes the relative direction of the wave attack generated by the wave generator and the corresponding angle  $\beta$ . The dotted arrow indicates the direction of the longshore current. According to HOLTHUIJSEN (2007) the current does not change the angle of wave attack but its energy direction by the combination of the two vectors current velocity  $v_x$  and relative group velocity  $c_{g,rel}$  marked with the corresponding arrow. As shown

in Fig. 25, negative angles of wave attack lead to smaller absolute values of the angle of wave energy  $\beta_e$  whereas positive angles of wave attack lead to higher angles of wave energy  $\beta_e$  than the angle of wave attack  $\beta$ .

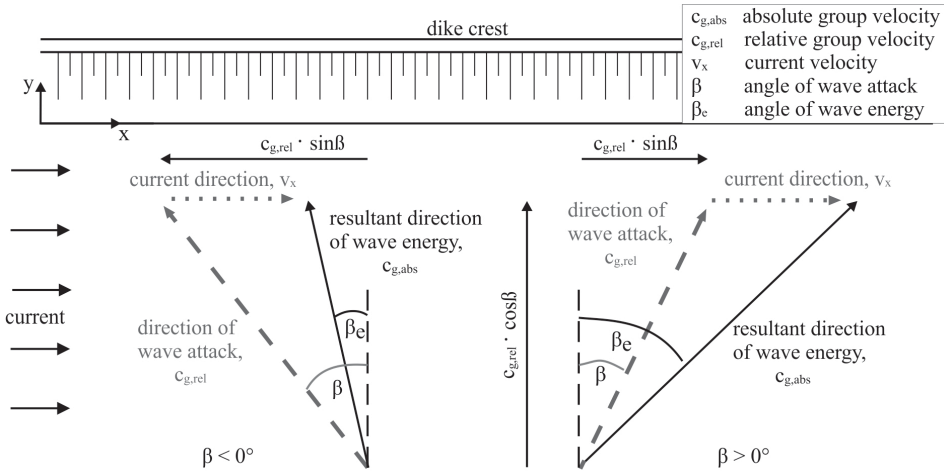


Figure 25: Interaction between wave direction and current.

The angle of wave energy  $\beta_e$  is determined by the relative group velocity  $c_{g,rel}$ , the angle of wave attack  $\beta$  and the current velocity  $v_x$  by the trigonometrical function (cf. Fig. 24):

$$\tan \beta_e = \frac{c_{g,rel} \cdot \sin \beta + v_x}{c_{g,rel} \cdot \cos \beta} \quad (8)$$

Herein the relative group velocity  $c_{g,rel}$  is determined by the following formula:

$$c_{g,rel} = \frac{\partial \omega}{\partial k} = \frac{\partial (\sqrt{g \cdot k \cdot \tanh(k \cdot d)})}{\partial k} \quad (9)$$

which leads to:

$$c_{g,rel} = 0.5 \cdot \frac{\omega_{rel}}{k} \left( 1 + \frac{2 \cdot k \cdot d}{\sinh(2 \cdot k \cdot d)} \right) \quad (10)$$

Fig. 26 shows how a current influences the angle of wave energy. On the abscissa the current is plotted. The ordinate shows the angle of wave attack (dashed line) and the angle of wave energy (continuous line). The graphs show different angles of wave attack with and against the current. For all angles of wave attack the angle of wave energy increases significantly depending on the current velocity. For currents higher than 4 m/s the changes in the angle of wave attack are lower and converge against 90° which is the direction of the current. For negative angles of wave attack (against the current, green and blue graph) the changing of the angle of wave energy is more significant than for the positive angles of wave attack (with the current, orange graph).

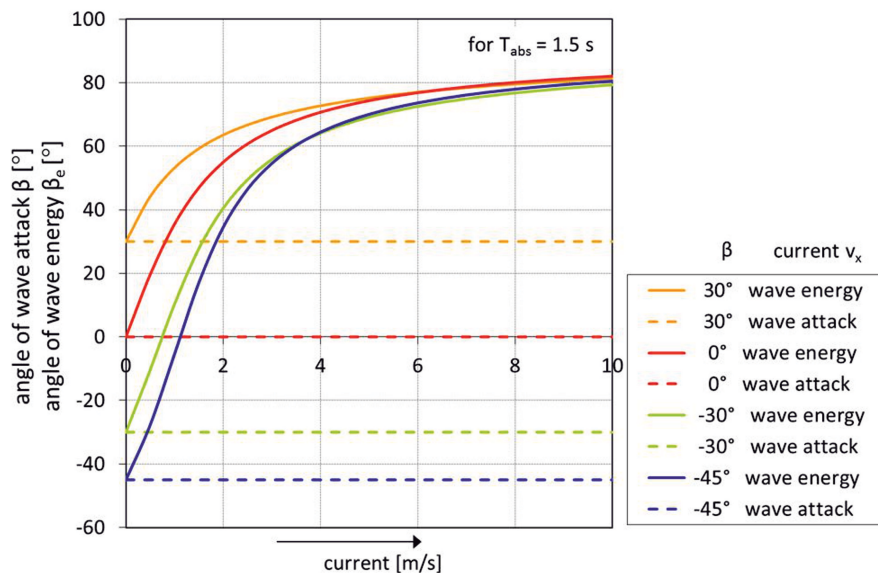


Figure 26: Angle of wave energy  $\beta_e$  divided by angle of wave attack  $\beta$  against the current for different angles of wave attack, water depth  $d = 0.5$  m,  $T_{abs} = 1.5$  s.

## 4.2 Wave run-up and wave overtopping influenced by current

As shown before, wave parameters are influenced by a current because of current induced refraction and current induced shoaling. ARTHUR (1950) shows, that the relative wave parameters are acting on a coastal structure, whereas VAN DER MEER (2010) applies the direction of the wave energy combining with the absolute wave parameters to determine the wave overtopping rate influenced by a current.

During a subproject of the OPTICREST-project (JENSEN and FRIGAARD 2000) the influence of a current parallel to the dike line on wave run-up was investigated by physical model tests. The current was varied between 0.5 m/s and 1.0 m/s and compared to tests without current. Hence an increasing wave run-up height up to 20 % was observed.

## 4.3 Influence of wind on waves

In the current research project the waves are induced by a wave generator. But the mechanically induced wind might change the wave parameters at the dike toe and influences the breaking process as well. GALLOWAY (1989) carried out wave observations at coasts to determine the influence of the wind direction on breaking waves. Wind in the direction of wave propagations leads to previous breaking of the waves which become surging waves. DE WAAL et al. (1996) included this knowledge in a formula for wave overtopping by reducing the breaker flow depth  $d_b$ . He determined the wind influenced flow depth  $d_{b(wind)}$  at the breaker point to:

$$\frac{d_{b(wind)}}{d_b} = \left( 1 + p \cdot \frac{u_{10}}{\sqrt{g \cdot d_b}} \right)^2 \quad (11)$$

with  $d_b$  flow depth at breaker point without wind [m]  
 $u_{10}$  wind velocity 10 m above still water level [m/s]

$$p = \frac{v_{crest,wind} - v_{crest,no\ wind}}{u_{10}} \approx 0.03 \quad (12)$$

with  $v_{crest,wind}$  flow velocity on the dike crest, wind  $u_{10} \neq 0$  m/s [m/s]  
 $v_{crest,no\ wind}$  flow velocity on the dike crest, wind  $u_{10} = 0$  m/s [m/s]

#### 4.4 Wave run-up and wave overtopping influenced by wind

The influence of onshore wind on wave run-up is a much younger research topic than current-wave-interaction. One reason might be that it is more complicated to transfer the results of physical model tests into prototype conditions because the scaling laws of Froude (wave propagation, wave run-up), Reynolds (shear forces) and Weber (interface between water and air) do not correspond and cannot be fulfilled in one model set-up. Nevertheless it is commonly assumed that onshore wind has an increasing effect on wave run-up. Single reasons for that are that onshore wind pushes the water up the slope and the velocity in the wave run-up tongue increases. In addition the effect of downwash on the subsequent wave might be reduced. Other changes can be distinguished in the breaking process. Wind induces an earlier breaking of the waves and a change of the breaking type as well as of the breaking point on the slope. These effects have been summarized but could only partly be quantified by GONZÁLES-ECRIVÁ (2006).

Different hydraulic model tests were conducted to investigate the influence of wind on wave run-up (e. g. WARD et al. 1996, MEDINA 1998). The chosen facilities were flumes and monochromatic waves were studied. Wind speed created by wind machines ranged between 6.5 m/s and 16 m/s. Whereas WARD et al. (1996) studied single slope structures, the investigation of MEDINA (1998) considered complex breakwater cross sections and the wave run-up was observed e. g. at a vertical wall on the crest. In general it was found that lower wind speeds ( $w < 6$  m/s) have no significant effect on wave run-up whereas higher wind speeds increase the wave run-up height substantially. This effect can be observed on smooth as well as on rough slope surfaces. In the case of flatter slopes the increasing effect is less. WARD et al. (1996) stated a linear increase of the equivalent wave run-up height (maximum wave run-up adjusted for the increase in still water level due to onshore wind) with the incident wave height for wind speed  $> 12$  m/s. But if the wind induces wave breaking before the waves reach the test structure the wave run-up decreases with increasing incident wave height.

The OPTICREST-project was focused on storm induced wave run-up and collected prototype measurement data as well as model test results (DE ROUCK et al. 2001). Two prototype locations, the Zeebrugge Breakwater (Belgium) and the Petten Sea-Defense (Netherlands), were investigated. While the first structure is a rubble mound breakwater the measured wave run-up height is strongly influenced by the permeability and the roughness of the slope surface. The second structure is a dike with a smooth

impermeable surface but a berm and a long shallow foreshore. Mainly the foreshore has a significant influence on the measured wave run-up height. Most of the model tests did not include a wind generation. Also the conformity between physical model and prototype was ensured by applying the wave spectra measured in the prototype. Altogether these measurement results are not appropriate for comparison with the FlowDike model tests.

GONZÁLES-ECRIVÁ (2006) found that wind increases the energy of the wave spectrum slightly but no differences in the spectral width could be distinguished.

Especially for small overtopping rates and vertical structures the effect of wind might be significant (DE WAAL et al. 1996). The influence of wind can be neglected for high overtopping rates and/or low wind velocities (WARD et al. 1996) but information on wind influence on wave overtopping is still scarce.

The main problem to consider wind experimentally and to quantify its effect is the inaccurate scaling of wind in small scale model tests. YAMASHIRO et al. (2006) recommend to scale the prototype wind by a factor 1/3 but the experiments are restricted to a model scale of 1/45.

## **5 Analysis of wave field and breaking processes**

### **5.1 General**

To analyze the wave evolution in front of the dike, the results from reflection and zero-down-crossing analysis were evaluated. The reflection analysis was done in frequency domain, the zero-down-crossing analysis in time domain.

### **5.2 Verification of measurements**

#### **5.2.1 General**

The measurements of the wave field had to be verified. Therefore the signals of the wave gauges recorded over the first seconds of the reference test were compared. Afterwards the zero-down-crossing analysis is described to see the distribution of the input signal of each wave gauge array. This signal should be Rayleigh distributed (HOLTHUIJSEN 2007). To verify the correctness of the reflection analysis the spectral moments of the measured, reflected and incident waves will be compared among each other. On the basis of the reflection analysis the wave parameters of the incident waves, used for the analysis on wave run-up and wave overtopping, will be determined. Additionally the wave breaking will be analyzed while comparing the reflection coefficient and the surf similarity parameter.

#### **5.2.2 Measured wave heights**

As a result of the zero-down-crossing analysis of the measured wave heights  $H$  in time domain, Fig. 27 depicts the Rayleigh distribution of wave heights exemplarily for the wave gauge array at the toe of 0.7 m high and 1:6 sloped dike. The Rayleigh distribution is

common for the analysis of JONSWAP spectra in deep water. The abscissa is fitted to a Rayleigh scale by means of the relation:

$$x' = \sqrt{-\ln\left(1 - \frac{100-x}{100}\right)} \tag{13}$$

with  $x$  probability of exceedance [%]  
 $x'$  probability of exceedance – Rayleigh distributed [%]

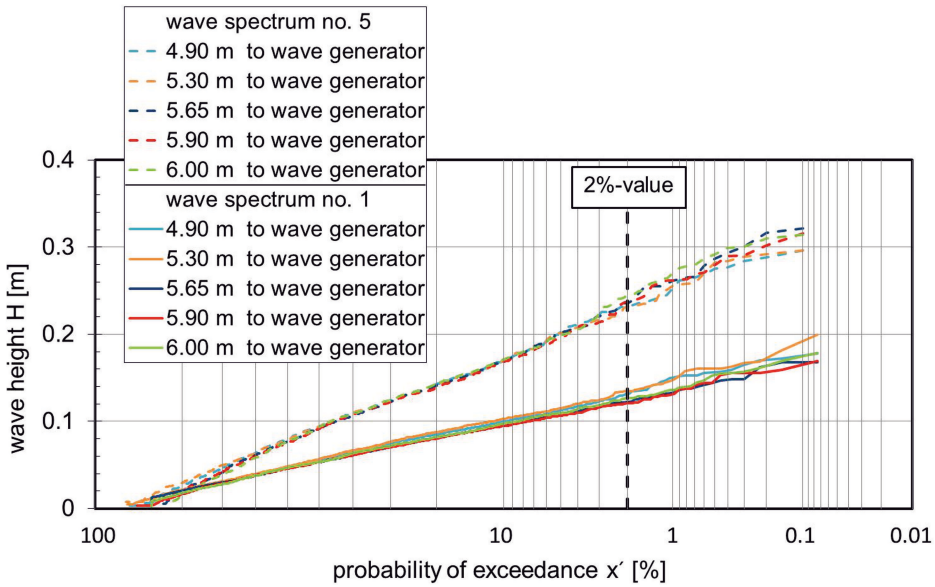


Figure 27: Linear distribution of wave height H over a Rayleigh scale for a Jonswap spectrum exemplarily for the wave gauges at the toe of the 0.7 m dike on the 1:6 sloped dike (wave no. 1 and wave no. 5).

The Rayleigh distributed x-values are the reason why a linear trend was found. The similarity of their shape indicates the homogeneous arrangement for both wave gauge arrays.

The wave height exceeded by 2 % of the waves  $H_{2\%}$  in [m] is a dimension for the homogeneity of the wave field as well as the correct measuring of the wave gauges. Fig. 28 and Fig. 29 show the standard deviation of the wave heights  $H_{2\%}$  of each wave gauge array for different tests (w1 to w6). The standard deviations of  $H_{2\%}$  of the tests on the 1:6 sloped dike are mainly smaller than 0.01 m. The comparative high standard deviation for the wave spectra 5 (steepest analyzed wave in this project, 1:3 sloped dike) and wave spectra 6 (1:6 sloped dike, 15° wave attack) can be traced back to prematurely breaking waves caused by superposition of incident and reflected wave. This has to be considered while interpreting the results on wave run-up and wave overtopping.

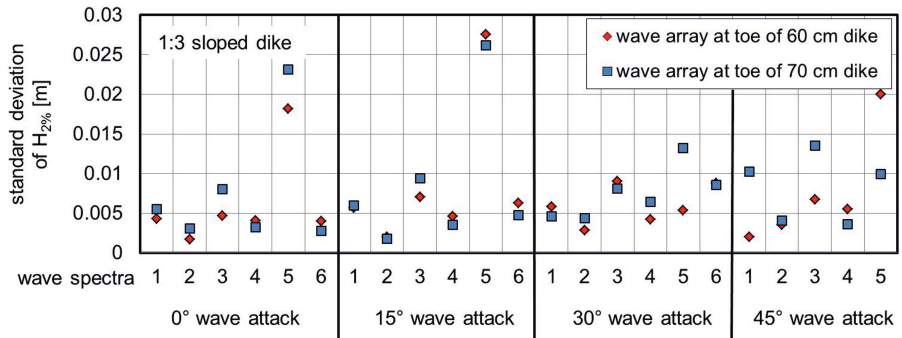


Figure 28: Standard deviation of  $H_{2\%}$ -values; 1:3 sloped dike.

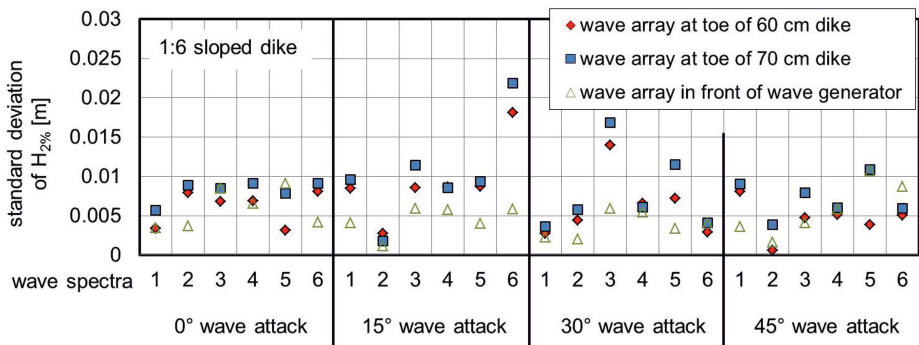


Figure 29: Standard deviation of  $H_{2\%}$ -values; 1:6 sloped dike.

### 5.2.3 Reflection analysis – frequency domain

From the reflection analysis, which is performed in frequency domain, the plotted distribution of energy density (reference tests, wave no. 1 and 5, toe at the 0.6 m high dike) in Fig. 30 corresponds to the theoretical assumption for a JONSWAP spectrum as a single peaked spectrum.

Under consideration of wave reflection one value  $H_{m0}$  for each wave gauge array was obtained. Fig. 31 gives the significant wave heights  $H_{m0}$  of the incident wave of the reference tests from the reflection analysis. The wave gauge arrays at the toe of the two dike heights give quite similar significant wave heights  $H_{m0}$  for each test phase (1:3 and 1:6 sloped dike). The right graph for the 1:6 sloped dike includes the wave heights in front of the wave generator. For the wave number 6 the wave height in front of the wave generator differs slightly from the wave heights at the toe of the dike. The maximum deviation of 0.01 m appears for wave spectrum number 5 ( $H_s = 0.15$  m).

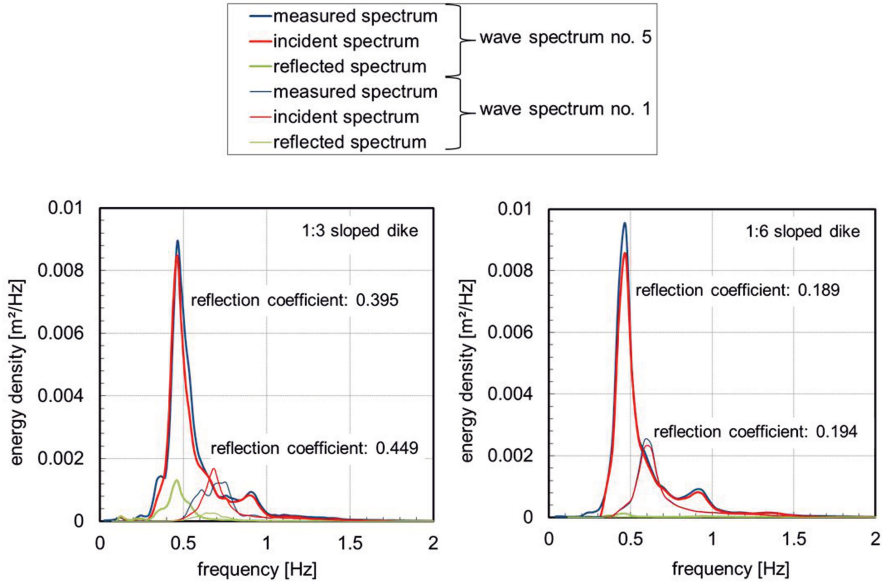


Figure 30: Energy density spectrum in front of 0.6 m crest of the 1:3 sloped dike (left) and 1:6 sloped dike (right).

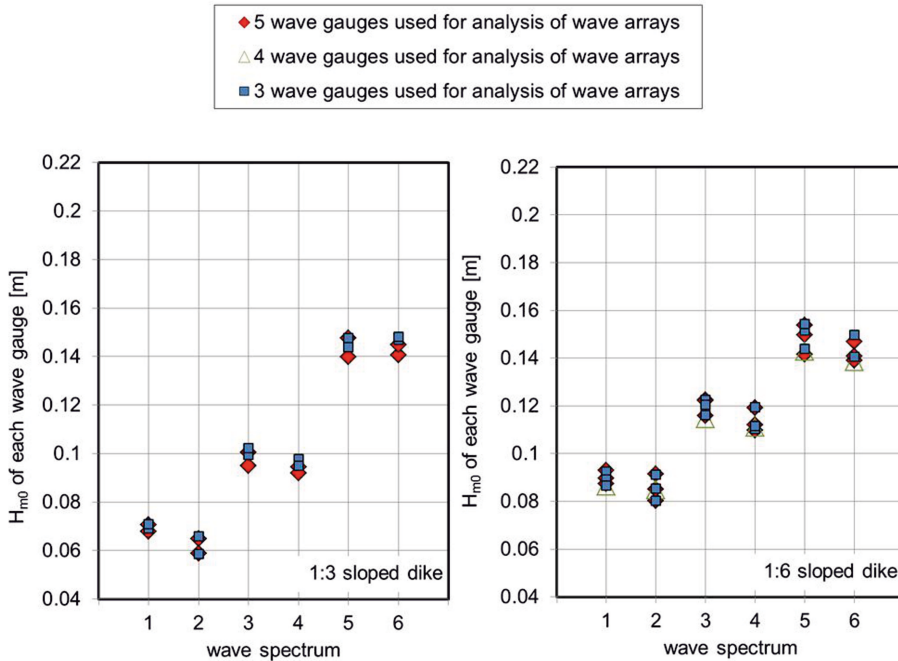


Figure 31: Significant incident wave height  $H_{m0}$  for the reference model tests calculated for each wave gauge array and the six wave spectra.

The spectral wave heights  $H_{m0}$  are determined for every test at the toe of the 0.6 m high dike and at the toe of the 0.7 m high dike. These two wave heights are plotted against each other in Fig. 32. The black graph demonstrates equal x and y values. The best fit lines of the wave heights on the 1:3 and 1:6 sloped dike correspond well with that graph. For both tests phases (1:3 and 1:6 sloped dike) the coefficient of determination of the two best-fit-lines is equal or higher than 0.90. Therefore both wave heights can be used for the following analyses on wave run-up and wave overtopping.

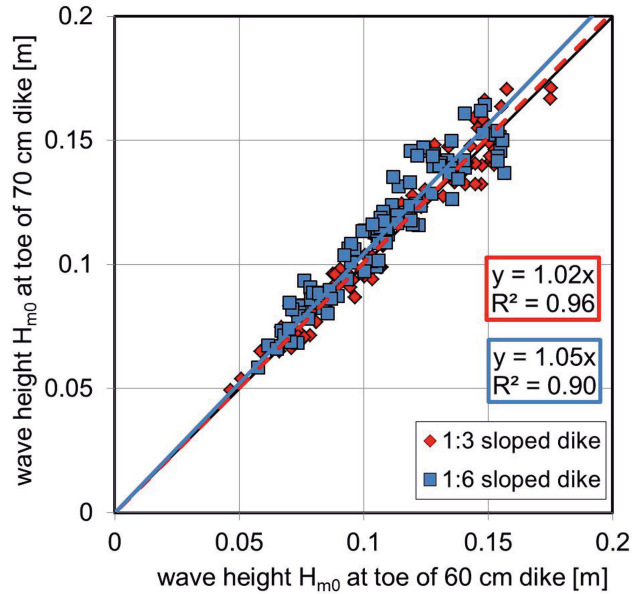


Figure 32: Spectral wave heights  $H_{m0}$  in front of 0.6 m high dike against wave heights  $H_{m0}$  in front of 0.7 m high dike; five wave gauges analyzed.

The zeroth moment of the average spectrum, which is equal to the measured spectrum, the zeroth moment of the incident spectrum and of the reflected spectrum has been determined for every test. In Fig. 33 the zeroth moment of the average wave spectrum is plotted against the sum of the incident and reflected spectrum. It should be:

$$m_{0,average} = m_{0,incident} + m_{0,reflected} \tag{14}$$

Fig. 33 shows the results of the reflection analysis. In the left graph the data points of the reference test are filled with a color and correspond well with the line of perfect equality. The data points in the right graph show the results for all tests without current and wind but with oblique wave attack. Therefore, small deviations in comparison to the line of perfect equality are noticeable.

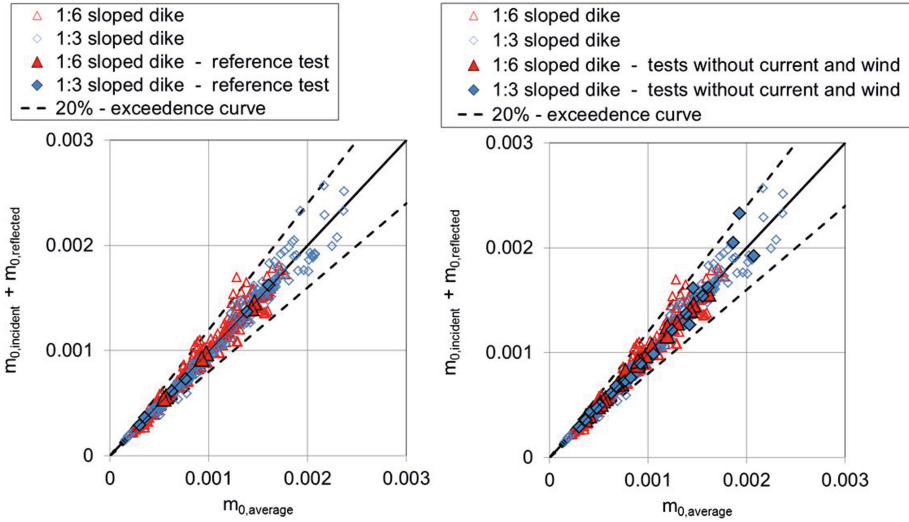


Figure 33:  $m_{0,average}$  as a function of the sum of  $m_{0,incident}$  and  $m_{0,reflected}$ , analysis with 5 wave gauges.

Many parameters, like the dimensionless run-up height and the dimensionless overtopping rate, are calculated using the spectral wave period  $T_{m-1,0}$  which is defined as

$$T_{m-1,0} = \frac{m_{-1}}{m_0} \tag{15}$$

with  $m_{-1}$  minus first moment of spectral density [ $m^2$ ]  
 $m_0$  zero order moment of spectral density [ $m^2/s$ ]

As a simplification for the spectral moment  $T_{m-1,0}$  is often used:

$$T_{m-1,0} = \frac{T_p}{1.1} \tag{16}$$

with  $T_p$  peak period [s]

Fig. 34 shows the calculated spectral wave period  $T_{m-1,0} = m_{-1} / m_0$  against the peak period  $T_p$ . The green graph shows the approximated function  $T_{m-1,0} = T_p / 1.1$ . The data points agree well with the approximated function. For further analyses the exact value of the calculated spectral period  $T_{m-1,0} = m_{-1} / m_0$  will be used.

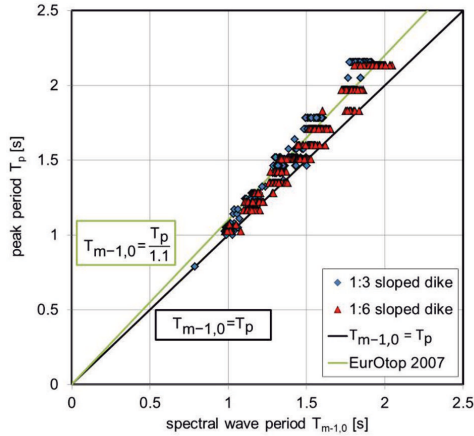


Figure 34: Spectral wave period  $T_{m-1,0}$  against peak period  $T_p$ .

### 5.3 Wave breaking

In Fig. 35 the surf similarity parameter  $\xi_{m-1,0}$  is plotted against the reflection coefficients  $K_R$  for the reference tests on the 1:3 and 1:6 sloped dike. The data points filled with color are the data points of the investigations on the 1:3 sloped dike. The reflection coefficients for the 1:6 sloped dike are lower because of less reflection. The reflection coefficients  $K_R$  of the FlowDike 1 and FlowDike 2 tests are slightly higher than given by BATIJES (1974) with:

$$K_R = 0.1 \cdot \xi^2 \tag{17}$$

The surf similarity parameter was determined using equation (18). The reflection coefficient is given by equation (19). Thereby no distinction was made between perpendicular and oblique wave attack.

$$\xi_{m-1,0} = \frac{\tan \alpha}{\sqrt{s_{m-1,0}}} = \frac{\tan \alpha}{\sqrt{\frac{H_{m0}}{L_{m-1,0}}}} \tag{18}$$

$$K_R = \sqrt{\frac{m_{0,reflected}}{m_{0,incident}}} \tag{19}$$

with  $m_{0,reflected}$  Energy density of the reflected wave spectrum [ $\text{m}^2/\text{s}$ ]  
 $m_{0,incident}$  Energy density of the incident wave spectrum [ $\text{m}^2/\text{s}$ ]

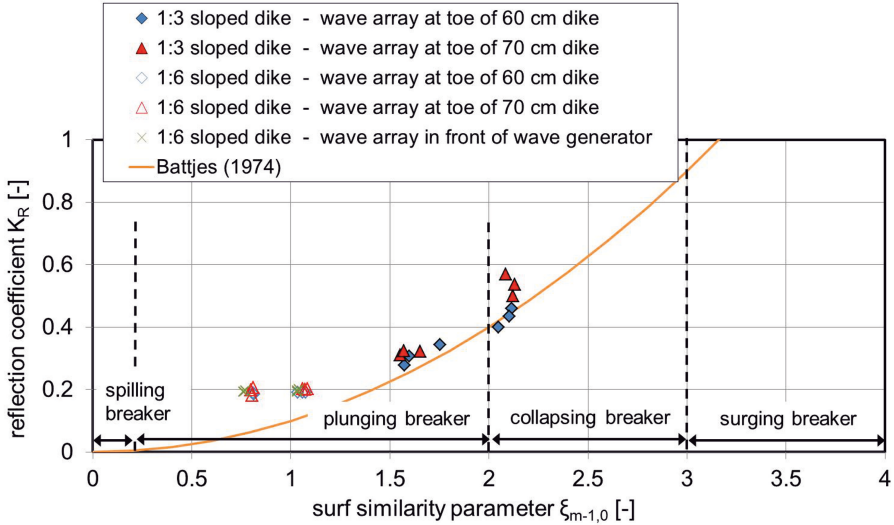


Figure 35: Surf similarity parameter  $\xi_{m-1,0}$  against reflection coefficient  $K_R$  for reference tests.

Fig. 36 shows the surf similarity parameter as a function of the reflection coefficient for all tests without current and wind but considering different angles of wave attack. The reflection coefficients  $K_R$  on the 1:6 sloped dike ( $\xi_{m-1,0} > 1.3$ ) correspond well with the reflection coefficients of the reference test. The reflection coefficients  $K_R$  on the 1:3 sloped dike ( $\xi_{m-1,0} > 1.3$ ) are higher than the values from the reference test.

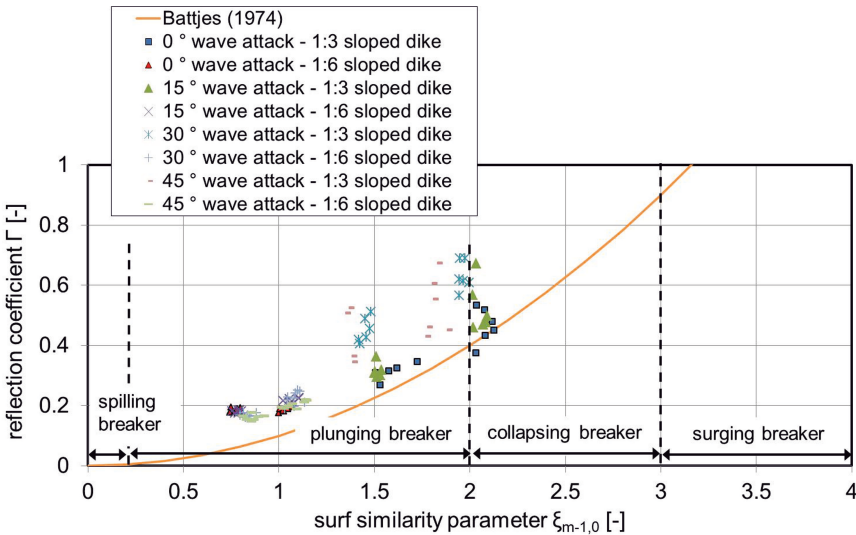


Figure 36: Surf similarity parameter  $\xi_{m-1,0}$  against reflection coefficient  $K_R$  for tests without current and wind, oblique wave attack.

In Fig. 37 the surf similarity parameters  $\xi_{m-1,0}$  are plotted against the reflection coefficients  $K_R$  for all tests. The data points filled with a color are the data points of the

investigations on the 1:3 sloped dike. The reflection coefficients cover a range between 0.26 and 0.71. The reflection coefficients for the 1:6 sloped dike are lower because of less reflection and their values lie between 0.16 and 0.35.

The waves on the 1:3 sloped dike can mainly be classified as plunging breakers. Some tests have to be related to collapsing breakers. The tests on the 1:6 sloped dike contain only plunging breakers.

For the analysis of wave overtopping on the 1:3 sloped dike, it has to be distinguished between breaking and non-breaking waves. On the 1:6 sloped dike only breaking waves are considered. The breaker coefficient was determined using equation (18). The surf similarity parameter is given below (cf. (19)).

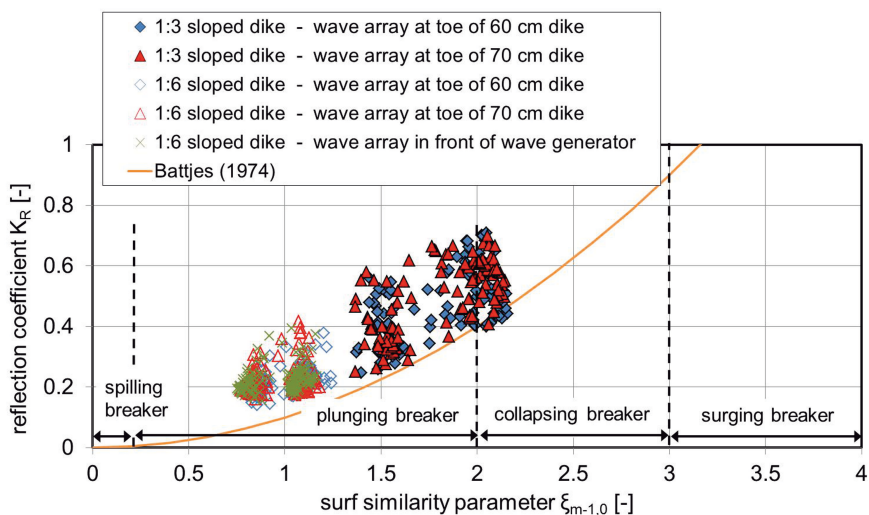


Figure 37: Surf similarity parameter  $\xi_{m-1,0}$  against reflection coefficient  $K_R$  of all tests.

## 6 Analysis of wave run-up and wave overtopping

### 6.1 Remarks

This section describes the measured wave run-up and wave overtopping analysis and how these flow processes are influenced by wind, current and oblique wave attack. The studied data set includes different combinations of only two or all influencing parameters, but can be subdivided in four main sub sets:

- perpendicular wave attack – as reference test
- oblique wave attack
- current influence on wave attack
- wind influence on wave attack

The basic set for perpendicular wave attack and the sub set for oblique wave attack are used for a first comparison of the tests to the currently applied formulae and former investigations (e. g. EUROTOP-MANUAL 2007, OUMERACI et al. 2002). This is done first to

validate the applied evaluation method. In addition the newly introduced variables, such as current and wind, are analyzed and compared to the basic tests.

The considered parameters are defined as following:

- wind velocity  $u$ :                    5 m/s  10 m/s  (1:3 sloped dike)  
    4 m/s  8 m/s    (1:6 sloped dike)
- current velocity  $v$ :                0.15 m/s  0.3 m/s  0.4 m/s (only 1:6 sloped dike)
- angle of wave attack  $\beta$ :        -45° -30° -15°  0° +15° +30°

Positive angles of wave attack describe a wave propagation with the current and negative angles of wave attack describe a wave propagation against the current.

The main objectives of measurement analysis are to estimate the influence of each parameter considered (direction of wave attack, current, wind) on the wave run-up height and to determine correction factors to the commonly used empirical formulae discussed in sec. 4.4.

## 6.2 Analysis on wave run-up

### 6.2.1 Comparison between capacitive gauge and video

Video analysis was processed regarding 10 stripes each 1/10 of the run-up board width. However data analysis does not include stripe 1 and stripe 10 because the measured values here are influenced by laterally flow processes as mentioned before. As brought up previously several regions were excluded from video analysis due to disturbing light reflection. This is the cause that for many videos of the FlowDike 1 test series (1:3 sloped dike) no values could be detected for stripe 4 and 5.

Fig. 38 shows the run-up height depending on time obtained by both measurement facilities – the capacitive gauge and video camera (model test 451, s4\_01a\_00\_w1\_00\_00). Data measured by video camera are represented by the two middle stripes (stripe 5 and stripe 6). Obviously there is a good agreement regarding the run-up process and the maximum values. This indicates that both measurement techniques are suitable to determine wave run-up.

A significant difference has to be acknowledged for the wave run-down. The capacitive gauge always detected a slower run-down process because the down-rushing water was decelerated by the rubber bands which assured a constant distance between the two wires and of course due to surface tension. On the contrary the detection of run-up tongue by video analysis could not identify the very thin and almost transparent water film during the run-down process because there was no significant change in pixel brightness here. Then the next up rushing wave was identified and its run-up tongue recognized.

The data plot displays also why it was necessary to choose a crossing level higher than zero. The measured data shows that the run-down of the wave tongue could not be sufficiently measured by capacitive gauge. After the wave tongue reaches its maximum height the water level decreases very slowly and a following smaller wave might be missed. Furthermore the measurement data for the time dependent run-up often did not reach the still water level between two up-rushing waves. With a crossing level equal to zero many wave run-up events would be missed.

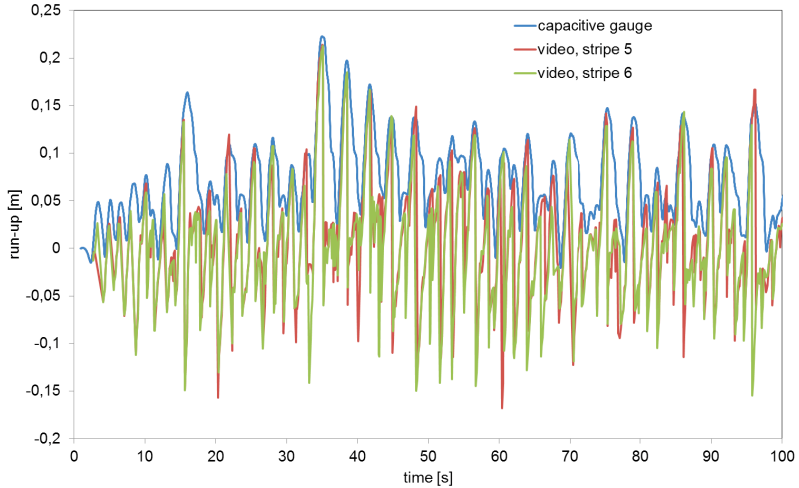


Figure 38: Wave run-up depending on time measured by capacitive gauge and video (stripe 5 and 6), model test s4\_01a\_00\_w1\_00\_00.

A comparison between calculated values of  $R_{u2\%}$  for both measurement devices for all model tests is presented in Fig. 39. The values on basis of capacitive gauge measurement are almost all lower than the maximum values obtained by video analysis considering the whole run-up board width. The best fit line shows average differences of about 9 %.

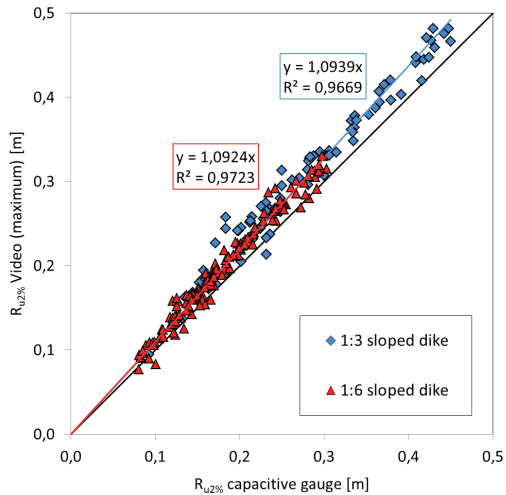


Figure 39: Wave run-up height  $R_{u2\%}$  for all model tests: comparison between maximum values obtained by video analysis considering the whole run-up board width and measured by capacitive gauge.

This is because of the different width of the capacitive gauge and the run-up board. The capacitive gauge was situated in the middle of the run-up plate and could only measure the wave run-up there although the run-up height differed across the plate width. Results

from video analysis represent here the maximum run-up height independent of its location across the run-up plate width.

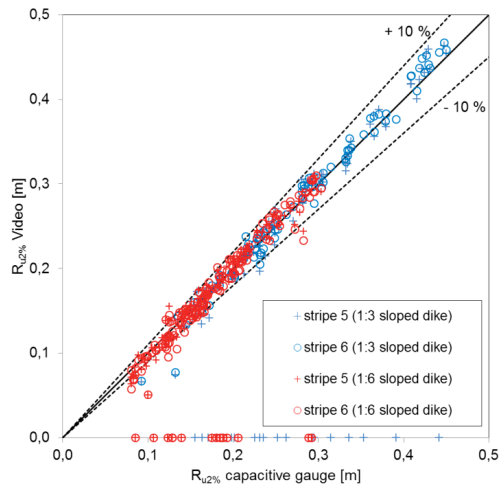


Figure 40: Comparison between wave run-up height  $R_{u2\%}$  measured by capacitive gauge and extracted from video films for two smaller stripes around the capacitive gauge.

A comparison between the result of the capacitive gauge and the two stripes around it (stripe 5 and stripe 6) should show no significant difference. This is proved in Fig. 40. The diagram shows smaller relative differences for higher values of  $R_{u2\%}$  which might indicate measurement errors.

The following discussion includes all  $R_{u2\%}$ -values obtained by video analysis (1:3 sloped dike: 6 stripes, 1:6 sloped dike: 8 stripes) and measured by the capacitive gauge.

### 6.2.2 Reference tests

To validate the overall model set-up, results from reference tests (1:3 dike as well as 1:6 dike) are compared to data of former investigations. Fig. 41 shows calculated values of relative wave run-up height  $R_{u2\%}/H_{m0}$  versus surf similarity parameter  $\xi_{m-1,0}$ . Two functions of former investigations have been added (cf. EUROTOP-MANUAL 2007). Values for  $H_{m0}$  were obtained analyzing measurement results of the wave gauge array which was situated closer to the run-up board. All measured values for wave run-up height are plotted within the graph. This gives an impression of the general variance within the model results regarding wave run-up.

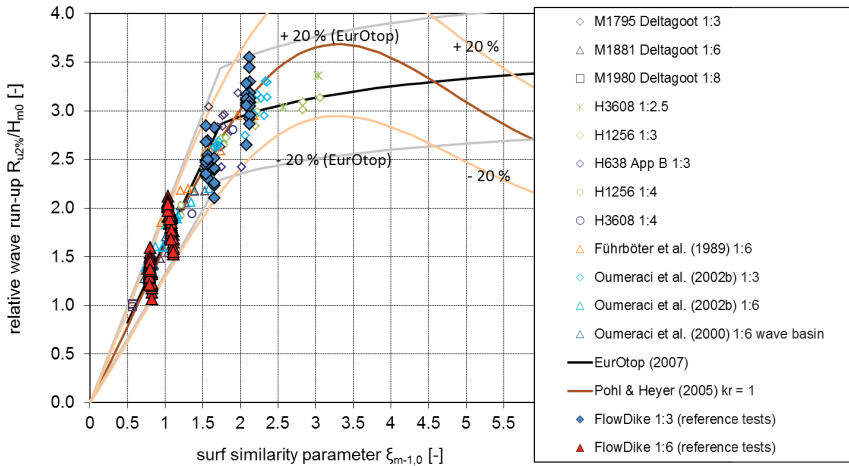


Figure 41: Relative wave run-up height  $R_{u2\%}/H_{m0}$  versus surf similarity parameter  $\xi_{m-1,0}$  – comparison between reference tests and former investigations (EUROTOP-MANUAL 2007).

The comparison shows a good agreement to former investigations and indicates that the general hydraulic model set-up was appropriate for the investigation planned. Surf similarity parameter  $\xi_{m-1,0}$  is between 1.5 and 2.1 for the FlowDike 1 model tests (1:3 sloped dike) and between 0.8 and 1.1 for the FlowDike 2 model tests (1:6 sloped dike).

### 6.2.3 Influence of angle of wave attack

Fig. 42 shows calculated values of relative wave run-up height  $R_{u2\%}/H_{m0}$  versus surf similarity parameter  $\xi_{m-1,0}$  for all model tests with oblique wave attack (tests without current and wind). The two functions by EUROTOP-MANUAL (2007) and by HEYER and POHL (2005) have been added to the figure. Results of the reference model tests (without current, without wind, perpendicular wave attack) were added for comparison reasons.

It is obvious that an oblique wave attack leads to smaller relative run-up heights. If the angle of wave attack is higher the resultant relative run-up height  $R_{u2\%}$  is smaller. This tendency is significant for angles of wave attack  $\beta > 40^\circ$  which is indicated by an arrow in the figure. For smaller angles of wave attack the influence is not obvious.

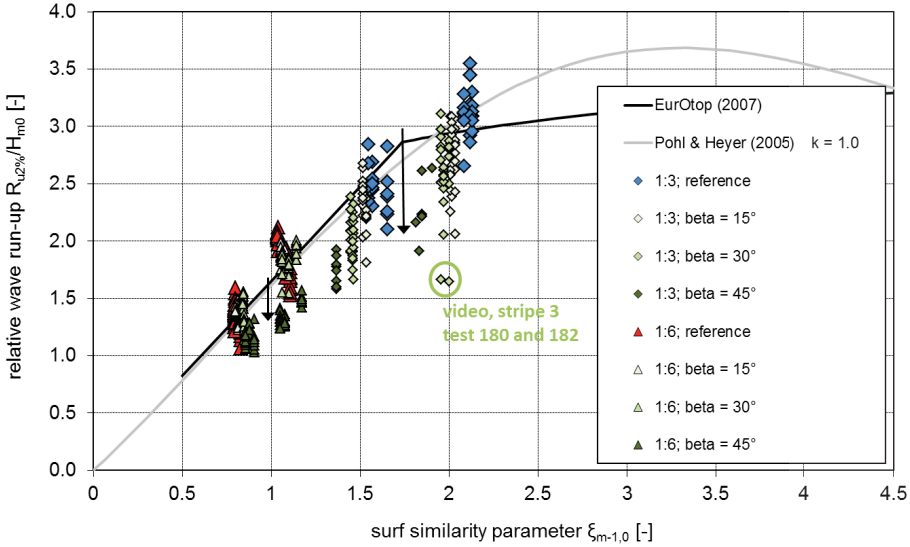


Figure 42: Relative run-up height  $R_{u2\%}/H_{m0}$  versus surf similarity parameter  $\xi_{m-1,0}$  for reference tests and tests with oblique wave attack.

To analyze the influence of the angle of wave attack on run-up the ratio  $\gamma_\beta$  is defined as follows:

$$\gamma_\beta = \frac{(R_{u2\%}/H_{m0})_\beta}{(R_{u2\%}/H_{m0})_{\beta=0}} \tag{20}$$

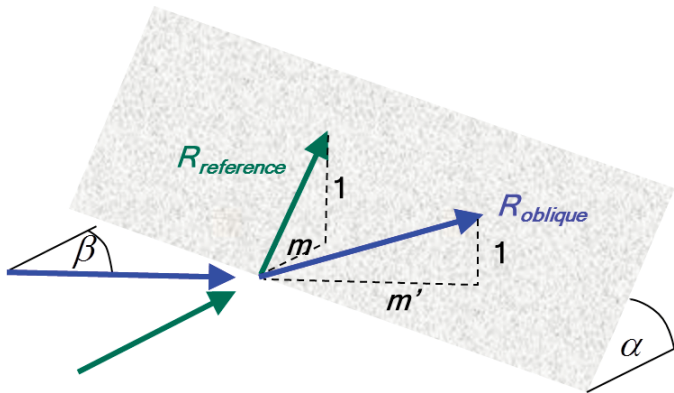


Figure 43: Relationship between wave run-up under perpendicular wave attack ( $R_{\beta=0}$ ) and oblique wave attack ( $R_{\beta \neq 0}$ ).

The influence of the angle of wave attack on wave run-up can be described using the function  $(\cos \beta)$  because dike slope ( $\tan \alpha = 1/m$ ) for perpendicular wave attack (see Fig. 43) and the according dike slope ( $\tan (\alpha') = 1/m'$ ) considering a wave attack under the angle  $\beta$  are related by:

$$\frac{\tan \alpha'}{\tan \alpha} = \cos \beta \tag{21}$$

Because the run-up is proportional to the dike slope the ratio  $\gamma_\beta$  is proportional to  $(\cos \beta)$  too. To estimate boundary value for a function  $\gamma_\beta = f(\beta)$  wave run-up on a very flat shore as well as at a vertical wall should be discussed further. On a very flat shore ( $\alpha \rightarrow 0^\circ$ ) a total refraction is possible. Wave direction in case of shore parallel waves ( $\beta = 90^\circ$ ) would be changed and resulted in an almost perpendicular wave attack and the run-up would be equal to that in case of  $\beta = 0^\circ$  (see Fig. 44, left side). It follows a ratio  $\gamma_{\beta=90^\circ} (\alpha \rightarrow 0^\circ) = 1$ . Waves propagating in the perpendicular direction ( $\beta = 90^\circ$ ) of a vertical wall ( $\alpha = 90^\circ$ ) create a run-up  $R = H$  (see Fig. 44, right side). If one considers a vertical wall and a wall parallel wave attack ( $\beta = 0^\circ$ ) the waves would propagate along the wall and create a hypothetical run-up of  $R = H/2$ . From this it follows that  $\gamma_{\beta=90^\circ} (\alpha \rightarrow 0^\circ) = 0.5$ .

A function capturing all these considerations could be:

$$\gamma_\beta = a_r \cdot \cos^2 \beta + b_r \tag{22}$$

The coefficients  $a_r$  and  $b_r$  depending at least on the dike slope (see Fig. 45) with  $a_r + b_r = 1$ . The coefficient  $b_r$  represents the boundary value  $\gamma_{\beta=90^\circ}$ . It has to be lower in the case of a steeper slope and higher in the case of a flatter slope (see Fig. 45).

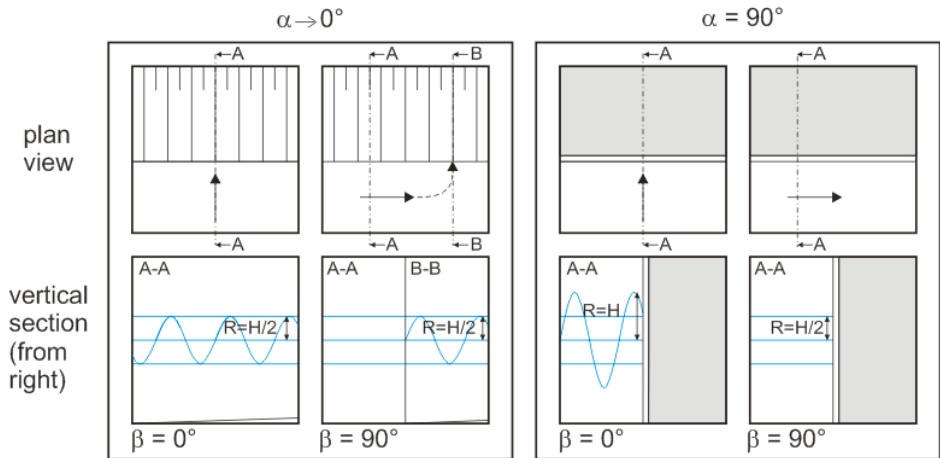


Figure 44: Wave run-up height: boundary values for perpendicular or parallel “run-up” and a very flat shore (left) and at a vertical wall (right).

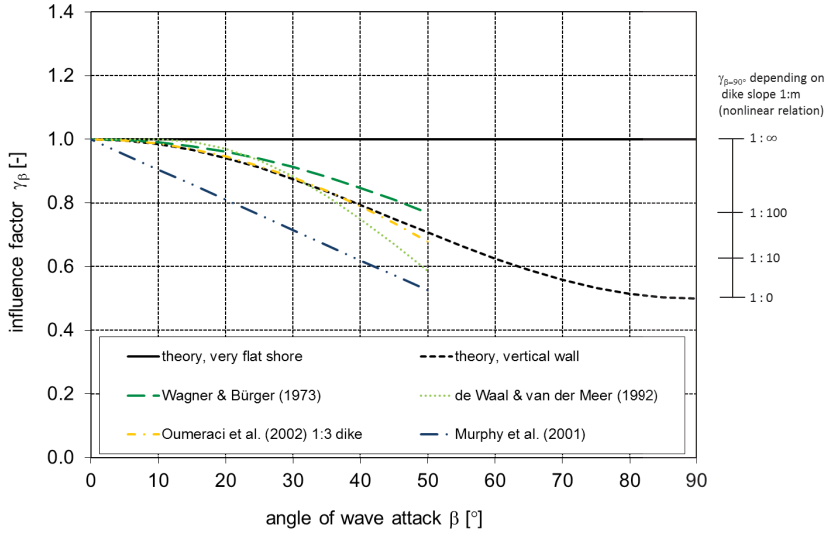


Figure 45: Empirical function for the influence factor  $\gamma_\beta$  in dependence on the angle of wave attack.

The calculated values  $\gamma_\beta$  for all tests with oblique wave attack but without wind and without a longshore current are presented in Fig. 46. Data includes measured values by capacitive gauge as well as extracted values from video analysis. Results from test 156 and test 445 were not considered within data analysis because they are characterized by significant differences between results from capacitive gauge and video analysis.

In general there is a decreasing tendency of  $\gamma_\beta$  with higher values of  $\beta$ . Only one data set (1:6 sloped dike,  $\beta = 30^\circ$ ) is not consistent with this tendency and was excluded from regression analysis. It has to be noticed that the measured data represent a more scattered data set.

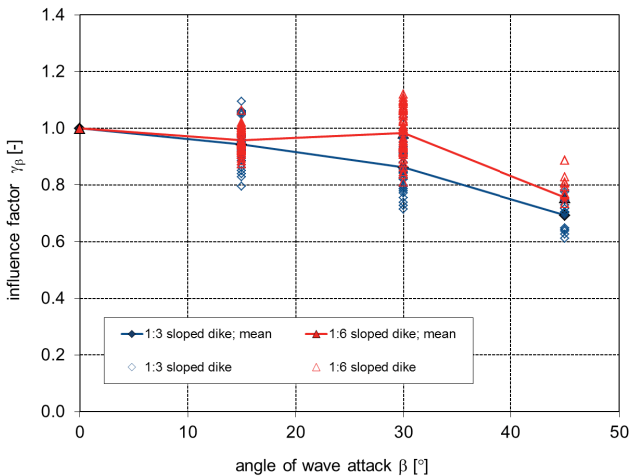


Figure 46: Influence factor  $\gamma_\beta$  in dependence on the angle of wave attack (tests without wind and current).

The results show good agreement with existing empirical functions (see Fig. 47). In general it could be stated that the results fit in former investigations and could be an additional prove that the hydraulic model set-up was appropriate chosen.

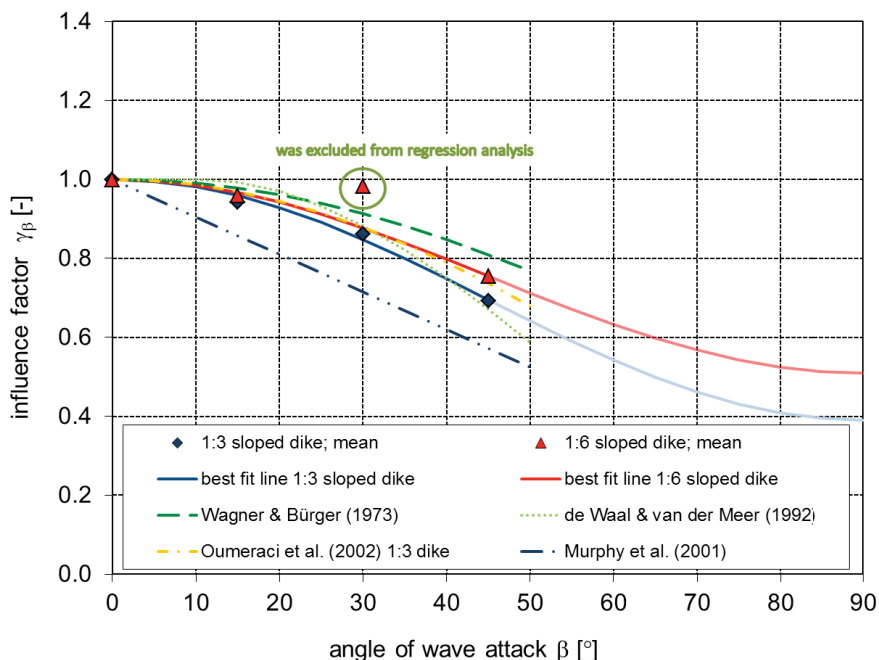


Figure 47: Influence factor  $\gamma_\beta$  in dependence on  $\cos^2\beta$ .

Two equations were fitted to the results according to the form derived above:

$$\gamma_\beta = 0.61 \cdot \cos^2 \beta + 0.39 \quad (1:3 \text{ sloped dike}) \quad (23)$$

$$\gamma_\beta = 0.49 \cdot \cos^2 \beta + 0.51 \quad (1:6 \text{ sloped dike}) \quad (24)$$

The derived functions confirm the theoretical discussion above. The value  $b_r = \gamma_{\beta=90^\circ}$  is higher for the 1:6 sloped dike than for the 1:3 sloped dike. Further investigations for  $\beta > 50^\circ$  are still needed to validate the formulae above for this co-domain.

### 6.2.4 Influence of wind

It is commonly assumed within the literature that onshore wind has an increasing effect on wave run-up (see chapter 4.4).

Fig. 48 displays the relative run-up height depending on surf similarity parameter for tests with wind and for reference tests. The dots cover similar regions within the diagram and no clear tendency is visible.

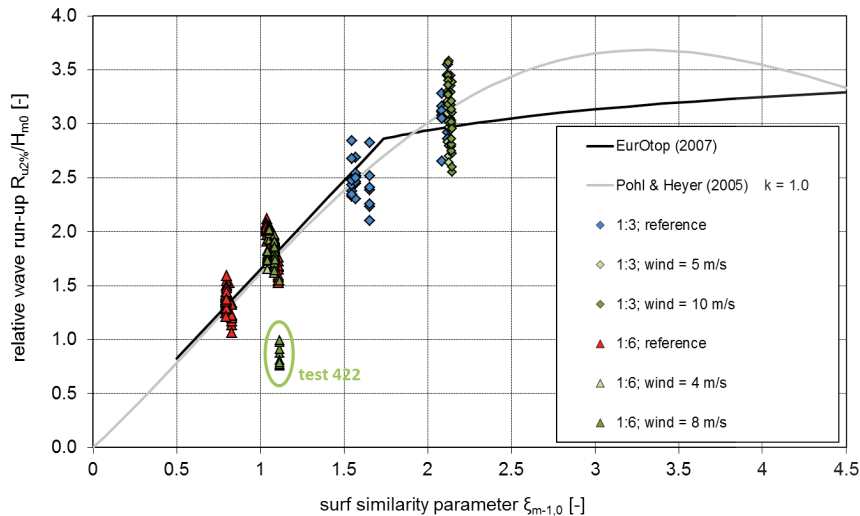


Figure 48: Relative run-up height  $R_{u2\%}/H_{m0}$  versus surf similarity parameter  $\xi_{m-1,0}$  for reference tests and tests with wind.

To analyze the influence of onshore wind the ratio  $\gamma_w$  is defined as follows:

$$\gamma_w = \frac{(R_{u2\%}/H_{m0})_w}{(R_{u2\%}/H_{m0})_{w=0}} \tag{25}$$

The calculated factors for each test with wind, rectangular wave attack and without a current are presented in Fig. 49. Data includes measured values by capacitive gauge as well as extracted values from video analysis.

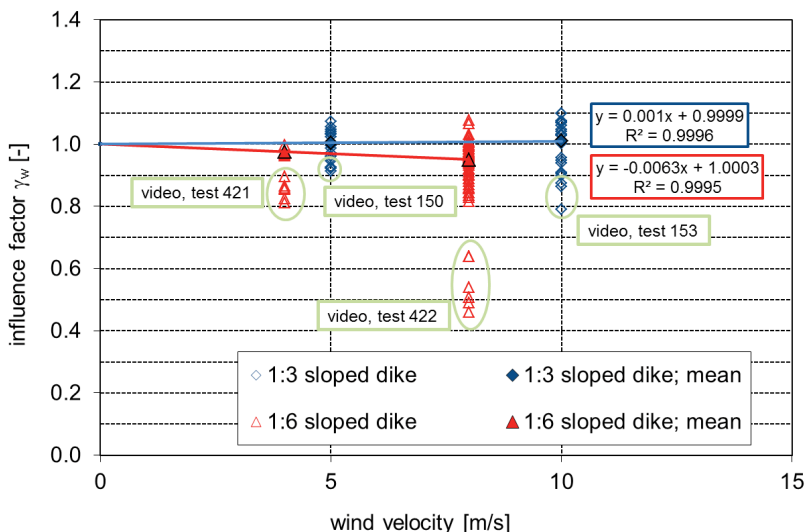


Figure 49: Influence factor  $\gamma_w$  in dependence on wind velocity (tests without current and perpendicular wave attack).

Video films for FlowDike 2 (1:6 sloped dike) and wind velocity of 4 m/s were defective as visible in the results of test 421. That's why the mean value was only calculated using data from capacitive gauge. Data extracted by video analysis for test 422 were excluded too because they did not fit with the value of the capacitive gauge and show a significant lower value of  $\gamma_w$  without any comprehensible reason. But it might be possible that reflections of light which occurred on the run-up board have interfered with run-up detection during video analysis. Out of the same reason test 150 and test 153 were not considered within further data analysis.

The results indicate no noteworthy increasing effect of wind on run-up as stated in the literature for wind speeds  $> 6$  m/s to 8 m/s. On the contrary there is a very slight decreasing effect in case of the 1:6 sloped dike. Because the presented study considered sea state the explanation of these results which are different to those from former investigations with monochromatic waves might lay herein. That the wind pushes a wave tongue up the sloped might be the case for monochromatic waves as well as sea state and would increase the wave run-up. In case of a reducing influence of downwash on the subsequent wave there might be a different effect. Because in a sea state a higher wave is in general followed by a smaller wave so that this effect may not come out so significant considering the wave run-up of higher waves in a sea state. An explanation for a decreasing effect could be that the wind induces an earlier breaking process of the waves on the dike slope and that's why the wave run-up is lower than without wind. It seems that in the case of a sea state these opposing effects balance each other.

To estimate the corresponding prototype wind speed out of model wind speed the formula presented in GONZÁLES-ECRIVÁ (2006) might be useful but very few data were used to establish it:

$$w = \frac{w_p}{c_w} \quad (26)$$

with  $w_p$  prototype wind speed [m/s]  
 $c_w$  constant factor  $c_w = 1.2$  to  $1.8$  [-]

### 6.2.5 Influence of current

The following ways of interaction between wave and current are possible and are stated here as hypotheses. They are focused on the change in wave height. On a first thought it seems that a current causes only a displacement of every single water drop parallel to the wave crest and no change of any wave parameter is happening, than no effect on run-up would be detectable. But if we consider in a second thought that the current causes a deflection of every water particle moving in circular paths, than every particle would move along a helix and has to travel a longer distance which would cause an additional energy loss and a lower wave run-up. If we consider a sea state we can distinguish further between its smaller and bigger waves. Particles in a smaller wave would have to move in a more stretched helix as particles in a bigger wave. As we are focused on larger waves because they cause the widely known  $R_{u2\%}$ , a run-up height which would be only exceeded by 2 % of the incoming waves, the effect described above may be not so significant in the whole.

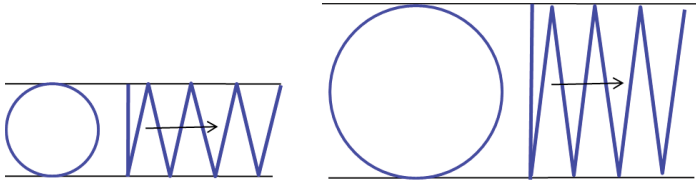


Figure 50: Moving path of a water drop in a smaller (left) and a bigger (right) wave of a sea state.

The change of the angular frequency and connected parameters as wave period and wave length can be calculated according to sec. 4.1.

But it is also possible that the current provides additional energy and this increases the wave energy and affects a higher wave run-up. The maximum attainable run-up height is equal to the kinetic energy head of the current ( $v^2/(2g)$ ). A component of the current in wave direction may also increase the run-up velocity and leads to a higher run-up.

If there is a component of the current in the direction of wave propagation the wave length would increase which leads to a higher run-up and vice versa. If the component of the current in wave direction is equal to zero (the wave propagates in a perpendicular direction relative to the current) there would be no change in wave length. But there would be still a change in the direction of wave energy transport, because some energy would propagate parallel to the wave crest.

Fig. 51 shows the relative wave run-up versus surf similarity parameter for both reference tests and tests with currents, without wind and perpendicular wave attack. Regarding this diagram it is not obvious if a higher current velocity has any effect on the wave run-up.

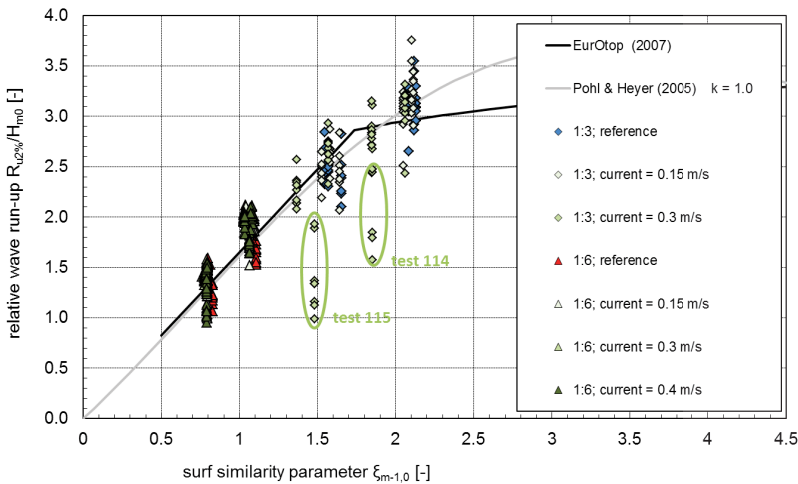


Figure 51: Relative run-up height  $R_{u2\%} / H_{m0}$  versus surf similarity parameter  $\xi_{m-1,0}$  for reference tests and tests with longshore current.

To analyze the influence of current on wave run-up the ratio  $\gamma_{cu}$  is defined as follows:

$$\gamma_{cu} = \frac{(R_{u2\%} / H_{m0})_{cu}}{(R_{u2\%} / H_{m0})_{cu=0}} \quad (27)$$

The so calculated influence factor  $\gamma_{cu}$  in dependence on current velocity is presented in Fig. 52. Green marked tests are characterized by significant differences between results from capacitive gauge and video analysis and were excluded from further analysis. The calculated values show no significant influence of current on run-up considering current velocities up to 0.4 m/s and perpendicular wave attack.

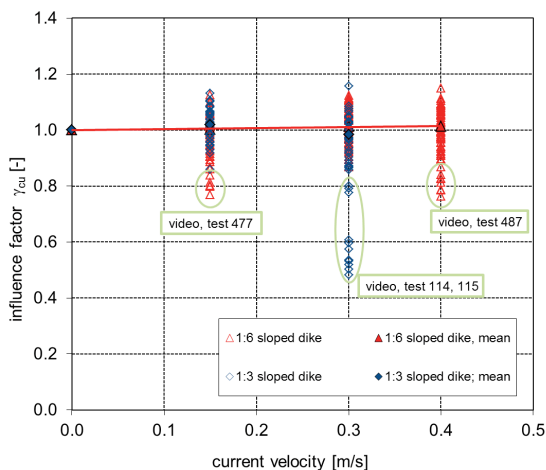


Figure 52: Influence factor  $\gamma_{cu}$  in dependence on current velocity (tests with current but without wind and perpendicular wave attack).

It seems that in case of oblique wave attack and longshore current the different and in part opposing effects mentioned above together with refraction and shoaling results in no change of run-up height.

### 6.2.6 Influence of current and oblique wave attack

In a second step the combined effect of oblique wave attack and a longshore current was investigated. It was described previously (chapter 4.1) that it is possible to include the change of wave parameters due to a longshore current by using the absolute wave parameters together with the angle of wave energy instead of the angle of wave attack.

But it is also possible that additional to the effect that a longshore current causes a deflection of the wave energy direction which decreases the wave run-up it increases the wave run-up velocity which would increase wave run-up. It is not obvious which effect might be dominated. It has to be considered too that all these effects will be superposed by refraction and shoaling as well.

The results of the current investigation show no obvious dependencies (Fig. 53 and Fig. 54) but it has to be considered that the relative wave run-up height  $R_{u2\%}/H_{m0}$  is a very sensitive parameter. Here no clear advantage is obvious in using absolute wave parameters and the angle of wave energy instead of the relative wave parameters together with the angle of wave attack.

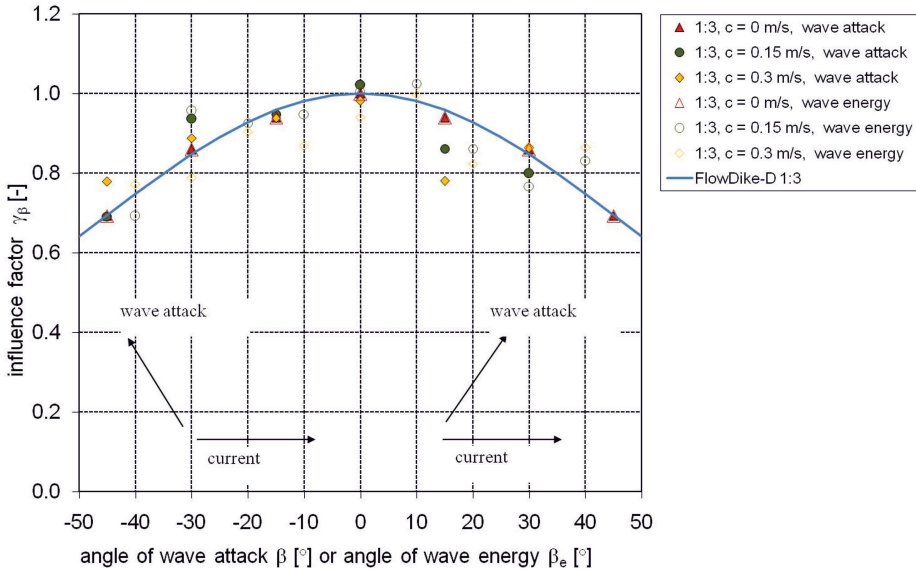


Figure 53: Influence factor  $\gamma_\beta$  in dependence on angle of wave attack or angle of wave energy respectively (1:3 sloped dike, tests with current and perpendicular and oblique wave attack but without wind).

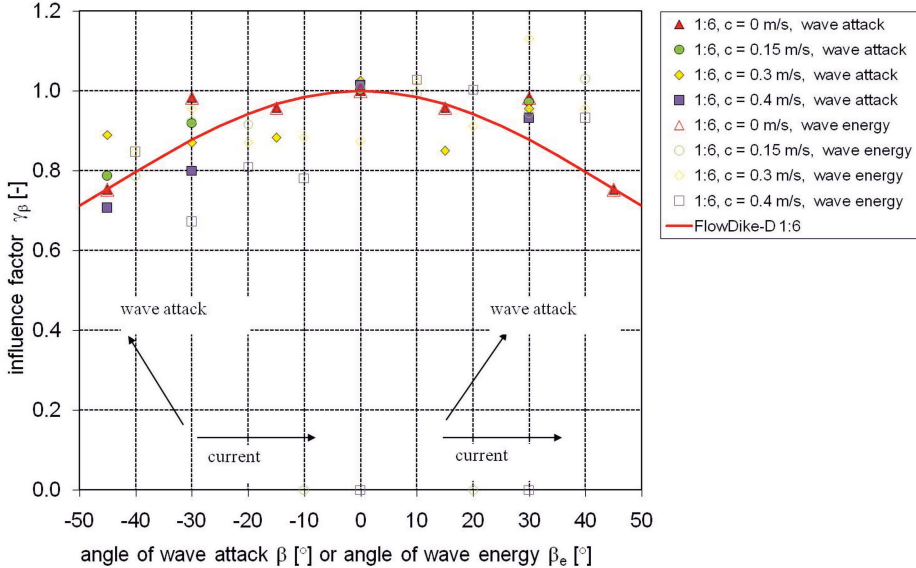


Figure 54: Influence factor  $\gamma_\beta$  in dependence on angle of wave attack or angle of wave energy respectively (1:6 sloped dike, tests with current and perpendicular and oblique wave attack but without wind).

### 6.2.7 Combination of all influence parameters

The third step within data analysis was the comparison between measured and calculated relative wave run-up. Calculation was done using the formula of EUROTOP-MANUAL (2007) together with the estimated influence factors  $\gamma_\beta$ ,  $\gamma_{cu}$  and  $\gamma_w$  (see chapters 6.2.3 to 6.2.5). Results are presented in Fig. 55 and Fig. 56.

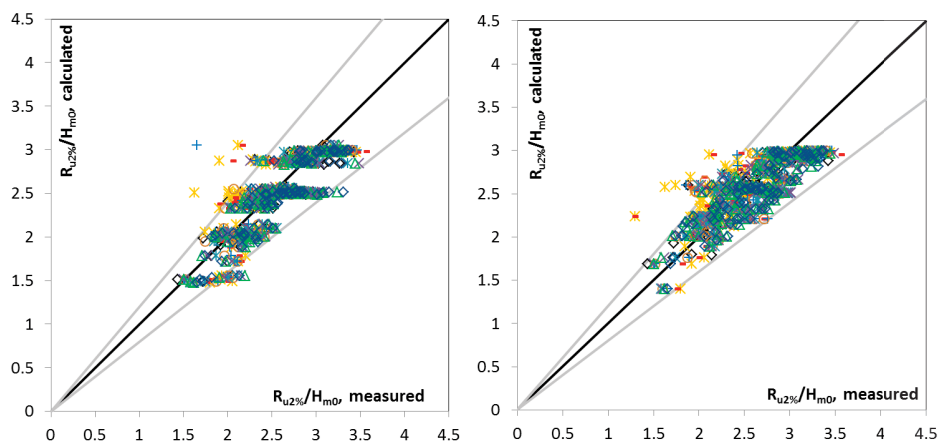


Figure 55: Comparison between measured and calculated relative wave run-up (1:3 sloped dike, calculation formulae by EUROTOP (2007) and the influence factors determined above; left: calculation using relative wave parameters; right: calculation using absolute wave parameters).

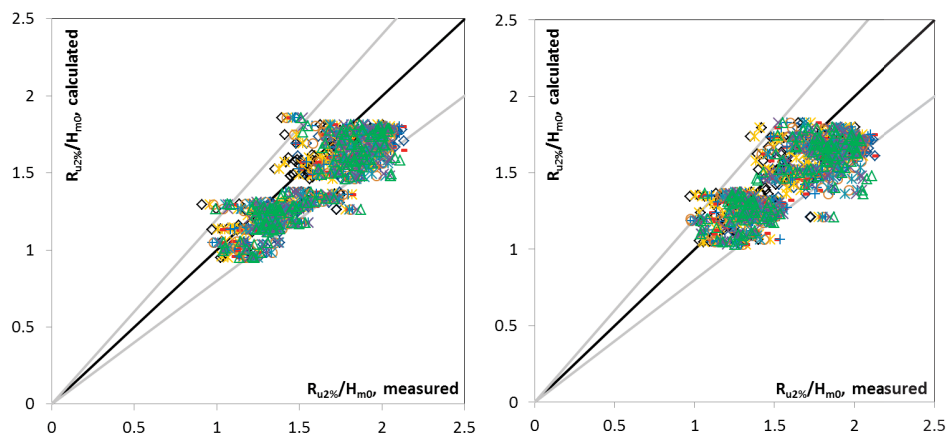


Figure 56: Comparison between measured and calculated relative wave run-up (1:6 sloped dike, calculation formulae by EUROTOP (2007) and the influence factors determined above; left: calculation using relative wave parameters; right: calculation using absolute wave parameters).

The comparison shows a good agreement between the measured and the calculated values. All pairs of values are in a range of  $\pm 20\%$ . The advantage in using absolute wave parameters together with the angle of wave energy instead of relative wave parameters together with the angle of wave attack is not obvious.

## 6.3 Analysis on wave overtopping

### 6.3.1 Reference test

In a first step the results from the basic test without wind and current are compared to the existing formulae from the EUROTOP-MANUAL (2007). The results on the 1:3 sloped dike and 1:6 sloped dike are illustrated below, together with their 95 % confidence range. First the results for both configurations fit well within the 95 % confidence range, which are displayed as dotted lines in the graphics. Most of the points fall below the average probabilistic trend (dashed blue line) from the EUROTOP-MANUAL (2007), but validate altogether the formulae.

Interpolated trend lines were added to the following diagrams to make them easier to understand. Due to the relation between the dimensionless overtopping discharge  $q_*$  and the dimensionless freeboard height  $R_{c*}$  an exponential function was chosen. After fitting the trend for the basic reference test, all following analysis will be done by regression analysis. For this purpose the inclinations of the slope  $b$  for each test series trend are compared to the inclination  $b$  of the reference test.

Fig. 57 shows the results of the reference tests for the 1:3 and 1:6 sloped dikes for breaking waves. In Fig. 58 the regression curve for non-breaking waves for the 1:3 sloped dike is given. All regression lines of the two dike slopes (dotted graph (1:3 dike) and dashed graph (1:6 dike)) are slightly lower than the recommended formula of the EUROTOP-MANUAL (2007), but still lying within the confidence range of 95 %. In the following analysis the inclination of the graph of the corresponding reference test is used to determine the influence factors  $\gamma_i$  for the three different conditions:

- 1:3 dike for breaking wave conditions
- 1:6 dike for breaking wave conditions
- 1:3 dike for non-breaking wave conditions

For better comparison with the formulae from the EUROTOP-MANUAL (2007), a regression with a fixed crossing on the y-axis was applied. The fixed interception  $Q_0$  remains the same as the y-axis crossing from the EUROTOP-MANUAL (2007) for each breaking condition.

The following trend was found for the 1:3 sloped dike (blue line):

- breaking waves:  $Q_0 = 0.067$   $b = -5.189$
- non-breaking waves:  $Q_0 = 0.2$   $b = -2.677$

The 1:6 sloped dike (red line) gives the following parameter:

- breaking waves:  $Q_0 = 0.067$   $b = -4.779$

In each case the results follow an average trend, which is just a bit lower than the stated equation from the EUROTOP-MANUAL (2007). Concluding for the analysis on wind, current and oblique wave attack, the crossing with the y-axis of the basic reference test can remain the same as in the formulae from EUROTOP-MANUAL (2007). The inclination of the slope  $b$  will influence the designated comparison of the results, as it is used to determine the influence of each variable within a parametric study.

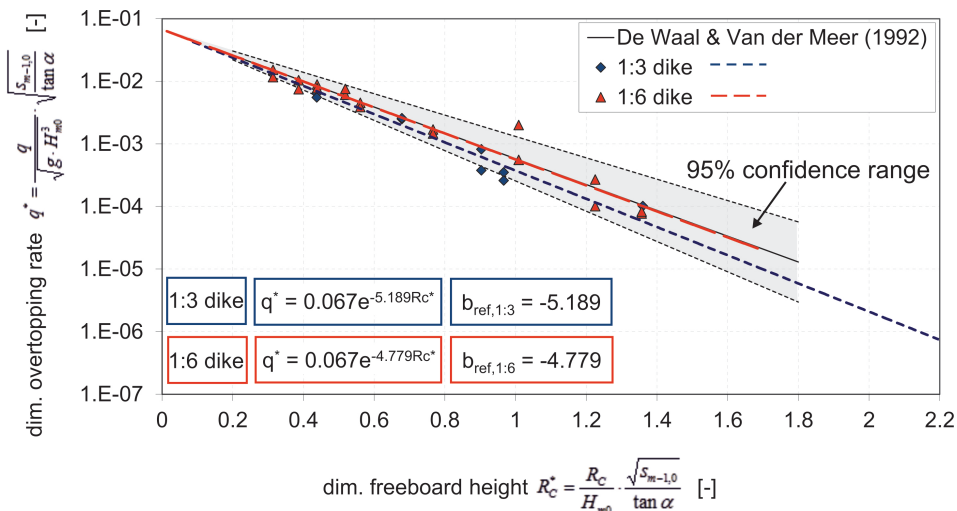


Figure 57: Dimensionless overtopping rate – reference tests for breaking wave conditions (1:3 dike, 1:6 dike).

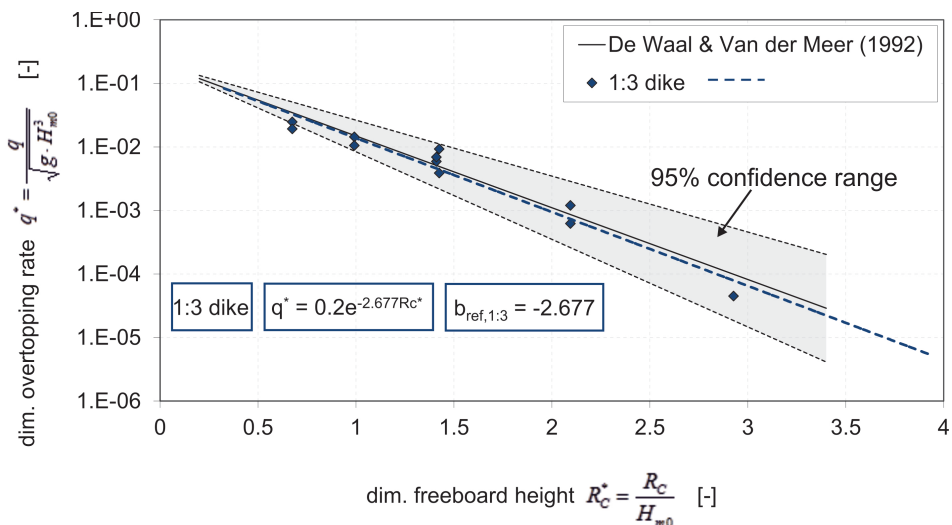


Figure 58: Dimensionless overtopping rate – reference test for non-breaking wave conditions (1:3 sloped dike).

Summarizing the first conclusions drawn in this section, it can be stated that:

- The results validate well the theory applied in EUROTOP-MANUAL (2007).
- The overtopping formula underestimates slightly the results found in FlowDike 1, but fits those of FlowDike 2 as well.
- The trend lines with fixed interception show an acceptable accuracy.
- The basic trend lines used for regression analysis of the following parametric set can be fixed on the y-axis to the interception values of formulae by the EUROTOP-MANUAL (2007).

- Between FlowDike 1 and FlowDike 2 a shift of the results has remained. This variance was about 8 % referring to the slope inclinations  $(b_{ref,1.6} / b_{ref,1.3}) = (-4.779 / -5.189) = 92\%$ .

### 6.3.2 Influence of wave spectra

Fig. 59 shows the results of former investigations on mostly 1:6 smooth sloped dikes. Most of the listed tests were performed during the German research project “Loading of the inner slope of sea dikes by wave overtopping” (BMBF KIS 009) where the investigation of different wave spectra was part of it. Also the test results during the project “Influence of oblique wave attack on wave run-up and wave overtopping – 3D model tests at NRC/Canada with long and short crested Waves” are included. In the left graph the data points of all tests are given. The corresponding regression curves are given in the right graph. It can be seen that the results for the double peak spectra and the TMA spectra is a bit smoother than the regression curve of FlowDike 1 and FlowDike 2 (1:3 and 1:6 sloped dike) and the sea state test.

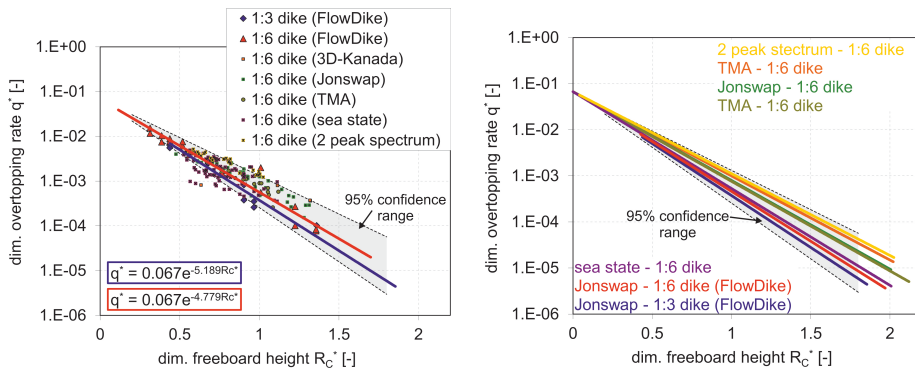


Figure 59: Influence of wave spectra on wave overtopping; Comparison of FlowDike 1 and FlowDike 2 results with former investigations by OUMERACI et al. (2002).

### 6.3.3 Influence of oblique wave attack without current

Oblique wave attack has been investigated before, so this section will only be an adaptation and verification. This is done with regard to the following analyses, which will consider the combined effects of obliqueness, currents and wind.

In the following figures (Fig. 60 to Fig. 62) all test results for oblique wave attacks are given. The trend lines have been determined with fixed interception for each angle of wave attack.

Again the data points lay very well around their exponential regression. Only the points for non-breaking waves with  $-15^\circ$  oblique waves seem to scatter too much (cf. Fig. 62). There is an obvious trend in both graphs, where the increase of obliqueness results in a reduction of overtopping. For larger angles the reduction increases, this means between  $0^\circ$  and  $15^\circ$  the reduction is lower than between  $30^\circ$  and  $45^\circ$ .

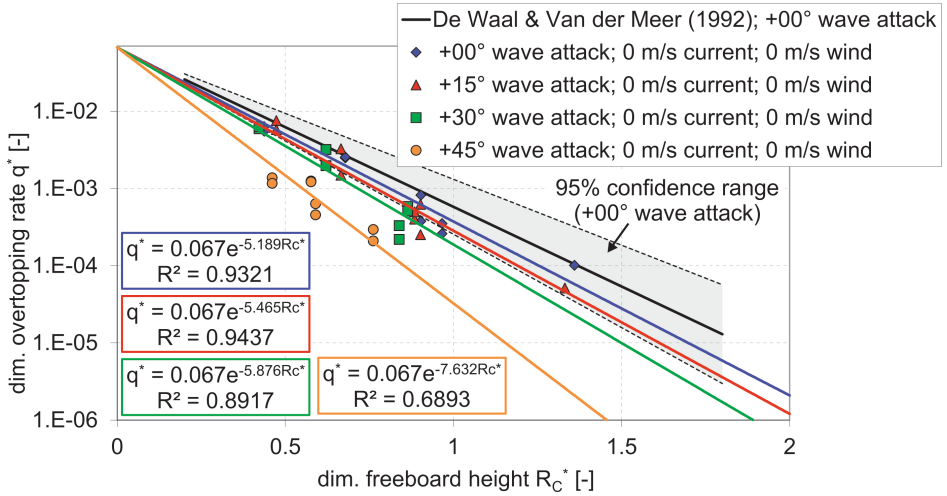


Figure 60: Influence of oblique wave attack on wave overtopping; 1:3 sloped dike (breaking conditions).

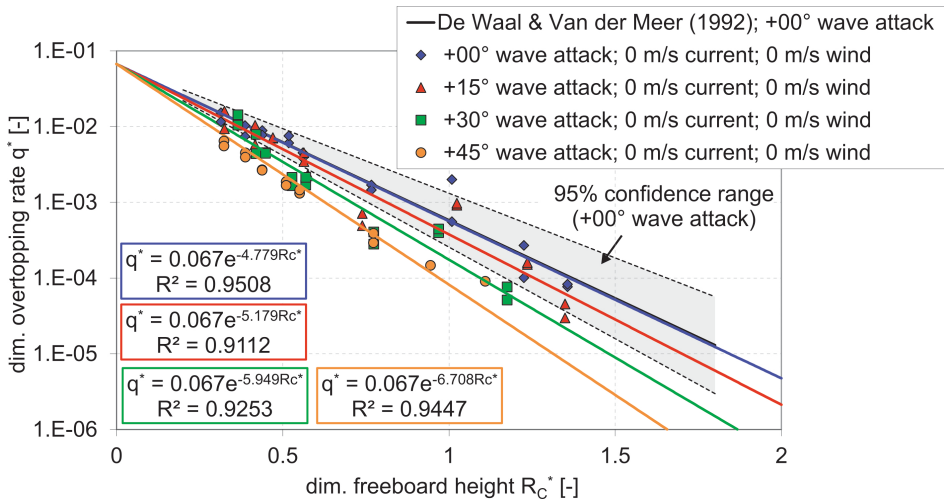


Figure 61: Influence of oblique wave attack on wave overtopping; 1:6 sloped dike (breaking conditions).

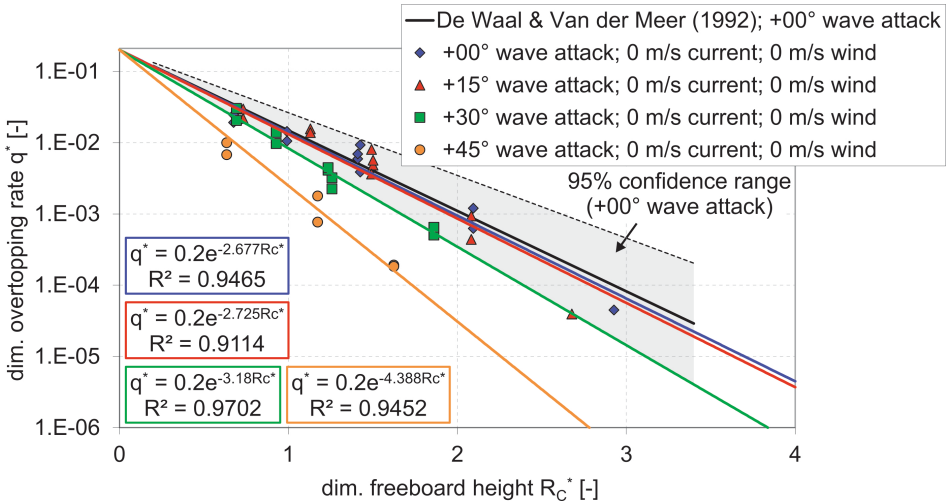


Figure 62: Influence of oblique wave attack on wave overtopping; 1:3 sloped dike (non-breaking conditions).

On the 1:6 sloped dike the trend lines and results for oblique wave attack for breaking conditions are illustrated in Fig. 61. A similar effect is obvious. The increase in obliqueness results in the reduction of overtopping, but this time the reduction, especially between 30° and 45°, is not as large as for the 1:3 sloped dike. It was mentioned before, that small overtopping amounts were expected and also recognized during testing due to the slope inclination. An explanation for less difference in the overtopping graphs for FlowDike 2 could be as well the smoother slope of the dike that leads to early breaking on the dike.

At a closer look one finds that the trend line slope  $b$  shows for all different angles of wave attack a shift between the 1:3 slope and the 1:6 slope. The shift was already perceived for the perpendicular waves (sec. 6.3.1) and will stay the same through the whole analysis (Tab. 2).

Table 2: Inclinations of the slopes  $b_{1:3}$  and  $b_{1:6}$  of tests without current and wind (cf. Fig. 60 to Fig. 61).

dike slope	wave conditions	wave attack			
		0°	15°	30°	45°
1:3	breaking waves	-5.189	-5.465	-5.876	-7.632
1:3	non-breaking waves	-2.677	-2.725	-3.180	-4.388
1:6	breaking waves	-4.779	-5.179	-5.949	-6.708

### 6.3.4 Statistical spread of tests

The slopes of the trend lines  $b$  (cf. figures above) are determined using the regression formula of Microsoft Excel 2010. To determine the statistical spreading of these values a slope  $b_i$  was determined for every measured value separately. The procedure is clarified in Fig. 63 while  $b_i$  can be calculated by

$$b_i = \frac{\ln\left(\frac{q^*}{a}\right)}{R_{c^*}} \quad [-] \quad (28)$$

with  $q^*$  dimensionless overtopping rate [-]  
 $a$  regression coefficient with  $a = 0.067$  for breaking conditions and  $b = 0.2$  for non-breaking conditions [-]  
 $R_{c^*}$  dimensionless freeboard height [-]

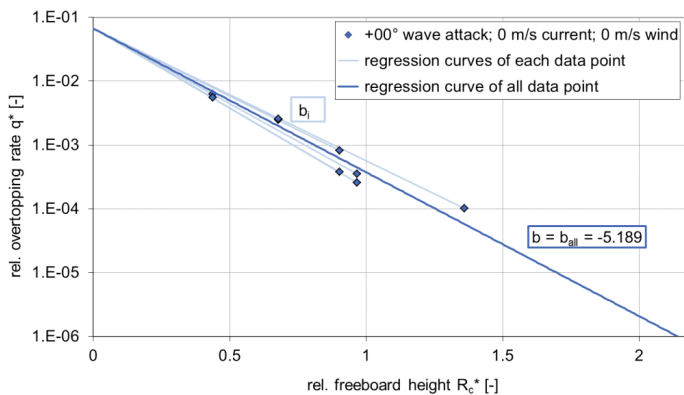


Figure 63: Determination of the slopes of the graphs for each data point  $b_i$  and the slope of the graph considering all data points  $b_{all}=b$  exemplary for the reference test on the 1:3 sloped dike (breaking conditions).

For each data point  $i$  and its slope of the graph  $b_i$ , an influence factor  $\gamma_i$  is determined separately for each data point and defined by the following formula:

$$\gamma_i = \frac{b_i}{b_{all,0^\circ}} \quad [-] \quad (29)$$

Like given in Tab. 2 the parameter  $b_{all,0^\circ}$  are determined as follows:

- 1:3 sloped dike, breaking waves:  $b_{all,0^\circ} = -5.189$
- 1:3 sloped dike, non-breaking waves:  $b_{all,0^\circ} = -2.677$
- 1:3 sloped dike, breaking waves:  $b_{all,0^\circ} = -4.779$

These influence factors are plotted in Fig. 64 to Fig. 65 against the angle of wave attack.

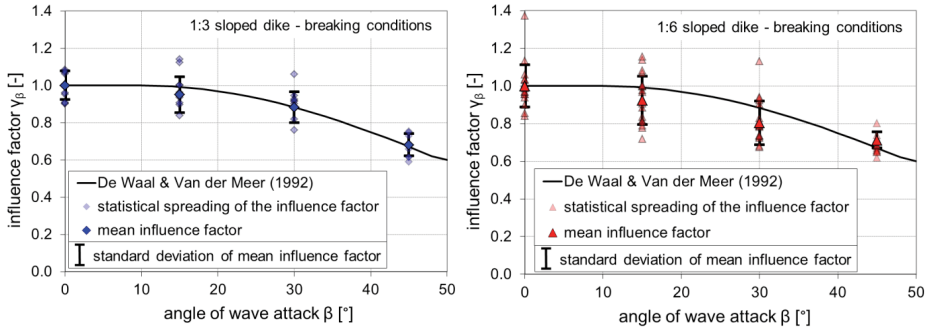


Figure 64: Influence of oblique wave attack on wave overtopping: statistical spreading of tests with oblique wave attack; breaking conditions (left: 1:3 sloped dike; right: 1:6 sloped dike).

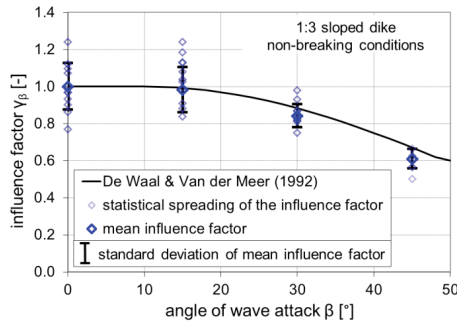


Figure 65: Influence of oblique wave attack on wave overtopping: statistical spreading of tests with oblique wave attack; 1:3 sloped dike (non-breaking wave conditions).

### 6.3.5 Comparison with former investigations

Influence factors for wave overtopping for obliqueness  $\gamma_\beta$  can be determined by comparing the exponential coefficients  $b_\beta$  for normal wave attack ( $\beta=0$ ) and oblique wave attack ( $\beta \neq 0$ ):

$$\gamma_i = \frac{b_\beta}{b_{\beta=0^\circ}} \tag{30}$$

The results of FlowDike 1 and FlowDike 2 validate well the trend of the former results like DE WAAL and VAN DER MEER (1992) (cf. Fig. 66). Most data points fall a little bit below the regression line.

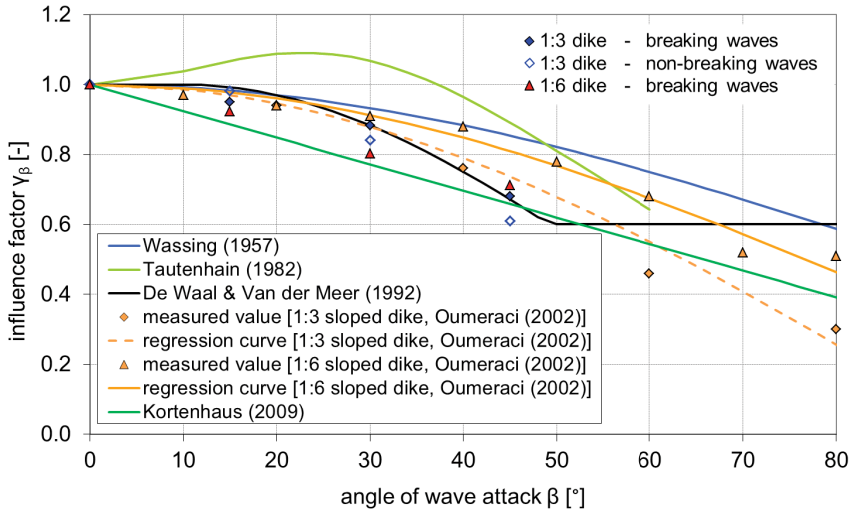


Figure 66: Comparison of influence factors for obliqueness – FlowDike 1 and FlowDike 2 (1:3 and 1:6 sloped dike) with former investigations.

### 6.3.6 Influence of current

To determine the influence of the longshore current, the influence factors  $\gamma_{cu}$  was introduced to take the influence of current  $v_x$  into account:

$$\gamma_{cu} = \frac{b_{cu}}{b_{cu=0}} \quad (31)$$

This influence factor is defined for tests with perpendicular wave attack and without wind. Fig. 67 gives these influence factors plotted against the current velocity for breaking and non-breaking conditions of each dike. The influence factors differ between 0.965 and 1.025, with the exception of the test on the 1:3 sloped dike under non-breaking wave conditions with a current velocity of 0.3 m/s.

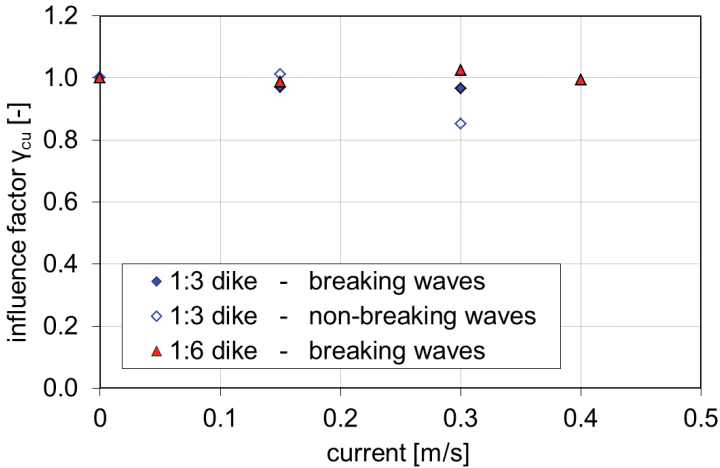


Figure 67: Influence of the current on wave overtopping, angle of wave attack  $\beta = 0^\circ$ , no wind.

These influence factors and their statistical spreading against the current are plotted in Fig. 68 and Fig. 69.

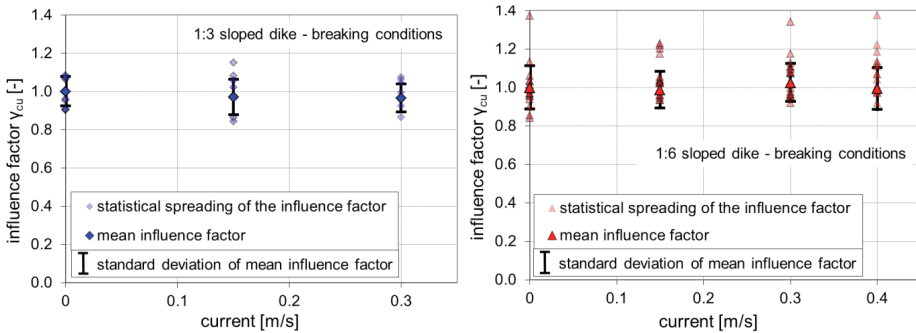


Figure 68: Influence of the current on wave overtopping: statistical spreading of tests with current, breaking conditions (left: 1:3 sloped dike; right: 1:6 sloped dike).

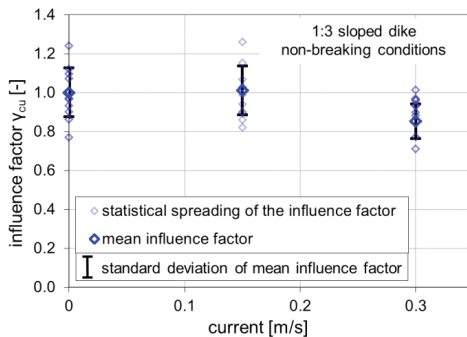


Figure 69: Influence of the current on wave overtopping: statistical spreading of tests with current; 1:3 sloped dike (non-breaking wave conditions).

### 6.3.7 Influence of wind

From the test program it can be seen that the test series on wind contain merely the wave spectra w1, w3 and w5 with a lower steepness than the wave spectra w2, w4 and w6. The steepness is a limiting factor for the surf similarity parameter, which is an input variable in the overtopping formulae. Due to this the generated waves for wind tests give only results for non-breaking conditions during FlowDike 1. For FlowDike 2 the influence of the slope was governing and still only breaking waves occurred. Another difference between FlowDike 1 and FlowDike 2 is the missing wind test for  $u = 4$  m/s, only two tests on this wind speed exist.

Though the effect in overtopping could be measured the detected events marked as points in the graphs show almost no influence for small and high overtopping events for the 1:3 sloped dike (cf. Fig. 70, left; lying nearly on the points of the reference test and in the 95 % confidence range of DE WAAL and VAN DER MEER (1992)). This does not correlate to the statement by WARD et al. (1996) and DE WAAL et al. (1996) that for smaller overtopping amounts a small increasing trend for the average overtopping can be established while no influence is noticeable for higher overtopping rates.

For FlowDike 2 the effect of increasing average overtopping amounts for the smaller wave spectra, such as w1 can be stated again. The first data points for high waves in the graph match again the points from the reference test. The regression curves are nearly the same, so that no influence of wind is recognizable (cf. Fig. 70, right). The influence factors and their statistical spreading are plotted in Fig. 71 against the wind.

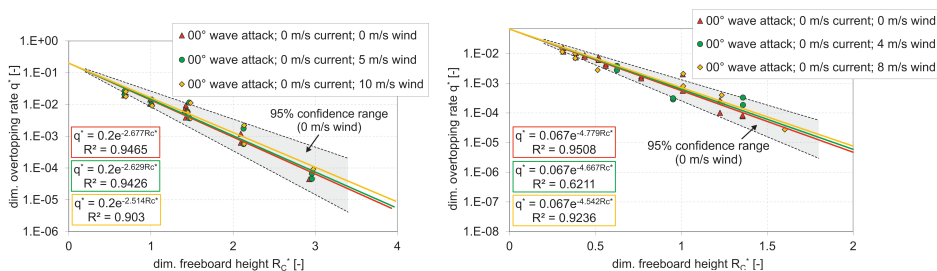


Figure 70: Wind influence on wave overtopping; left: 1:3 sloped dike – FlowDike 1; 1:6 sloped dike – FlowDike 2.

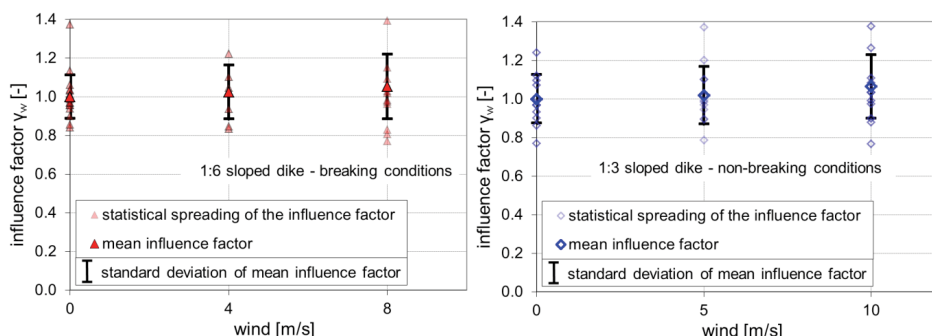


Figure 71: Statistical spreading of tests with wind; left: 1:6 sloped dike (breaking conditions); right: 1:3 sloped dike (non-breaking conditions).

### 6.3.8 Influence of oblique wave attack and current

To present the results of oblique wave attack and current on wave overtopping a distinction has to be done between the results for the 1:3 sloped dike for breaking and non-breaking waves (cf. Fig. 73) and the results for the breaking waves on the 1:6 sloped dike (cf. Fig. 74). In the following the results are presented for different combinations of the angle of wave attack and the angle of wave energy respectively the absolute and relative wave parameters (cf. Fig. 72):

- angle of wave attack and absolute wave parameters
- angle of wave attack and relative wave parameters
- angle of wave energy and absolute wave parameters

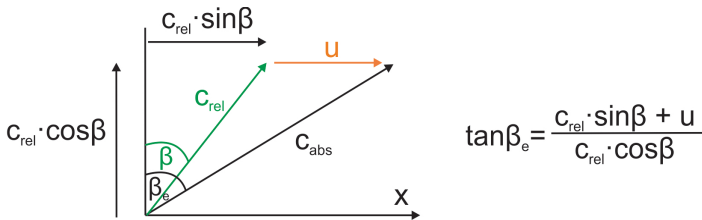


Figure 72: Relationship of the angle of wave attack, angle of wave energy, relative group velocity and absolute group velocity (cf. Fig. 25).

### 6.3.9 Angle of wave attack and absolute wave parameters

In a first step, a characteristic factor was applied to determine the influence of a combination of oblique waves and longshore current. The absolute wave parameters are used. The triangles show the influence factors for tests without current. An increase of the influence factor for increasing current velocity, shown by the circles (0.15 m/s), diamonds (0.30 m/s) and squares (0.40 m/s only 1:6 dike) is noticeable for breaking wave conditions. For non-breaking wave conditions (1:3 sloped dike) the influence factor increases for angles of wave attack of  $-45^\circ$ ,  $-30^\circ$  and  $+15^\circ$  and decreases for angles of wave attack of  $-15^\circ$  and  $+30^\circ$ . For non-breaking waves the influence factor of the tests under perpendicular wave attack and with a current of 0.30 m/s is quite smaller than with no current or a current of 0.15 m/s.

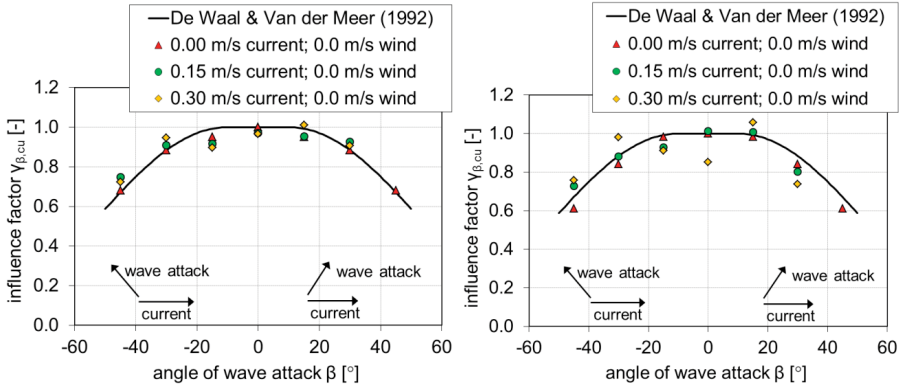


Figure 73: Current influence on wave overtopping, 1:3 sloped dike, left: breaking waves; right: non-breaking waves.

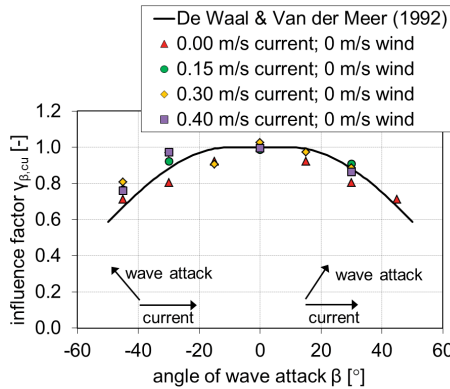


Figure 74: Current influence on wave overtopping, 1:6 sloped dike, breaking waves.

### 6.3.10 Angle of wave attack and relative wave parameters

For non-breaking waves the dimensionless overtopping rate and the dimensionless free-board height were determined independent of the wave period (cf. Fig. 57 and Fig. 58). Hence using the relative wave period only changes the influence factor  $\gamma_{\beta,eu}$  for breaking wave conditions and not for non-breaking conditions. The corresponding graphs are given below for the 1:3 and the 1:6 sloped dike (Fig. 75 and Fig. 76). The filled data points are results considering the absolute wave period  $T_{abs,m-1,0}$ . The non-filled data points were determined by using the relative wave period  $T_{rel,m-1,0}$ . The influence factor decreases for positive angles of wave attack. For negative angles of wave attack the relative wave periods become smaller. Consequently the influence factors increase to high values and cannot be used for describing the influence of currents. The here presented data corresponding to the relative wave period investigation are preliminary data and do not fit the data of further graphs.

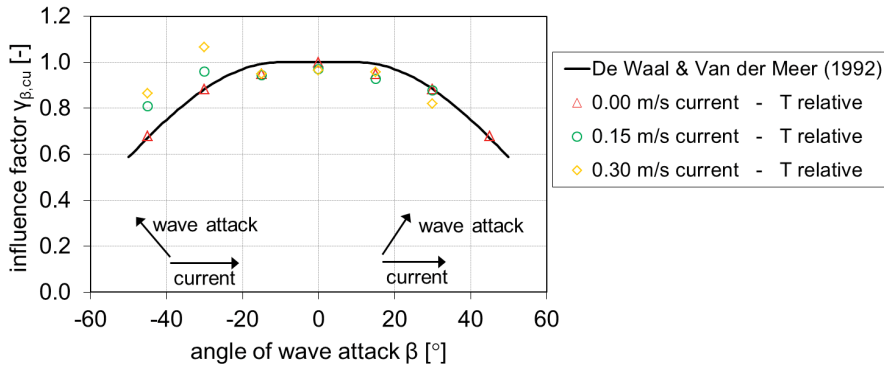


Figure 75: Current influence on wave overtopping including the relative wave period, 1:3 sloped dike, br. waves.

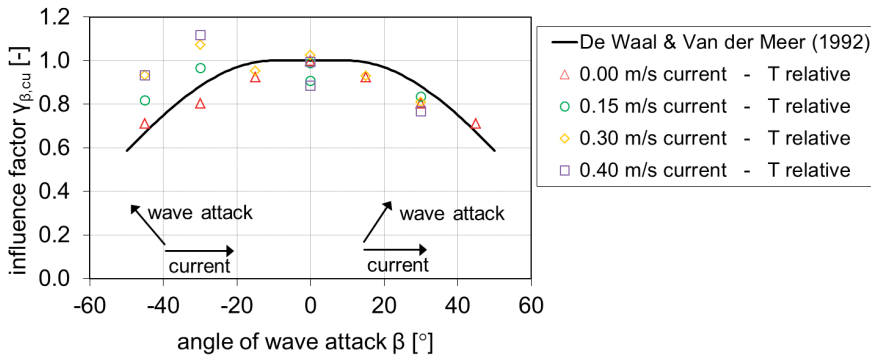


Figure 76: Current influence on wave overtopping including the relative wave period, 1:6 sloped dike, br. waves.

### 6.3.11 Angle of wave energy and absolute wave parameters

In the following, the theory of the wave energy direction is applied to the test results in Fig. 77 to Fig. 79 for the 1:3 and 1:6 sloped dike for breaking and non-breaking (only 1:3 sloped dike) waves. The filled data points are plotted against the angle of wave energy  $\beta_e$ . The data using the direction of wave energy lie further to the right than the data points that consider only the wave direction and not its energy direction and correspond fairly well to the graph of DE WAAL and VAN DER MEER (1992).

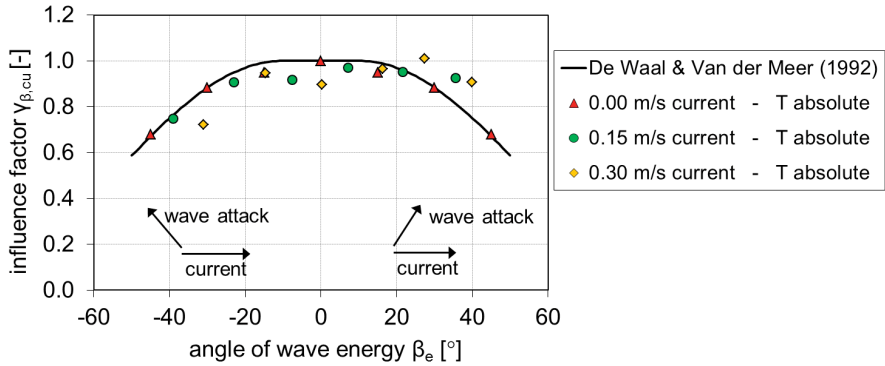


Figure 77: Current influence on wave overtopping including the angle of wave energy, 1:3 sloped dike, br. waves.

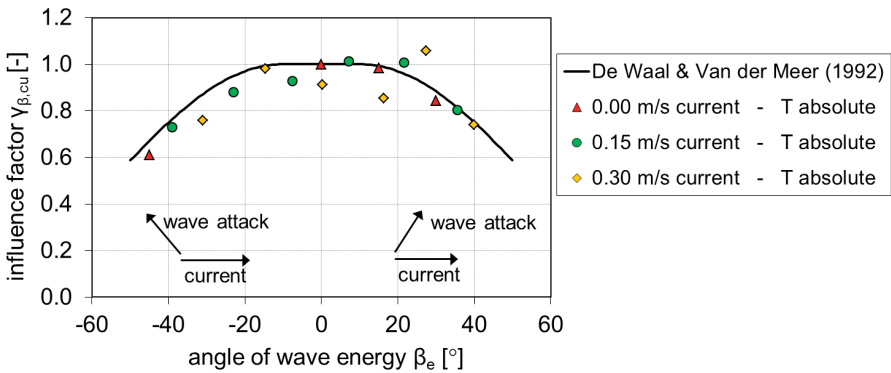


Figure 78: Current influence on wave overtopping incl. the angle of wave energy, 1:3 sloped dike, non-br. waves.

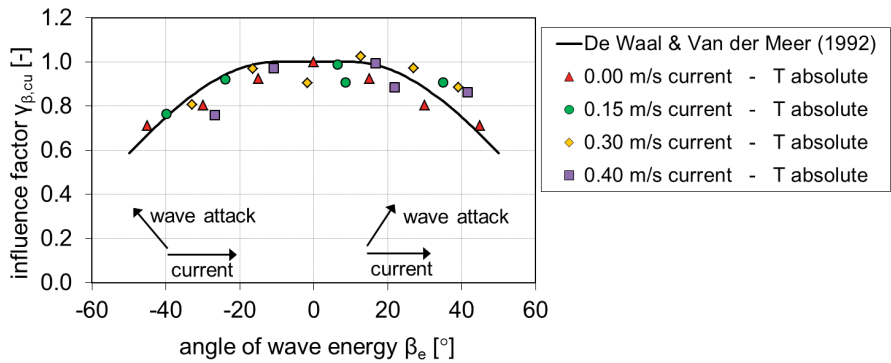


Figure 79: Current influence on wave overtopping including the angle of wave energy, 1:6 sloped dike, br. waves.

### 6.3.12 Conclusion

The influence of a longshore current combined with oblique wave attack has been analyzed. In the following a brief conclusion will be given for the three different combinations of the angle of wave attack and the angle of wave energy respectively the absolute and relative wave parameters:

- angle of wave attack and absolute wave parameters:
  - no significant influence of the current on wave overtopping could be measured
  - for breaking waves an insignificant increasing of wave overtopping is identifiable for current  $> 0$  m/s
  - for non-breaking waves (1:3 sloped dike): the wave overtopping increases with a higher current velocity with negative angles of wave attack; the wave overtopping decreases with a higher current velocity with positive angles of wave attack
- angle of wave attack and relative wave parameters
  - the dimensionless overtopping rate increases inexplicable using relative wave parameters
- angle of wave energy and absolute wave parameters
  - influence factors correspond more or less with the formula for  $\gamma_{\beta}$  by EUROTOP-MANUAL (2007)

Because of the slight influence of a longshore current on wave overtopping it is recommended to use the angle of wave attack and absolute wave parameters as analyzing method.

## 6.4 Comparison of wave run-up and wave overtopping

This section summarizes the influences of the angle of wave attack, the longshore current and wind on wave run-up and wave overtopping. For every data set the influence factor  $\gamma$  is given in Tab. 3 to Tab. 10 for the 1:3 sloped (breaking and non-breaking wave conditions) dike and the 1:6 sloped dike (breaking wave conditions). The influence factors determined by the analysis on wave run-up correspond well with the influence factors determined by wave overtopping analysis. As described in sec. 6.2 for wave run-up and 6.3 for wave overtopping only some tests give unclear influence factors. These factors are written in gray in the following tables.

Table 3: Influence factors  $\gamma_{\beta}$  for oblique wave attack.

angle of wave attack	1:3 sloped dike			1:6 sloped dike	
	run-up	overtopping br. waves	overtopping non-br. waves	run-up	overtopping br. waves
0°	1.00	1.00	1.00	1.00	1.00
-15°	0.94	0.95	0.98	0.96	0.92
-30°	0.86	0.88	0.84	0.98	0.80
+45°	0.69	0.68	0.61	0.75	0.71

Table 4: Influence factors  $\gamma_{cu}$  for current.

current	1:3 sloped dike			1:6 sloped dike	
	run-up	overtopping br. waves	overtopping non-br. waves	run-up	overtopping br. waves
0 m/s	1.00	1.00	1.00	1.00	1.00
0.15 m/s	1.02	0.97	1.01	1.00	0.99
0.30 m/s	0.98	0.97	0.85	1.01	1.02
0.40 m/s	-	-	-	1.01	0.99

Table 5: Influence factors  $\gamma_w$  for wind.

wind	1:3 sloped dike			1:6 sloped dike	
	run-up	overtopping br. waves	overtopping non-br. waves	run-up	overtopping br. waves
0 m/s	1.00	-	1.00	1.00	1.00
4 m/s or 5 m/s	1.00	-	1.02	0.98	1.02
8 m/s or 10 m/s	1.01	-	1.07	0.95	1.05

Table 6: Influence factors  $\gamma_{\beta,cu}$  for current, oblique wave attack  $\beta = -45^\circ$ , 0 m/s wind.

current	1:3 sloped dike			1:6 sloped dike	
	run-up	overtopping br. waves	overtopping non-br. waves	run-up	overtopping br. waves
0 m/s	0.69	0.68	0.61	0.75	0.71
0.15 m/s	0.69	0.75	0.73	0.79	0.76
0.30 m/s	0.78	0.72	0.76	0.89	0.81
0.40 m/s	-	-	-	0.71	0.76

Table 7: Influence factors  $\gamma_{\beta,cu}$  for current, oblique wave attack  $\beta = -30^\circ$ , 0 m/s wind.

current	1:3 sloped dike			1:6 sloped dike	
	run-up	overtopping br. waves	overtopping non-br. waves	run-up	overtopping br. waves
0 m/s	0.86	0.88	0.84	0.98	0.80
0.15 m/s	0.94	0.91	0.88	0.92	0.92
0.30 m/s	0.89	0.95	0.98	0.87	0.97
0.40 m/s	-	-	-	0.80	0.97

Table 8: Influence factors  $\gamma_{\beta, cu}$  for current, oblique wave attack  $\beta = -15^\circ$ , 0 m/s wind.

current	1:3 sloped dike			1:6 sloped dike	
	run-up	overtopping br. waves	overtopping non-br. waves	run-up	overtopping br. waves
0 m/s	0.94	0.95	0.98	0.96	0.92
0.15 m/s	0.95	0.92	0.93	-	-
0.30 m/s	0.94	0.90	0.91	0.88	0.90
0.40 m/s	-	-	-	-	-

Table 9: Influence factors  $\gamma_{\beta, cu}$  for current, oblique wave attack  $\beta = +15^\circ$ , 0 m/s wind.

current	1:3 sloped dike			1:6 sloped dike	
	run-up	overtopping br. waves	overtopping non-br. waves	run-up	overtopping br. waves
0 m/s	0.94	0.95	0.98	0.96	0.92
0.15 m/s	0.86	0.95	1.01	-	-
0.30 m/s	0.78	1.01	1.06	0.85	0.97
0.40 m/s	-	-	-	-	-

Table 10: Influence factors  $\gamma_{\beta, cu}$  for current, oblique wave attack  $\beta = +30^\circ$ , 0 m/s wind.

current	1:3 sloped dike			1:6 sloped dike	
	run-up	overtopping br. waves	overtopping non-br. waves	run-up	overtopping br. waves
0 m/s	0.86	0.88	0.84	0.98	0.80
0.15 m/s	0.80	0.93	0.80	0.97	0.91
0.30 m/s	0.86	0.91	0.74	0.96	0.89
0.40 m/s	-	-	-	0.93	0.86

## 6.5 Analysis of flow processes on dike crests

### 6.5.1 Plausibility of the measured data

Nowadays, the research on wave run-up and wave overtopping intends to describe also the flow processes on the crest. SCHÜTTRUMPF (2001) and VAN GENT (2002) describe these processes related to wave run-up and wave overtopping by flow parameters such as flow depth  $h_{2\%}$  and flow velocity  $v_{2\%}$ . A formula resulting from a simplified energy equation is given to determine the flow depths on the seaward dike crest  $h_{2\%}$  which are exceeded by 2 % of the incoming waves with the formula

$$\frac{h_{2\%}}{H_s} = c_h \cdot \frac{R_{u2\%} - R_c}{H_s} [-] \tag{32}$$

with  $H_s$  significant wave height [m]

- $R_{u2\%}$  run-up height exceeded by 2 % of the incoming waves [m]
- $R_c$  freeboard height [m]
- $c_h$  empirical coefficient determined by model tests[-]

Additionally flow velocities on the seaward dike crest  $v_{2\%}$  are given by

$$\frac{v_{2\%}}{\sqrt{g \cdot H_s}} = c_v \cdot \sqrt{\frac{R_{u2\%} - R_c}{H_s}} \quad [-] \quad (33)$$

- $c_v$  empirical coefficient determined by model tests [-]

Experimental investigations on the overtopping flow parameters were performed in small and large wave flumes but the three dimensionality of the process was not investigated so far.

For each test of the 1:3 and 1:6 sloped dike the coefficients  $c_h$  and  $c_v$  were determined by using the described formula (32) and (33) by SCHÜTTRUMPF and VAN GENT (2003). To exclude measuring errors a selection of tests was made: flow velocities of wind tests and with a corresponding flow depth on the crest lower than 1 cm are not usable because the micro propeller was not able to deliver correct results under these conditions. These flow velocities are not considered in the following analysis. Fig. 80 and Fig. 81 show the coefficients  $c_h$  and  $c_v$  for all four dike configurations on the seaward side. These coefficients  $c_h$  and  $c_v$  are determined using the mentioned formula by SCHÜTTRUMPF and VAN GENT (2003):

$$c_h = \frac{R_{u2\%} - R_c}{H_s} \cdot \frac{H_s}{h_{2\%}} \quad [-] \quad (34)$$

$$c_v = \sqrt{\frac{R_{u2\%} - R_c}{H_s}} \cdot \frac{\sqrt{g \cdot H_s}}{v_{2\%}} \quad [-] \quad (35)$$

- with
- $H_s$  significant wave height [m]
  - $R_{u2\%}$  run-up height exceeded by 2 % of the incoming waves [m]
  - $R_c$  freeboard height [m]
  - $c_h$  empirical coefficient determined by model tests [-]

In Fig. 80 and Fig. 81 the standard-deviations  $\pm\sigma$ ,  $\pm2\sigma$  and  $\pm3\sigma$  of the coefficients  $c_h$  and  $c_v$  are plotted respectively.

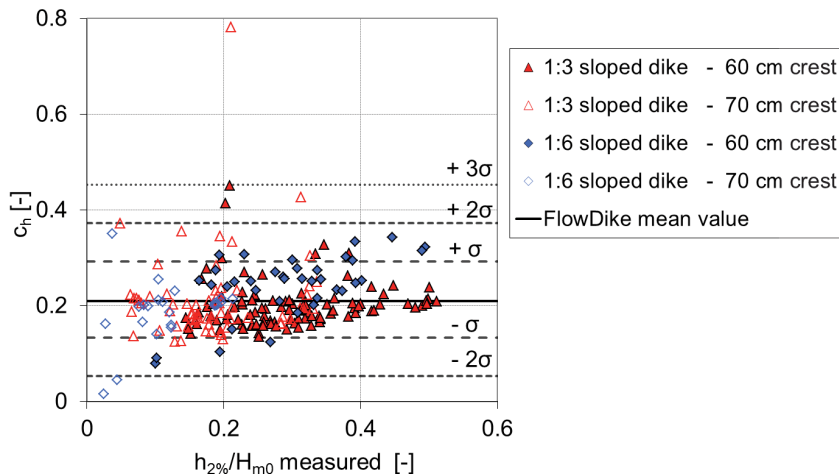


Figure 80: Coefficient  $c_h$  as a function of  $h_{2\%}/H_{m0}$  without tests with wind or flow depth under 1 cm.

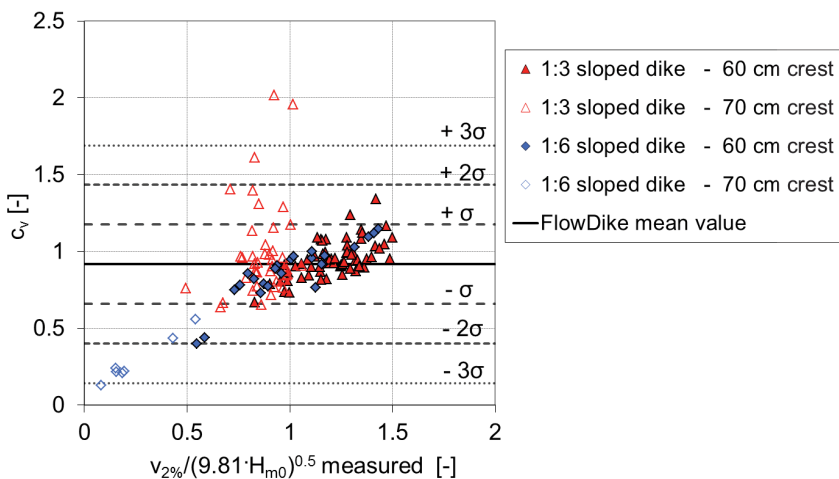


Figure 81: Coefficient  $c_v$  as a function of  $v_{2\%}/(9.81H_{m0})^{0.5}$  without tests with wind or flow depth under 1 cm.

Furthermore, as a result of these distributions the data which are located outside the  $3\sigma$ -interval are excluded from the following analysis and new mean values are determined.

To verify the coefficients for each dike configuration the average coefficient of each dike configuration and the average coefficient of all dike configurations are shown in Fig. 82. The standard deviation refers to every single test. The coefficient  $c_v$  of the 1:6 sloped and 0.7 m high dike gives quite different values than the other dike configurations (cf. red-lined circle in Fig. 82). Therefore this dike configuration will be omitted for the determination of the coefficient  $c_v$ . Fig. 83 shows the new distribution of coefficients and the final constant empirical coefficients  $c_h$  and  $c_v$ :

$$c_h = 0.21 \quad \text{and} \quad c_v = 0.94$$

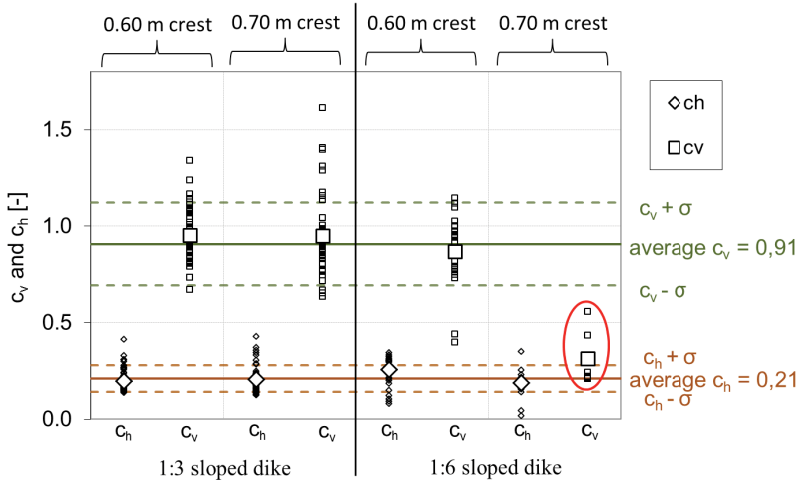


Figure 82: Average coefficients of every single dike configuration and of all configurations together.

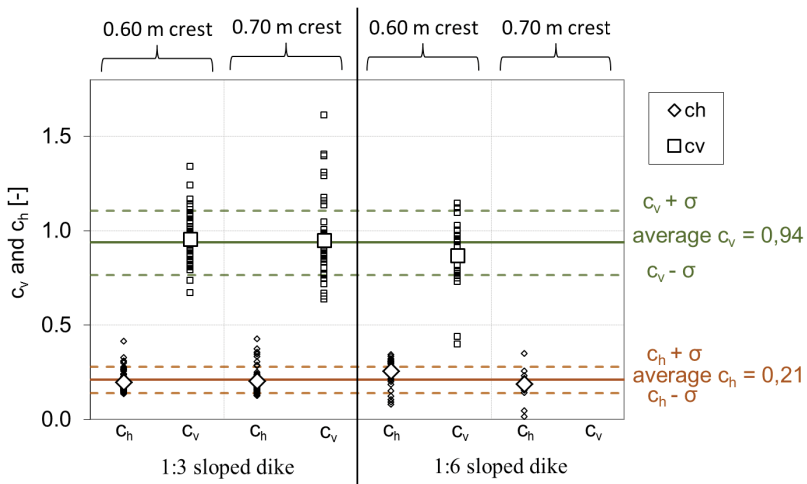


Figure 83: Average coefficients of every single dike configuration and of all configurations together excluding  $c_v$  of 1:6 sloped and 0.7 m high dike.

It is possible to determine the flow depths and flow velocities on the seaward side by using the modification of empirical coefficients used in formula (32) and (33) by SCHÜTTRUMPF and VAN GENT (2003).

Fig. 84 shows that the new empirical coefficient  $c_h = 0.21$  is lower than the coefficient by SCHÜTTRUMPF (2001)  $c_h = 0.33$  and is slightly higher than the value by VAN GENT (2002)  $c_h = 0.15$ . The coefficient  $c_v = 0.94$  for the results of FlowDike 1 and FlowDike 2 is lower than the coefficients by SCHÜTTRUMPF (2001)  $c_v = 1.37$  and VAN GENT (2002)  $c_v = 1.30$ . The coefficients by SCHÜTTRUMPF (2001) have been determined

by flow depth and flow velocities on the dike slope, while flow depths on the dike crest have been used in FlowDike 1 and FlowDike 2.

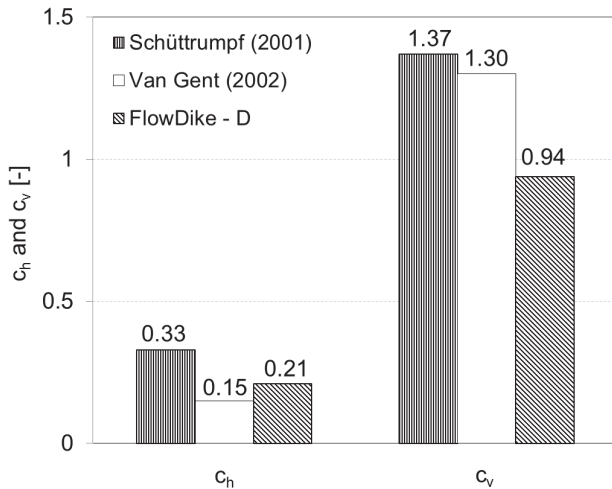


Figure 84: Coefficients  $c_h$  and  $c_v$  of former investigations compared with the new coefficients by FlowDike 1 and FlowDike 2.

With the new empirical coefficients  $c_h$  and  $c_v$  flow depths  $h_{2\%}$  and flow velocities  $v_{2\%}$  were calculated and plotted against the measured values (Fig. 85). According to the modification of empirical coefficients used in formulas by SCHÜTTRUPF and VAN GENT (2003) it is possible to determine the flow depths and flow velocities on the seaward side of the crest on the 1:3 sloped dike (Fig. 85) and 1:6 sloped dike (Fig. 86). Further analysis considering the influence of current and wind on flow processes on dike crests has not been carried out yet.

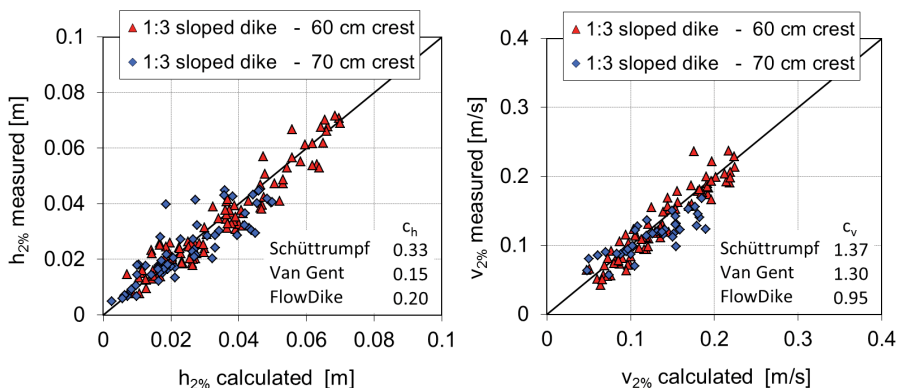


Figure 85: Measured and calculated flow depths  $h_{2\%}$  and flow velocities  $v_{2\%}$  on the seaward side of the dike crests using the new empirical coefficients, 1:3 sloped dike.

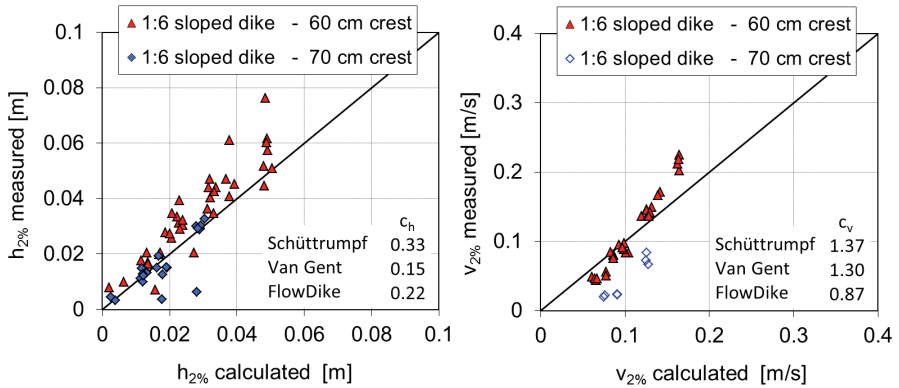


Figure 86: Measured and calculated flow depths  $h_{2\%}$  and flow velocities  $v_{2\%}$  on the seaward side of the dike crests using the new empirical coefficients, 1:6 sloped dike.

### 6.5.2 Influence of oblique wave attack on flow processes on dike crests

In the following section the influence of oblique wave attack on flow depth on dike crests will be analyzed. Following the previous chapter, the flow velocities on the dike crests do not give clear results. Therefore they will not be used for the determination of the influence of oblique wave attack on flow processes on dike crests.

The dimensionless flow depth  $h^*$  can be determined using the following formula:

$$h^* = \frac{h_{2\%}}{H_s} \quad [-] \tag{36}$$

with  $h_{2\%}$  flow depths on seaward dike crest, which is exceeded by 2 % of the incoming waves [m]  
 $H_s$  significant wave height [m]

Fig. 87 and Fig. 88 give the dependency between the dimensionless flow depth  $h^*$  and the dimensionless freeboard height  $R_c^*$  for the different angles of wave attack. The interception with the y-axis of the regression curves is defined as  $h^*=1$ . This means that the flow depths on the seaward dike crest  $h_{2\%}$  have the same value as the significant wave height  $H_s$ . The inclination of the graphs of the tests with perpendicular wave attack is lower than the slopes of the graphs of the test with oblique wave attack. The higher the angle of wave attack the smaller is the dimensionless flow depth  $h^*$  for unchanged dimensionless freeboard height  $R_c^*$ . This behavior corresponds well with the characteristic of the wave overtopping rate (cf. section 6.3).

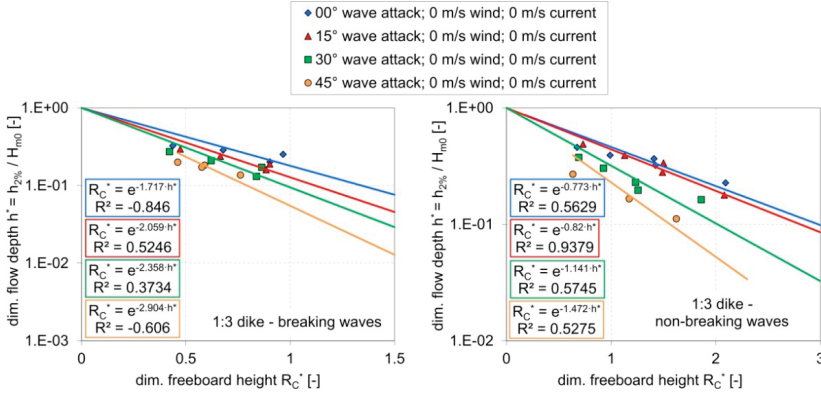


Figure 87: Influence of oblique wave attack on flow depth on dike crests; 1:3 sloped dike (left: breaking conditions; right non-breaking conditions).

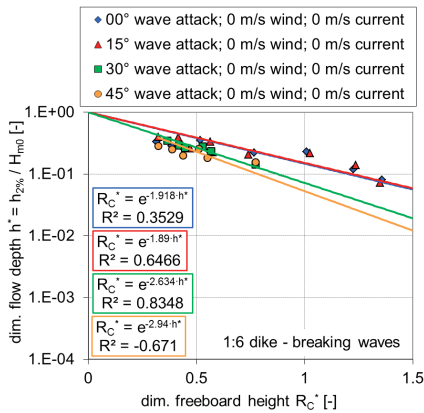


Figure 88: Influence of oblique wave attack on flow depth on dike crests; 1:6 sloped dike (breaking conditions).

## 7 Conclusion

The investigations of FlowDike 1 and FlowDike 2 focussed on the effects of onshore wind and longshore current on wave run-up and wave overtopping for perpendicular and oblique wave attack. These variables were two of the missing effects in freeboard design and therefore a main interest for design purposes. Model tests were carried out in the shallow water wave basin at DHI (Hørsholm, Denmark) and included the configuration of a 1:3 sloped dike (FlowDike 1) and a 1:6 sloped dike (FlowDike 2).

The data analysis on wave run-up was based on an advanced data extraction from video films considering 10 separate stripes of the run-up board which provided additional measurement results. In a first step the measured wave run-up was analyzed with respect to the influence of a single parameter: oblique wave attack, onshore wind and a longshore current.

Results considering oblique wave attack confirm former empirical investigations. The increasing effect of onshore wind on wave run-up as described regarding former model

tests with monochromatic waves could not be validated by the FlowDike test results. The investigated onshore wind speed of  $< 10$  m/s had no significant effect on the wave run-up in the model tests with the 1:3 sloped dike and a very slightly decreasing effect in the model tests with the 1:6 sloped dike. Furthermore no significant effect on wave run-up in case of a longshore current velocity  $< 0.4$  m/s and a perpendicular wave attack was obtained.

In a second step the combined effect of oblique wave attack and a longshore current was investigated. The results show non obvious dependencies but it has to be considered that the relative wave run-up height is a very sensitive parameter.

The third step within data analysis was the comparison between measured and calculated relative wave run-up. Calculation was done using the formula of EUROTOP-MANUAL (2007) together with the estimated influence factors  $\gamma_{\beta}$ ,  $\gamma_{cu}$  and  $\gamma_w$ . The comparison shows a good agreement between the measured and the calculated values. All pairs of values are in a range of  $\pm 20$  %.

The tests on perpendicular wave attack without influencing parameter were validated with existing wave overtopping formulae from the EUROTOP-MANUAL (2007). For both model tests the data points of the reference tests fit well within the 95 % confidence range of the formula.

All wind tests confirmed the stated assumptions by GONZÁLEZ-ECRIVA (2006) and DE WAAL et al. (1996) concerning the significant wind impact on small overtopping discharges. For high overtopping discharges practically no influence is noticeable as the data points for wind match those of the reference test, this validates the stated theory of WARD et al. (1996).

The influence of oblique waves on overtopping was analyzed as a last resort. In a first attempt the results found for both investigations validate the trend for obliqueness to reduce wave overtopping. The influence factors found for FlowDike 1 validate well the regression trend found for former investigations.

For wave overtopping the combination of oblique wave attack and longshore current was analyzed by determining an influence factor  $\gamma_{\beta, cu}$ . Using therefore the relative wave period  $T_{rel, m-1, 0}$  instead of the absolute wave period  $T_{abs, m-1, 0}$  leads to rather high values and does not account the current influence on wave overtopping. Instead of that the influence-factor  $\gamma_{\beta, cu}$  can be determined by using the angle of wave energy  $\beta_e$  instead of the angle of wave attack  $\beta$ .

The influence factors for the angle of wave attack, the longshore current and wind on wave run-up correspond well to the influence factors on wave overtopping. For both analysis on wave run-up and wave overtopping the absolute wave parameters and the angle of wave attack should be used.

According to the modification of empirical coefficients used in formulae by SCHÜTTRUMPF and VAN GENT (2003) it is possible to determine the flow depths and flow velocities on the seaward side of the crest. Additionally, the dimensionless flow depths for different dimensionless freeboard height and different angles of wave attack have been analyzed. The higher the angle of wave attack the smaller is the dimensionless flow depth for unchanged dimensionless freeboard heights. This behavior corresponds well with the characteristics of the wave overtopping rate.

Further investigations on very oblique wave attack with  $\beta > 45^\circ$  are planned within the HYDRALAB-IV project CornerDike.

## 8 List of abbreviations

br	breaking wave conditions
nbr	non-breaking wave conditions
SWL	still water level
w1	wave condition number 1
w2	wave condition number 2
w3	wave condition number 3
w4	wave condition number 4
w5	wave condition number 5
w6	wave condition number 6

## 9 Notation

a	[-]	regression coefficient with $a=0.067$ for breaking conditions and $a=0.2$ for non-breaking conditions
$a_r$	[-]	coefficient depending at least on the dike slope to determine the influence factor $\gamma_\beta$
$b_{all}, b_{all,0^\circ}$	[-]	slope of the graph considering all data points (for normal wave attack)
$b_i$	[-]	slopes of the graphs for each data point
$b_r$	[-]	coefficient depending at least on the dike slope to determine the influence factor $\gamma_\beta$
$b_{ref,1:3}$	[-]	slopes of the graph of the reference test (1:3 sloped dike)
$b_{ref,1:6}$	[-]	slopes of the graph of the reference test (1:6 sloped dike)
$b_\beta$	[-]	exponential coefficients for normal or oblique wave attack
$c_{abs}$	[m/s]	absolute velocity of waves
$c_{g,abs}$	[m/s]	absolute group velocity of waves
$c_{g,rel}$	[m/s]	relative group velocity of waves
$c_h$	[-]	empirical coefficient determined by model tests concerning flow depth on crest
$c_{rel}$	[m/s]	relative velocity of waves
$c_v$	[-]	empirical coefficient determined by model tests
$c_w$	[-]	constant factor to determine the wind speed by GONZÁLES-ECRIVÁ (2006)
d	[m]	flow depth, water depth
$d_b$	[m]	flow depth at breaker point without wind
$d_{b(wind)}$	[m]	flow depth at breaker point with wind
g	[m/s <sup>2</sup> ]	acceleration due to gravity ( $= 9.81 \text{ m/s}^2$ )
$h^*$	[-]	dimensionless flow depth on seaward dike crest
$h_{2\%}$	[m]	flow depth on dike crest exceeded by 2 % of the incoming waves
$H_{2\%}$	[m]	wave height exceeded by 2 % of the waves
$H_{m0}$	[m]	significant wave height from spectral analysis
$H_s$	[m]	significant wave height
$H_s$	[m]	significant wave height (defined as highest one-third of wave heights)

$k$	[rad/m]	wave number with $k = 2 \cdot \pi / \omega$
$K_R$	[-]	reflection coefficient
$k_{rel}$	[rad/m]	relative wave number $k = 2 \cdot \pi / \omega_{rel}$
$L_{m-1,0}$	[m]	deep water wave length $L_{m-1,0} = \frac{T_{m-1,0}}{2\pi}$
$m$	[-]	slope of the dike: 1 unit vertical corresponds to $m$ units horizontal
$m'$	[-]	adapted slope of the dike for oblique wave attack: 1 unit vertical corresponds to $m$ units horizontal
$m_0$	[m <sup>2</sup> /s]	zero order moment of spectral density
$m_{0,incident}$	[m <sup>2</sup> /s]	energy density of the incident wave spectrum
$m_{0,reflected}$	[m <sup>2</sup> /s]	energy density of the reflected wave spectrum
$m_{-1}$	[m <sup>2</sup> ]	minus first moment of spectral density
$p$	[-]	probability of wave overtopping event
$q$	[m <sup>3</sup> /(sm)]	mean overtopping rate per meter structure width
$q^*$	[-]	dimensionless overtopping discharge
$Q_0$	[-]	interception with the y-axis
$R_c$	[m]	freeboard height of the structure
$R_{c^*}$	[-]	dimensionless freeboard height
$R_{u2\%}$	[m]	run-up height exceeded by 2 % of the incoming waves
$s_{m-1,0}$	[-]	wave steepness defined by $s_{m-1,0} = H_{m0} / L_{m-1,0}$
$T_{abs}$	[s]	absolute wave period
$T_{m-1,0}$	[s]	spectral wave period defined by $T_{m-1,0} = m_{-1} / m_0$
$T_p$	[s]	spectral peak wave period
$u$	[m/s]	wind velocity
$u_{10}$	[m/s]	wind velocity 10 m above still water level
$v$	[m/s]	current velocity parallel to the dike crest
$v_{2\%}$	[m/s]	flow velocity on dike crest exceeded by 2 % of the incoming waves
$v_{crest,no wind}$	[m/s]	flow velocity on the dike crest, wind $u_{10} = 0$ m/s
$v_{crest,wind}$	[m/s]	flow velocity on the dike crest, wind $u_{10} \neq 0$ m/s
$v_\beta$	[m/s]	component of current velocity in the direction of wave propagation
$w$	[m/s]	wind speed by GONZÁLES-ECRIVÁ (2006)
$w_p$	[m/s]	prototype wind speed by GONZÁLES-ECRIVÁ (2006)
$x$	[m]	horizontal coordinate parallel to the dike crest
$x'$	[-]	probability of exceedance – Rayleigh distributed [%]
$y$	[m]	horizontal coordinate perpendicular to the dike crest
$z$	[m]	vertical coordinate
$\alpha$	[°]	slope of the front face of the structure
$\alpha'$	[°]	adapted slope of the dike for oblique wave attack
$\beta$	[°]	angle of wave attack relative to normal on structure; perpendicular wave attack: $\beta=0^\circ$ ; oblique wave attack: $\beta \neq 0^\circ$
$\beta_e$	[°]	angle of wave energy relative to normal on structure
$\gamma_{cu}, \gamma_{\beta,cu}$	[-]	correction factor to take the influence of current $v_x$ (and the angle of wave attack) into account
$\gamma_i$	[-]	influence factor of each data point
$\gamma_w$	[-]	correction factor to take the influence of wind into account

$\gamma_{\beta}$	[-]	correction factor for oblique wave attack considering run-up and ov. design
$\xi$	[-]	surf similarity parameter
$\xi_{m-1,0}$	[-]	surf similarity parameter based on $s_{m-1,0}$
$\sigma$	(varying)	standard deviation
$\omega$	[rad/s]	angular frequency
$\omega_{abs}$	[rad/s]	absolute angular frequency
$\omega_{rel}$	[rad/s]	relative angular frequency

## 10 References

- ARTHUR, R. S.: Refraction of shallow water waves: The combined effect of currents and underwater topography, Transactions, American Geophysical Union, Vol. 31-4, 549–552, doi: 10.1029/TR031i004p00549, 1950.
- BATTJES, J. A.: Computation of set-up, longshore currents, run-up and overtopping due to wind-generated waves, Vol. 74-2, Delft, Netherlands, 1974.
- DE ROUCK, J.; BOONE, C. and VAN DE WALLE, B.: The optimisation of crest level design of sloping coastal structures through prototype monitoring and modelling: OPTICREST; Detailed scientific and technical report, Ghent, Belgium, Ghent University, (contract; MAS3-CT97-0116), 2001.
- DE ROUCK, J.; TROCH, P.; VAN DE WALLE, B.; VAN GENT, M. R. A.; VAN DAMME, L.; DE RONDE, J.; FRIGAARD, P. and MURPHY, J.: Wave run-up on sloping coastal structures prototype measurements versus scale model tests, Proceedings of the international Conference on Breakwaters, coastal structures and coastlines, 233–244, London, England, 2002.
- DE WAAL, J. P. and VAN DER MEER, J. W.: Wave runup and overtopping on coastal structures, Proceedings of the 23rd International Conference on Coastal Engineering, 1772–1784, 1992.
- DE WAAL, J. P.; TÖNJES, P. and VAN DER MEER, J. W.: Wave overtopping of vertical structures including wind effect, Proceedings of the 25th International Conference on Coastal Engineering, 2216–2229, Singapore, Singapore, 1996.
- DHI WASY WATER & ENVIRONMENT: WS Wave Analysis Tools – User Guide, [DHI Software 2007], 2007.  
[http://www.hydroasia.org/jahia/webdav/site/hydroasia/shared/Document\\_public/Project/Manuals/WRS/MIKEZero\\_WSWAnalysisTools.pdf](http://www.hydroasia.org/jahia/webdav/site/hydroasia/shared/Document_public/Project/Manuals/WRS/MIKEZero_WSWAnalysisTools.pdf) (access on 27th October 2011)
- EUROTOP-MANUAL; PULLEN, T.; ALLSOP, N. W. H.; BRUCE, T.; KORTENHAUS, A.; SCHÜTTRUMPF, H. and VAN DER MEER, J. W.: EurOtop, wave overtopping of sea defences and related structures: Assessment manual, Die Küste, 73, 2007.  
<http://www.overtopping-manual.com/eurotop.pdf> (04-18-12)
- FÜHRBÖTER, A. and WITTE, H.-H.: Wellenbelastung an Seedeichen – Strömungsgeschwindigkeiten beim Wellenaufbau auf einer Böschung der Neigung 1 : n = 1 : 6 (Experimentelle Untersuchungen im Großen Wellenkanal Hannover), In: Sonderdruck aus dem Jahrbuch der Hafentechnischen Gesellschaft, Band 44, 176–194, 1989.

- GALLOWAY, J. S.; COLLINS, M.B. and MORAN, A. D.: Onshore/offshore influence on breaking waves: An Empirical Study. Coastal Engineering 13. Elsevier Science Publishers, 1989.
- GONZÁLES-ECRIVÁ, J. A.: The role of wind in wave runup and wave overtopping of coastal structures, Proceedings of the 30th International Conference, Vol. 5, 4766–4778, Singapore, 2006.
- HEDGES, T. S.: Combinations of Waves and Currents – An Introduction, Proceedings of the Institution of Civil Engineers Part 1-Design and Construction, Vol. 82, 567–585, London, England, 1987.
- HEYER, T. und POHL, R.: Der Auflauf unregelmäßiger Wellen im Übergangsbereich zwischen branden und Schwingen, Wasser und Abfall, Vol. 5, 34–38, Sindelfingen, Germany, 2005.
- HOLTHUIJSEN, L. H.: Waves in oceanic and coastal waters, New York, 2007.
- JENSEN, M. S. and FRIGAARD, P.: The optimisation of crest level design of sloping coastal structures through prototype monitoring and modelling: OPTICREST; Final edition; Zeebrugge model: Wave runup under simulated prototype storms (II); The influence on wave run-up introducing a current, Aalborg, Denmark, Aalborg University (contract; MAS3-CT97-0116), 2000.
- LE MÉHAUTÉ, B.: Similitude in Coastal Engineering. Journal of the Waterways, Harbors and Coastal Engineering, Vol. 102, 317–335, 1976.
- MEDINA, J.: Wind effects on run-up and breakwater crest design. Proceedings International conference on coastal engineering. Copenhagen, 1998.
- MURPHY, J.; SCHÜTTRUMPF, H. and LEWIS, T.: Wave run-up and overtopping of sea dikes: results from new model studies, In: Fourth International Symposium on Ocean Wave Measurement and Analysis: September 2-6, 2001 in San Francisco, California, United States / Edge, Billy L., Hemsley, J. Michael [Ed.] – New York, American Society of Civil Engineers, 1575–1584, 2001.
- OUMERACI, H.; SCHÜTTRUMPF, H.; SAUER, W.; MÖLLER, J. and DROSTE, T.: Physical model tests on wave overtopping with natural sea states – 2D model tests with single, double and multi peak wave energy spectra, Vol. LWI-Bericht 852, Braunschweig, Germany, 2000.
- OUMERACI, H.; MÖLLER, J.; SCHÜTTRUMPF, H.; ZIMMERMANN, C.; DAEMRICH, K.-F. und OHLE, N.: Schräger Wellenauflauf an Seedeichen, Vol. LWI 881, FI 643/V, Braunschweig, Germany, 2002.
- SCHÜTTRUMPF, H.: Wellenüberlaufströmung bei Seedeichen – Experimentelle und theoretische Untersuchungen, Braunschweig, Germany, 2001.
- SCHÜTTRUMPF, H. and VAN GENT, M. R. A.: Wave overtopping at seadikes, 431–443, Vicksburg, MS, 2003.
- TRELOAR, P. D.: Spectral wave refraction under the influence of depth and current, Coastal Engineering, Vol. 9, Issue 5, 439–452, Amsterdam, Netherlands, 1986.
- VAN DER MEER, J. W.: Hydralab-Flowdike; Influence of wind and current on wave run-up and wave overtopping; detailed analysis on the influence of current on wave overtopping, Heerenveen, The Netherlands: Van der Meer Consulting B.V., Coastal Engineering Consultancy & Research, (Project number; vdm08310), 2010.
- VAN GENT, M. R. A.: Wave overtopping events at dikes, Proceedings of the 28th International Conference, Singapore, 2002.

- WAGNER, H. und BÜRGER, W.: Kennwerte zur Seedeichbemessung, *Wasserwirtschaft Wassertechnik*, Vol. 23, Issue 6, 204–207, Berlin, Germany, 1973.
- WARD, D. L.; ZHANG, J.; WIBNER, C. G. and CINOTTO, C. M.: Wind effects on runup and overtopping of coastal structures, *Proceedings of the 29th International Conference on Coastal Engineering*, 2206–2215, Singapore, 1996.
- YAMASHIRO, M.; YOSHIDA, A.; HASHIMOTO, H. and IRIE, I.: Conversion ratio of wind velocity from prototype to experimental model on wave overtopping. *Proceedings of the International Conference on Coastal Engineering*, San Diego, 2006.